I.

L. Havelková, B. Bashta, M. Vaňková, J. Zedník, J. Brus, A.Vagenknechtová, Jan Sedláček: Functionalized hyper-cross-linked porous homopolymers of ring substituted 1,3-diethynylbenzenes and their physisorption activity. *Odesláno 25.8.2023*

European Polymer Journal

Functionalized hyper-cross-linked porous homopolymers of ring-substituted 1,3-diethynylbenzenes and their physisorption activity

--Manuscript Draft--

Manuscript Number:	
Article Type:	Research paper
Section/Category:	Regular Paper
Keywords:	Porous organic polymers; hyper-cross-linked; polyacetylenes; heteroatom functional groups; CO2 adsorption; water vapour sorption
Corresponding Author:	Lucie Havelková CZECH REPUBLIC
First Author:	Lucie Havelková
Order of Authors:	Lucie Havelková
	Bogdana Bashta, Dr.
	Michaela Vaňková
	Jiří Zedník, Dr.
	Jiří Brus, Dr.
	Alice Vagenknechtová, Dr.
	Jan Sedláček, Prof.
Abstract:	An atom-economic one-step chain-growth coordination homopolymerization providing high yields of functionalized hyper-cross-linked polyacetylenes with a permanent micro/mesoporous texture and a specific surface area of up to 1062 m2/g is reported. Substituted 1,3-diethynylbenzenes used as monomers in this synthesis simultaneously provide both functionalization and hyper-cross-linking of the resulting products. The homopolymerization is highly compatible with the heteroatom groups of the monomers and allows the preparation of well-defined porous networks with a wide spectrum of univalent groups (-F, -Cl, -Br, -NO2, -COOCH3, -CH2OH, -COOH) present in the networks in a high content of 7.87 mmol/g. The physisorption activity of the prepared networks is significantly affected by the character of the functional groups. Functional groups generally increase the capacity of reversible CO2 capture. Networks with oxygen-containing groups show high and potentially application-interesting capacities of cyclic reversible capture of water vapour from the air (capacity up to 314 mg/g, at a relative humidity of 90%). Halogenated networks, on the other hand, are highly active in the reversible capture of benzene vapour (capacity up to 971 mg/g at room temperature).
Suggested Reviewers:	Toshio Masuda, Prof. Shanghai University School of Materials Science and Engineering toshio.masuda.78z@st.kyoto-u.ac.jp
	David Pahovnik, Dr. National Institute of Chemistry Slovenia David.Pahovnik@ki.si
	Pierre Lutz Charles Sadron Institute pierre.lutz@ics-cnrs.unistra.fr
	Asim Bhaumik, Prof. Indian Association for the Cultivation of Science School of Materials Sciences msab@iacs.res.in
	Neil Bruce McKeown, Prof. The University of Edinburgh School of Chemistry

Functionalized hyper-cross-linked porous homopolymers of ring-substituted 1,3-diethynylbenzenes and their physisorption activity

Lucie Havelková[1,*], *Bogdana Bashta*[1], *Michaela Vaňková*[1], *Jiří Zedník*[1], *Jiří Brus*[2], *Alice Vagenknechtová*[3], *Jan Sedláček*[1,*]

[1] Department of Physical and Macromolecular Chemistry, Faculty of Science, Charles University, Hlavova 2030, Prague 2, 128 43, Czech Republic

[2] Institute of Macromolecular Chemistry, Czech Academy of Sciences, Heyrovský Sq. 2, Prague 6, 162 00, Czech Republic

[3] Department of Gaseous and Solid Fuels and Air Protection, University of Chemistry and Technology in Prague, Technická 5, Prague 6, 166 28 Czech Republic

* Correspondence: lucie.havelkova@natur.cuni.cz, jan.sedlacek@natur.cuni.cz

Keywords

Porous organic polymers, hyper-cross-linked, polyacetylenes, heteroatom functional groups, CO_2 adsorption, water vapour sorption.

Abstract

An atom-economic one-step chain-growth coordination homopolymerization providing high yields of functionalized hyper-cross-linked polyacetylenes with a permanent micro/mesoporous texture and a specific surface area of up to 1062 m^2/g is reported. Substituted 1,3-diethynylbenzenes used as monomers in this synthesis simultaneously provide both functionalization and hyper-cross-linking of the resulting products. The homopolymerization is highly compatible with the heteroatom groups of the monomers and allows the preparation of well-defined porous networks with a wide spectrum of univalent groups (-F, -Cl, -Br, $-NO_2$, $-COOCH_3$, $-CH_2OH$, -COOH) present in the networks in a high content of 7.87 mmol/g. The physisorption activity of the prepared networks is significantly affected by the character of the functional groups. Functional groups generally increase the capacity of reversible CO_2 capture. Networks with oxygen-containing groups show high and potentially

application-interesting capacities of cyclic reversible capture of water vapour from the air (capacity up to 314 mg/g, at a relative humidity of 90 %). Halogenated networks, on the other hand, are highly active in the reversible capture of benzene vapour (capacity up to 971 mg/g at room temperature).

1. Introduction

Polyacetylene $[-HC=CH-]_n$ and its mono- and disubstituted derivatives, $[-HC=CR-]_n$ and $[-^1RC=CR^2-]_n$, are probably the first described well-defined π-conjugated polymers.[1] The π-conjugated nature of these polymers is due to the alternation of single and double bonds between the carbon atoms of the main chains. Thanks to this, conjugated chains of polyacetylenes can easily mediate or support the transport and transformation of energy or charges. As a result, polyacetylenes attract interest for their potential applications in electronics, optics and optoelectronics.[2–8] At the same time, conjugated polyacetylene chains are relatively rigid, allowing substituted polyacetylenes to adopt various regular conformations.[5] This enabled, for example, the formation of liquid crystalline polyacetylenes, providing that the aromatic/aliphatic groups of a proper length were selected as substituents of these polymers.[9-11] If polyacetylenes carry enantiomerically pure chiral substituents their chains can be helically twisted in a one-handed direction and polyacetylenes with so-called helical chirality can be achieved.[5,12–14] The rigidity of polyacetylenes may hinder their dense packing in the solid phase. In particular, the morphology of disubstituted polyacetylenes often includes various microvoids, which are interesting from the point of view of transport or capture of gases, vapours, and liquids in these polymers. Optimally casted membranes prepared from linear disubstituted polyacetylenes, (e.g. from poly[1-(trimethylsilyl)propyne], ref. [15]) were reported to exhibit excellent performance in the separation of O_2/N_2, ethanol/water and other mixtures.[16,17] Kwak et al.[18] showed that aromatic disubstituted polyacetylenes, poly[1-phenyl-2-(4-trimethylsilyl)phenylacetylene] and poly(1,2-diphenylacetylene), exhibited the properties of so-called Polymers of Intrinsic Microporsity (PIMs).[19,20] The Brunauer-Emmett-Teller specific surface area (S_{BET}) from 341 to 635 m^2/g was reported for these covalently very simple and readily accessible linear and mostly soluble polyacetylenes.[18] Polyacetylene PIMs were applied in the rapid determination of the viscosity of various oils based on monitoring the rate of change in the luminescence of these PIMs due to penetrating liquids.[21]

Substituted polyacetylenes are prepared by transition metal-catalysed chain-growth coordination polymerization of acetylenes, HC≡CR and $^1RC≡CR^2$. The application potential of

this polymerization is quite wide and diverse [2–4,22]: several hundred monosubstituted and disubstituted acetylenes have been successfully polymerized so far, including monomers with very bulky substituents [23] and monomers with substituents containing heteroatom groups of various polarity and reactivity.[24] Regarding the product architecture, the research was mainly focused on the preparation of linear (often well soluble) polyacetylenes. In contract, significantly lower attention was paid to polyacetylenes with a branched or cross-linked architecture. Several articles described chemically or thermally induced postpolymerization cross-linking of properly substituted linear polyacetylenes.[11,25–29] For example, Goto et al. cross-linked benzoxazine-substituted polyacetylenes into highly stable resins in which the polyacetylene chains were preserved.[25] Some authors dealt with chain-growth copolymerizations of mono- and diethynylated comonomers aimed at the preparation of hyperbranched or slightly cross-linked polyacetylenes suitable for further covalent modification or for the construction of membranes or nanoparticles.[2,30–33] Dong and Ye reported a comprehensive study of the copolymerization of phenylacetylene with 1,3- and 1,4-diethynylbenzenes catalyzed by an *in situ* generated Pd-based catalyst. They succeeded in preventing cross-linking (gelation) of the products and prepared (in moderate yields) a large series of soluble hyperbranched poly(phenylacetylene)s differing in branching density.[33] Unlike Dong and Ye, our group decided to use the chain-growth polymerization of acetylenes to prepare densely cross-linked (hyper-cross-linked) insoluble polyacetylene networks. Di-, tri-, and tetraethynylarenes [diethynylbenzenes, 1,3,5-triethynylbenzene and tetrakis(4-ethynylphenyl)methane] were used as monomers and their homopolymerization was optimized towards the high cross-linking density. Using polymerization catalysts based on Rh complexes and optimized reaction conditions, the desired networks were achieved in high (often quantitative) yields. The networks consisted of polyacetylene chains interconnected by arene links.[34–36] Due to the hyper-cross-linking and the rigidity of polyacetylene main chains, the segments of the networks were not tightly packed in the solid state, and the networks exhibited permanent microporosity that was formed without the need for additional postpolymerization cross-linking. The S_{BET} values of the networks were mostly from 600 to 1400 m^2/g which were typical S_{BET} values reported for Hyper-cross-linked Porous Polymers [37,38] prepared by other methods, e.g. by knitting polymerization of arenes [39] or by the radical polymerization of vinyl monomers followed by postpolymerization cross-linking.[40]

For functional applications of polymers with permanent porosity, the functionalization of these materials with heteroatom groups and segments serving, for example, as sorption or catalytically active centres was usually necessary.[37,41] We showed that the functionalization

of polyacetylene networks aimed at the preparation of porous materials active in selective sorption and catalysis can be performed both by prepolymerization [42–47] and postpolymerization [48,49] methods. The prepolymerization introduction of heterocyclic segments [42,43] and bivalent functional groups [44] was smooth, as these segments and groups simultaneously contributed to the formation of the porous scaffold of the polyacetylene networks. Prepolymerization functionalization with univalent heteroatom functional groups mostly required a copolymerization approach consisting in copolymerization of functionalized acetylene monomers with ethynylated cross-linkers.[46,47] This somewhat reduced the content of functional groups in the prepared networks. Therefore, we have developed and report here a homopolymerization method leading to porous hyper-cross-linked polyacetylene networks with a high content of univalent functional groups. Substituted 1,3-diethynylbenzenes were used as monomers, which simultaneously ensured functionalization and hyper-cross-linking of the resulting networks. The homopolymerization was compatible with the heteroatom groups of the monomers and allowed the preparation of well-defined porous poly(1,3-diethynylbenzene)s with a wide spectrum of univalent functional groups. Covalent, morphological and textural characterization of the prepared networks are also described and discussed in this article, as well as the effect of functional groups on the activity of the networks in the sorption of gases and vapours.

2. Experimental Section

2.1. Materials

(Acetylacetonato)(norbornadiene)rhodium(I), [Rh(nbd)acac], (>98%), 1,3-diethynylbenzene (M1), (>96%), 4,6-dimethyl-1,3-diethynylbenzene (M2), (>98%) (all TCI Europe), 1,3-diethynyl-5-fluorobenzene (M5), (98%), 1,3-diethynyl-5-chlorobenzene (M6), (98%), 1,3-diethynyl-5-bromobenzene (M7), (98%), 1,3-diethynyl-5-nitrobenzene (M8), (98%), 3,5-diethynylbenzoic acid methyl ester (M9), (98%), 3,5-diethynylbenzyl alcohol (M10), (98%), 3,5-diethynylbenzoic acid (M11), (98%), (all Spectra Group Limited, Inc.), methanol (≥99 %) and benzene (anhydrous, 99.8%) (both from Merck) were used as obtained. 5-Methyl-1,3-diethynylbenzene (M3) was prepared according to ref. [50] using 1,3-dibromo-5-methylbenzene and (trimethylsilyl)acetylene (both from TCI Europe) and 5-*n*-hexyl-1,3-diethynylbenzene (M4) was prepared from 1,3-dibromo-5-*n*-hexyl-benzene and (trimethylsilyl)acetylene (both from TCI Europe) according to ref. [51]. Dichloromethane (99.95%, Lach-Ner) was distilled with P_2O_5.

2.2. Synthesis of the networks

All networks were synthesized by chain-growth coordination polymerization using complex [Rh(nbd)acac] as a catalyst. As a polymerization solvent, we used distilled dichloromethane (M1-M9) or methanol (M10-M11) regarding the solubility of the monomers. The initial concentrations of the monomer and catalyst were 0.3 mol/dm^3 and 15 mmol/dm^3, respectively. The polymerizations were started by adding the catalyst solution to the solution of the monomer. The polymerizations were performed under the Ar atmosphere in the sealed thick-wall ampoules at 75°C. The precipitated polymer networks were separated, washed thoroughly with dichloromethane or methanol, and dried under the vacuum for 2 days at room temperature. The yield was determined gravimetrically.

2.3. Methods

The ^{13}C CP/MAS NMR spectra were acquired with a Bruker Avance III 500 WB/US NMR spectrometer (Bruker GmbH, Karlsruhe, Germany, 2013), at a field strength of 11.7 T and a spinning frequency of 18 kHz. To obtain accurate results, a 90° (^{1}H) pulse of 2.5 μs and a 64 kHz spin-locking field $B_1(^1H,^{13}C)$ (expressed in frequency units $\omega_1/2\pi = \gamma B_1$) was applied to the sample. The recycle delay was 6 s and the cross-polarization contact time was 3 ms. During the acquisition of NMR signals, SPINAL64 decoupling at a frequency of 89.3 kHz was applied to improve the resolution of measured spectra. Active cooling was used to counterbalance the frictional heating of rotating samples.[52]

Scanning Electron Microscopy (SEM) measurements were performed using the Tescan Lyra3 apparatus (TESCAN Brno, Ltd., Czech Republic) at an accelerating voltage of 10 kV.

Thermogravimetric analysis (TGA) was performed on the Setsys Evolution apparatus (Seteram, Caluire-et-Cuire, France) under a nitrogen atmosphere using a heating rate of 10 °C/min in the temperature range from 40 to 800 °C.

The adsorption/desorption isotherms of nitrogen (at 77 K) and CO_2 (in the temperature range from 273 to 313 K) on the polymer networks were obtained using the Triflex V4.02 apparatus (Micromeritics Instrument Corporation, Norcross, GA, USA). Before the sorption measurements, a sample was degassed using a Micromeritics SmartVacPrep instrument. This involved gradually heating the sample from room temperature to 353 K and keeping it there for 1 hour, then increasing the temperature to 383 K and degassing for 5 hours. After that, the tube with the sample was filled with nitrogen and cooled back to room temperature. To start the adsorption measurement, the tube with the sample was evacuated at vacuum level 1.3 Pa at 30 °C for 30 minutes. The specific surface area (S_{BET}) was determined using nitrogen adsorption data in the relative pressure range from 0.05 to 0.2 and the Brunauer-Emmett-Teller (BET) method. The micropore volume V_{mi} was determined based on the amount of nitrogen trapped at $p/p_0 = 0.1$. The total pore volume V_{tot} was determined from the amount of nitrogen trapped at $p/p_0 = 0.97$. Finally, to determine the pore size distribution the N2-DFT (Nitrogen Adsorption-Desorption using Density Functional Theory) theoretical method was utilized. To obtain the isosteric heat of CO_2 adsorption, the Clausius-Clapeyron equation was used.[53]

Dynamic water vapour sorption from air (at 297 K) was performed using a DVS Advantage 2 instrument (Surface Measurement Systems Ltd., London, UK). Prior to the adsorption, the polymer network was preheated to 100 °C for 120 min. The adsorption/desorption experiment was performed with a relative humidity (RH) setting of 0 % – 90 % – 0 % – 90 % – 0 % (with intermediate steps of 10 % RH) and a setting of 180 min for each step.

Benzene vapour sorption from air (at room temperature) was studied using a home-made setup consisting of a desiccator containing on its bottom an excess of liquid benzene. In the desiccator, the samples (placed in Petri dishes) were exposed to saturated benzene vapour ($p_{benzene} = 13$ kPa). The amount of benzene adsorbed was determined gravimetrically after 24 hours. Prior to the sorption experiment, the polymer networks were dried for 12 hours at 75 °C.

3. Results and discussion

3.1. Synthesis and characterization

We report a series of hyper-cross-linked porous polyacetylene networks prepared from ring-substituted 1,3-diethynylbenzenes by chain-growth coordination homopolymerization catalysed by [Rh(nbd)acac] complex.[54] The homopolymerizations were performed in either dichloromethane or methanol, the reaction time was mostly three days at 75 ºC. In the course of polymerization, the ethynyl groups of the monomers underwent conversion into rigid conjugated polyacetylene (polyene) chains. Due to the presence of two ethynyl groups per monomer molecule, a dense cross-linking of polyacetylene chains via 1,3-phenylene cross-links occurred during the polymerization. Most polymerizations provided respective networks in quantitative yields.

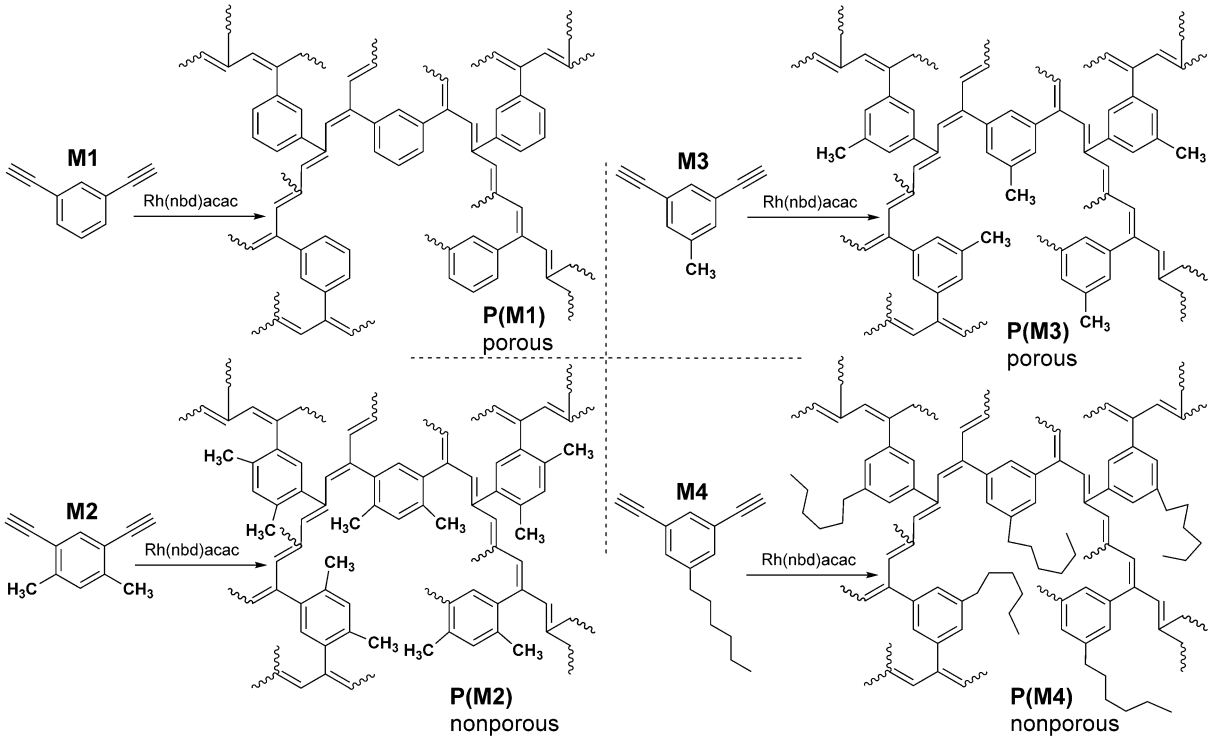

Scheme 1 Preparation of networks from 1,3-diethynylbenzene (M1), 4,6-dimethyl-1,3-diethynylbenzene (M2), 5-methyl-1,3-diethynylbenzene (M3) and 5-*n*-hexyl-1,3-diethynylbenzene (M4).

Table 1 Yield and specific surface area, S_{BET}, micropore volume, V_{mi}, and total pore volume, V_{tot} of networks prepared by homopolymerization of M1, M2, M3, and M4 in CH_2Cl_2 (reaction time three days at 75 ºC).

network code	Y [%]	S_{BET} [m^2/g]	V_{mi} [cm^3/g]	V_{tot} [cm^3/g]
P(M1)	100	1287	0.46	1.98
P(M2)	80	8	not determined	
P(M3)	100	1159	0.40	0.94
P(M4)	100	3	not determined	

Polymerization of 1,3-diethynylbenzene (monomer M1) provided poly(1,3-diethynylbenzene), labelled as P(M1) in quantitative yield (see Scheme 1 and Table 1). The ^{13}C CP/MAS NMR spectrum of P(M1) (Figure 1) showed an intensive broad signal (δ = 120 – 150 ppm) ascribed to the sp^2 hybridized carbon atoms of both benzene rings and polyene main chains. A weak signal at δ = 72-84 ppm corresponded to sp hybridized carbon atoms of unreacted ethynyl groups present in a small amount in P(M1). The low intensity of this signal indicated that most monomeric units of P(M1) were involved in cross-linking through the polymerization transformation of both ethynyl groups of monomer molecules. The textural characterization of P(M1) by N_2 adsorption/desorption at 77 K showed the micro/mesoporous character of this network with the following parameters: Brunauer-Emmett-Teller specific surface area, S_{BET} = 1287 m^2/g, micropore volume, V_{mi} = 0.46 cm^3/g and total pore volume, V_{tot} = 1.98 cm^3/g. The high S_{BET}, V_{mi}, and V_{tot} values reflected the high extent of cross-linking and the rigidity of the segments of P(M1).

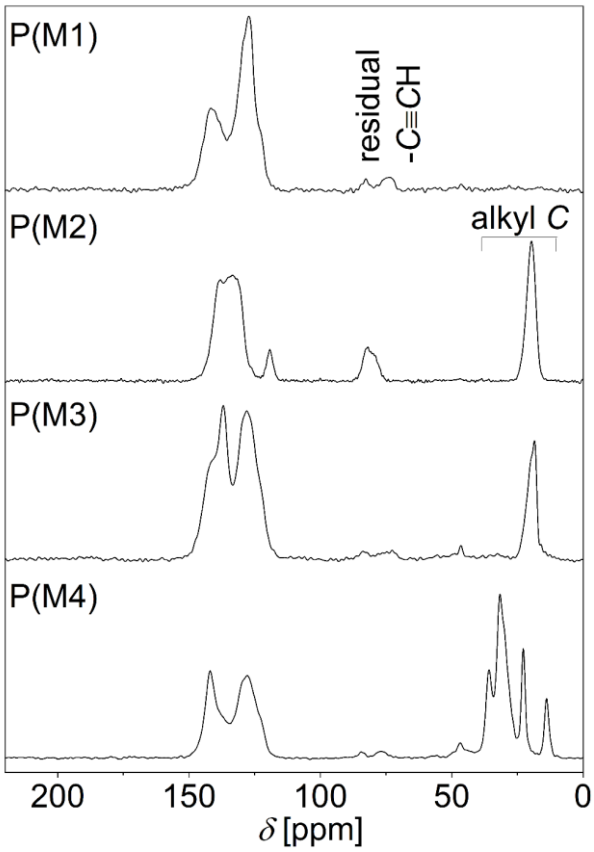

Figure 1 ^{13}C CP/MAS NMR spectra of networks P(M1), P(M2), P(M3) and P(M4).

The 1,3-diethynylbenzene molecule offers various positions for ring substitution. In order to assess the impact of the position and the size of the substituent on the 1,3-diethynylbenzene ring on the polymerizability of the monomer and on the texture of the resulting network, we employed three various alkylated 1,3-diethynylbenzenes as monomers: 4,6-dimethyl-1,3-diethynylbenzene (M2), 5-methyl-1,3-diethynylbenzene (M3) and 5-*n*-hexyl-1,3-diethynylbenzene (M4). Monomer M2 contained two methyl groups in adjacent positions to the ethynyl groups. Monomers M3 and M4 contained one alkyl group of various size in position 5 on the benzene ring. Consequently, these groups were separated from ethynyl groups by one unsubstituted aromatic carbon atom. All monomers provided respective networks P(M1), P(M2), and P(M3) in high yield (Scheme 1, Table 1). The presence of alkyl groups in P(M2), P(M3), and P(M4) was well manifested by signals in the region at δ = 10 - 40 ppm in the ^{13}C CP/MAS NMR spectra of the networks (see Figure 1). The N_2 adsorption/desorption showed that P(M2) was virtually nonporous. Most likely, the methyl groups adjacent to the ethynyl groups in M2 sterically hindered sufficient cross-linking of P(M2) necessary for a porous texture. This was consistent with the finding that the signal of the carbon atoms of the unreacted ethynyl groups was more intense in the ^{13}C CP/MAS NMR spectrum of P(M2) than

in the ^{13}C CP/MAS NMR spectrum of P(M1) (see Figure 1). Unlike P(M2), P(M3) showed a micro/mesoporous texture with high values of S_{BET}, V_{mi}, and V_{tot} (Table 1, Figure S1). These values were close to those obtained for the unsubstituted network P(M1) (see Table 1). The micro/mesoporous texture of P(M3) corresponded well with the high degree of conversion of ethynyl groups and thus also with the high cross-linking efficiency achieved in the polymerization of M3 (see ^{13}C CP/MAS NMR spectrum of P(M3) in Figure 1). Evidently, the substitution of 1,3-diethynylbenzene in position 5 with a (small) methyl group did not negatively affect the cross-linking efficiency and the micro/mesoporosity of the prepared network. A high conversion of ethynyl groups and a high extent of cross-linking were also achieved in the polymerization of M4 (see ^{13}C CP/MAS NMR spectrum of P(M4) in Figure 1). Despite this, the P(M4) network was virtually nonporous. Very likely, the bulky and flexible *n*-hexyl substituents effectively occupied the microporous voids formed in P(M4) thanks to the cross-linking and rigidity of the unsaturated network segments. We, therefore, concluded that for obtaining substituted poly(1,3-diethynylbenzene)s with permanent porosity, ring-substituted 1,3-diethynylbenzenes with not too bulky substituents in position 5, appear as promising monomers.

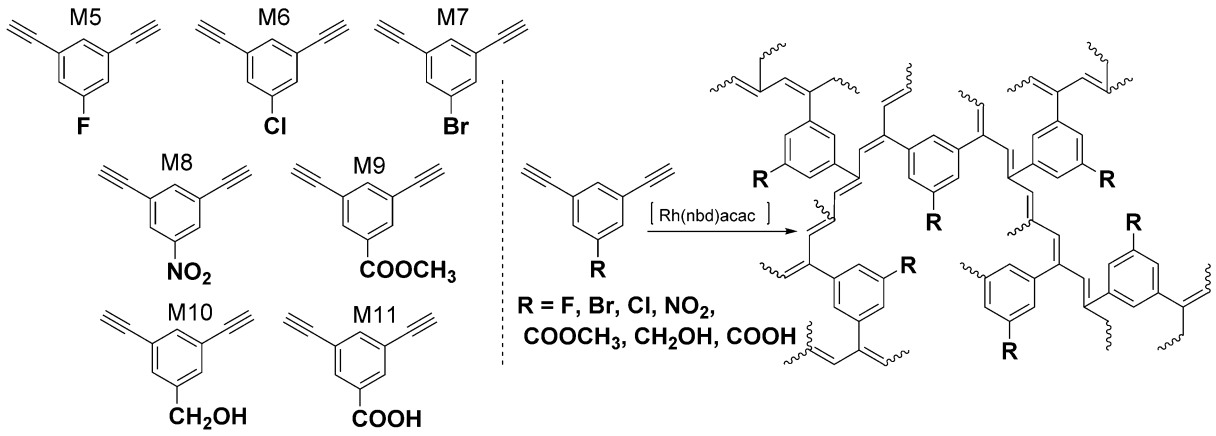

Scheme 2 1,3-Diethynylbenzenes substituted in position 5 and the preparation of porous networks from these monomers.

We selected a series of 1,3-diethynylbenzenes substituted in position 5 by following univalent heteroatom groups: -F (monomer M5), -Cl (M6), -Br (M7), -NO_2 (M8), -$COOCH_3$ (M9), -CH_2OH (M10) and -COOH (M11) (see Scheme 2). Monomers M5-M9 were polymerized in dichloromethane, monomers M10 and M11 were polymerized in methanol due to their poor solubility in dichloromethane. All polymerizations provided respective networks, P(M5)-P(M11), in quantitative yields, which testified to the good compatibility of the used

homopolymerization with diverse functional groups of the monomers. ^{13}C CP/MAS NMR spectra of P(M5)-P(M11) showed only weak signals of carbon atoms of unreacted ethynyl groups that indicated a high extent of cross-linking of all networks (Figure 2). The heteroatom substituents on benzene rings of the networks influenced the shape and broadness of the ^{13}C CP/MAS NMR signals of the aromatic carbon atoms. In particular, the signals of carbon atoms bearing -F and -NO_2 groups were well resolved in the ^{13}C CP/MAS NMR spectra of P(M5) and P(M8) at δ = 162 ppm and δ = 148 ppm, respectively (Figure 2). The signals of carbon atoms of -$COOCH_3$, -CH_2OH, and -COOH substituents were well evident in ^{13}C CP/MAS NMR spectra of P(M9), P(M10), and P(M11). Carbon atoms of hydroxymethyl substituents of P(M10) resonated at δ = 64 ppm. The ^{13}C CP/MAS NMR spectrum of P(M9) contained signals at δ = 51 ppm (-CH_3 groups) and δ = 165 ppm [-C(O)O- groups]. Carbon atoms of carboxyl groups of P(M11) resonated at δ = 167 ppm. The ^{13}C CP/MAS NMR spectrum of P(M11) contained also a weak signal at δ = 51 ppm which indicated that a small fraction of -COOH groups of P(M11) was converted into methyl ester groups due to the esterification with methanol used as a polymerization solvent.

Figure S2 of the Supplementary Material shows the results of the TGA analysis which confirmed the relatively high thermal stability of the prepared networks. The weight loss of all networks was less than 2 % at 200 °C. The t_{95} values (the temperature at which a weight loss of 5 % was detected) are summarized in Table 2. The t_{95} values of around 400 ºC resulted for unsubstituted and halo-substituted networks. The networks with -CH_2OH, -COOH, and -$COOCH_3$ showed t_{95} ranging from 302 to 380 ºC. A lower t_{95} = 268 ºC was found for nitro groups containing P(M8), which corresponded to the generally known lower stability of various nitroaromatic substances.

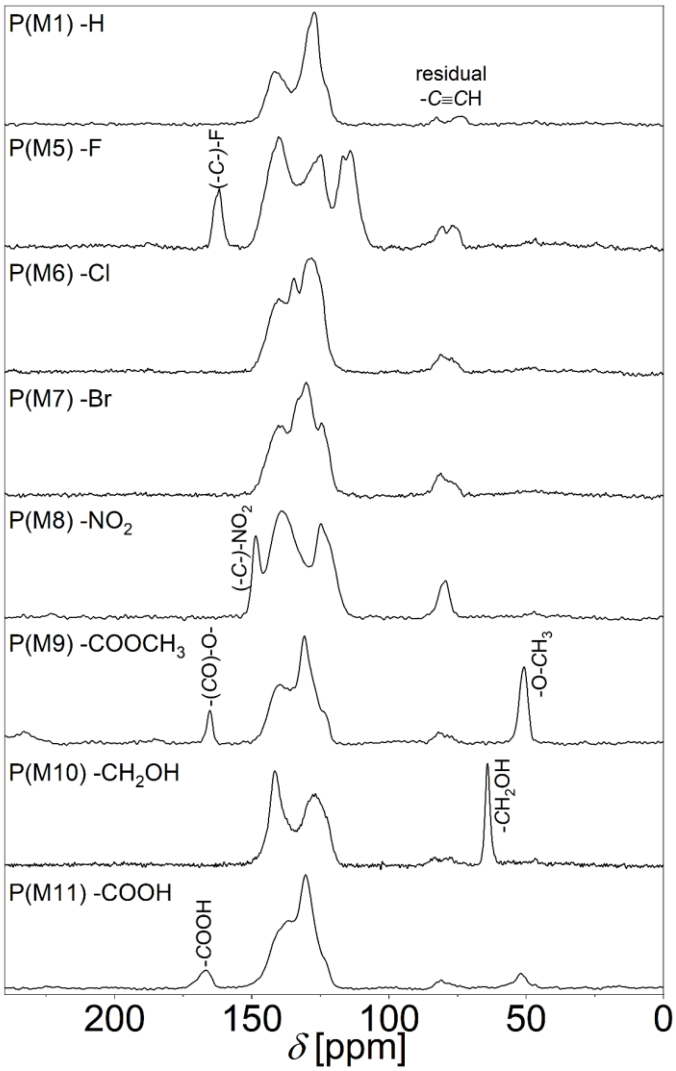

Figure 2 ^{13}C CP/MAS NMR spectra of networks P(M1), P(M5) - P(M11).

Table 2 Specific surface area, S_{BET}, micropore volume, V_{mi}, total pore volume, V_{tot} and mesopore volume, V_{me} of networks prepared by homopolymerization of respective monomers (reaction time three days at 75 ºC). t_{95} stands for the temperature at which a 5 % weight loss was detected by the TGA method.

network code	substituent	S_{BET} [m^2/g]	V_{mi} [cm^3/g]	V_{tot} [cm^3/g]	V_{me} [cm^3/g]	t_{95} [°C]
P(M1)[a)]	-H	1287	0.46	1.98	1.52	384
P(M5)[a)]	-F	1062	0.38	1.29	0.91	417
P(M6)[a)]	-Cl	969	0.35	0.94	0.59	400
P(M7)[a)]	-Br	593	0.22	0.83	0.61	395
P(M8)[a)]	$-NO_2$	488	0.20	0.26	0.06	268
P(M9)[a)]	$-COOCH_3$	626	0.25	0.35	0.10	380
P(M10)[b)]	$-CH_2OH$	450	0.17	0.30	0.13	302
P(M11)[b)]	-COOH	532	0.21	0.34	0.13	326

[a)]prepared in dichloromethane
[b)]prepared in methanol

The N_2 adsorption/desorption at 77 K showed the micro/mesoporous texture of all networks from Table 2 (see Figure 3 for N_2 adsorption/desorption isotherms). The S_{BET} values of halo-substituted networks decreased with increasing size and weight of the halo-substituent from 1062 m^2/g for F-substituted P(M5) to 593 m^2/g for Br-substituted P(M7). The S_{BET} values of the networks with oxygen-containing substituents ranged from 450 to 626 m^2/g. Surprisingly, the value of 626 m^2/g was attained for P(M9) with the most bulky -$COOCH_3$ substituents. The S_{BET} values of P(M10) and P(M11) with less bulky -CH_2OH and -COOH groups were slightly lower. We speculate that the porosity of these networks may have been negatively affected by the hydrogen bonding or other interactions between their polar substituents. The values of V_{mi} of the networks ranged from 0.17 cm^3/g [P(M10)] to 0.38 cm^3/g, [P(M5)].

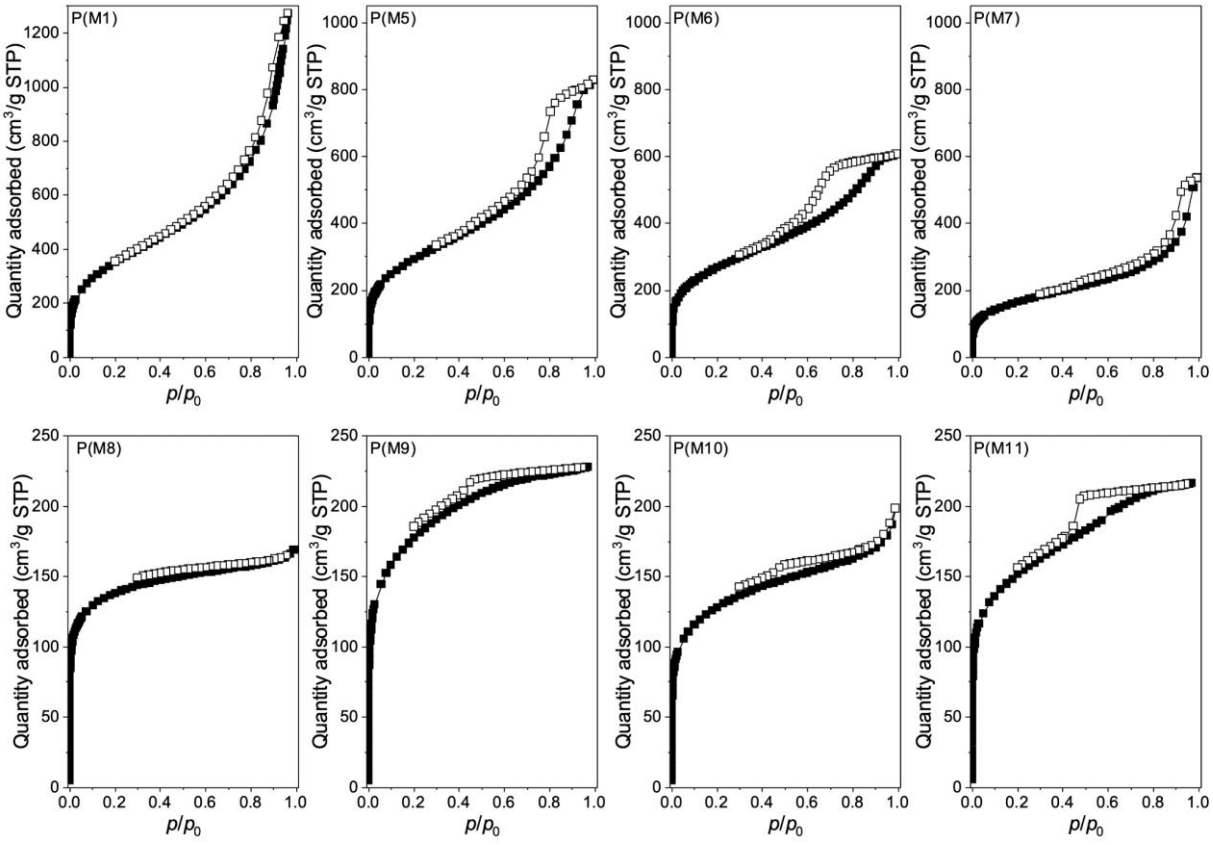

Figure 3 N_2 adsorption (full points) and desorption (empty points) isotherms (77 K) on networks P(M1), P(M5) - P(M11).

The DFT method was used to calculate differential pore size distributions from N_2 adsorption isotherms. Results are shown in Figure 4. All networks from Table 2 contained micropores with a diameter in the interval from 0.6 to 2 nm. In addition to micropores, larger mesopores and/or interparticle void volume were present in all networks. The larger pores in

the networks were responsible for the hysteresis on the adsorption/desorption isotherms of all the networks. The content and size of the pores with a diameter > 2 nm varied considerably in individual networks. The unsubstituted P(M1) and halo-substituted P(M5), P(M6), and P(M7) contained mesopores with a broad distribution of diameters ranging from 2 nm to ca. 20 nm. Networks with oxygen-containing groups, P(M8)-P(M11), contained mesopores with a diameter ranging from 2 to about 5 nm. Table 2 shows the values of mesopore volume, V_{me}, for individual networks determined as the difference between V_{tot} and V_{mi} values. The V_{me} values of the unsubstituted and halo-substituted networks ranged from 0.59 to 1.52 cm^3/g and exceeded the values of V_{mi}, contributing substantially to the total pore volume. In the case of the P(M8)-P(M11) networks the V_{me} values were significantly lower (from 0.06 to 0.13 cm^3/g).

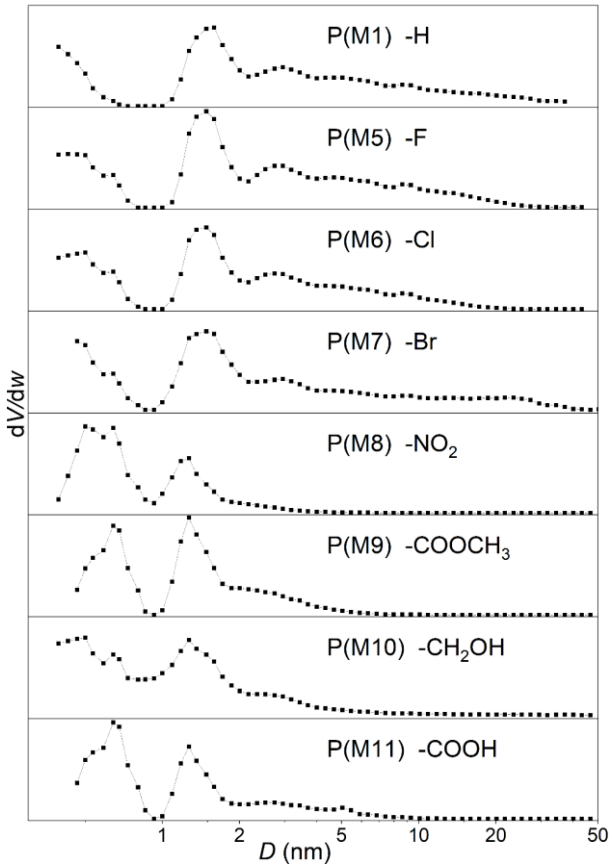

Figure 4 DFT pore size distributions of the networks P(M1), P(M5) - P(M11).

Figure 5 shows the Scanning Electron Microscopy (SEM) images of the networks. We speculate that the networks were composed of small particles formed by a polymer with a microporous texture. As evident from SEM images, the size of these particles as well as the dimensions of the interparticle voids increased depending on the network type in the following order: P(M9) ~ P(M11) < P(M1) ~ P(M5) ~ P(M6) ~ P(M7) < P(M8) ~ P(M10). The networks

P(M8) and P(M10) were formed by relatively large partially aggregated spherical particles of about 1 μm diameter and a large interparticle free volume. In contrast, P(M9) and P(M11) networks showed a compact morphology and minimal detectable interparticle free volume. The particle size was below the detection limit of the used SEM method. P(M1), P(M5) P(M6) and P(M7) networks consisted of small tightly aggregated or (partially) interconnected particles with a diameter of about 50-100 nm. The free voids between particles of P(M1), P(M5) P(M6) and P(M7) had dimensions falling mostly in the mesoporous size range and very likely contributed to the capillary condensation of N_2 observed when measuring N_2 adsorption/desorption isotherms on these networks. The morphological differences revealed by the SEM technique could be related to the different course of phase separation of individual covalently differing networks during their formation and isolation.

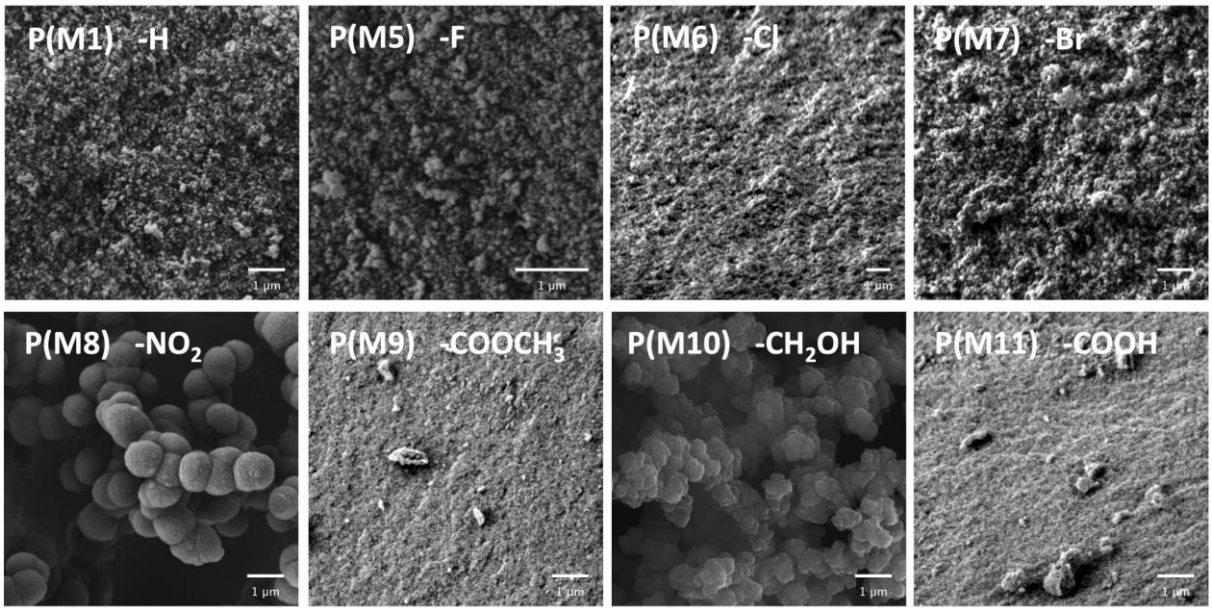

Figure 5 SEM images of P(M1) and P(M5) - P(M11) prepared by homopolymerization of respective monomers (reaction time three days at 75 ºC).

As discussed above, the prepared networks varied in both texture and morphology. Probably the most pronounced difference in this regard was observed between the unsubstituted P(M1) network and P(M8) network decorated with NO_2 groups. We, therefore, studied the formation of P(M1) and P(M8) networks in more detail, focusing on the effect of reaction time on their texture and morphology. In addition to the already discussed P(M1) and P(M8) prepared using a reaction time of 3 days, P(M1) and P(M8) networks were prepared and characterized, which were isolated from the polymerization system after 15 and 60 min of reaction. The results of this study are presented in Table 3 and in Figure 6 and Figure 7.

M1 and M8 provided porous polymer networks in high yield even when shorter reaction times were applied (Table 3). As the polymerization time increased, the values of the textural parameters S_{BET}, $V_{mi,}$ and V_{tot} increased, both in the case of P(M1) and P(M8) type networks. The specific surface areas of the networks formed after 3 days of polymerization were roughly double compared to the specific surface areas of the networks isolated after 15 min of polymerization. For the networks prepared from M8, the character of the pore size distribution did not change with the polymerization time. The networks prepared from M8 always had a predominantly microporous texture with a low contribution of mesopores to the total porosity (V_{me} = 0.05 - 0.07 cm^3/g). Conversely, the pore size distribution depended significantly on the polymerization time in the case of networks prepared from M1 monomer, as can be seen in Figure 6. The P(M1) network isolated after 15 min of reaction was predominantly microporous with a low contribution of mesopores to the total porosity (V_{me} = 0.07 cm^3/g, V_{me}/V_{tot} = 0.23). Extending the reaction time to just 60 min led to a significant increase in the mesopore volume (V_{me} = 0.37 cm^3/g, V_{me}/V_{tot} = 0.51). In the network isolated after 3 days of polymerization, mesopores contributed dominantly to the total porosity (V_{me} = 1.52 cm^3/g, V_{me}/V_{tot} = 0.77), as discussed earlier.

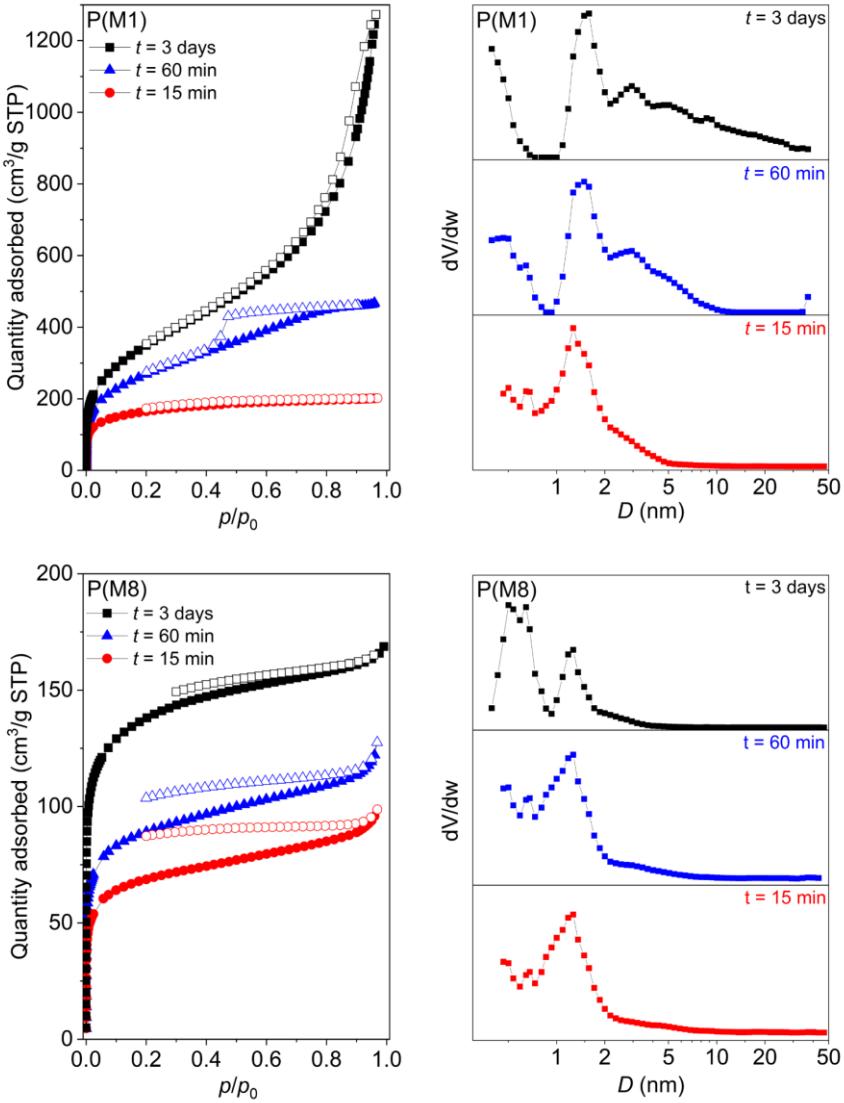

Figure 6 N_2 adsorption (full points) and desorption (empty points) isotherms (77 K) and DFT pore size distributions of P(M1) and P(M8) prepared at various reaction times.

Table 3 Yield and specific surface area, S_{BET}, micropore volume, V_{mi}, total pore volume, V_{tot}, and mesopore volume, V_{me} of networks P(M1) and P(M8) prepared by homopolymerization of M1 and M8 in CH_2Cl_2 at 75 ºC as a function of reaction time.

network code	reaction time	Y [%]	S_{BET} [m^2/g]	V_{mi} [cm^3/g]	V_{tot} [cm^3/g]	V_{me} [cm^3/g]	V_{me}/V_{tot}
P(M1)	15 min	63	582	0.24	0.31	0.07	0.23
	60 min	99	976	0.36	0.73	0.37	0.51
	3 days	100	1287	0.46	1.98	1.52	0.77
P(M8)	15 min	98	238	0.10	0.15	0.05	0.33
	60 min	100	308	0.13	0.20	0.07	0.35
	3 days	100	488	0.20	0.26	0.06	0.23

The polymerization time also affected the morphology of P(M1) and P(M8) (Figure 7). With the reaction time, the size of the particles forming both P(M1) and P(M8) increased slightly. The larger particles observed in the SEM images of the networks isolated after three days of polymerization were probably formed in the later stages of the reactions by linking (fusion) of the initially formed smaller particles. The size of the particles forming the P(M8) networks ranged from roughly 0.3 μm (reaction time 15 min) to 1 μm (reaction time 3 days) and the free space between the particles always had a macroporous character. Regarding P(M1) networks, it was possible to estimate the particle size (50 – 100 nm) only for the network isolated after three days of polymerization. The particles of P(M1) networks isolated after 15 or 60 min were smaller and the used SEM method did not allow for their more accurate characterization. The SEM characteristics and pore size distributions ascertained from N_2 adsorption/desorption isotherms correlated well in the case of P(M1) networks. For the micro/mesoporous P(M1) network isolated after 3 days of reaction, the SEM image showed free interparticle voids of mesoporous dimension (Figure 7), which apparently contributed to the capillary condensation of N_2 observed when measuring the N_2 adsorption/desorption isotherm (Figure 6). On the contrary, in the case of the microporous P(M1) network isolated after 15 min of reaction, in which only a very low contribution of mesopores to the total porosity was demonstrated by N_2 adsorption (V_{me} = 0.07 cm^3/g) (Figure 6), free interparticle voids were not visible in the SEM image (Figure 7).

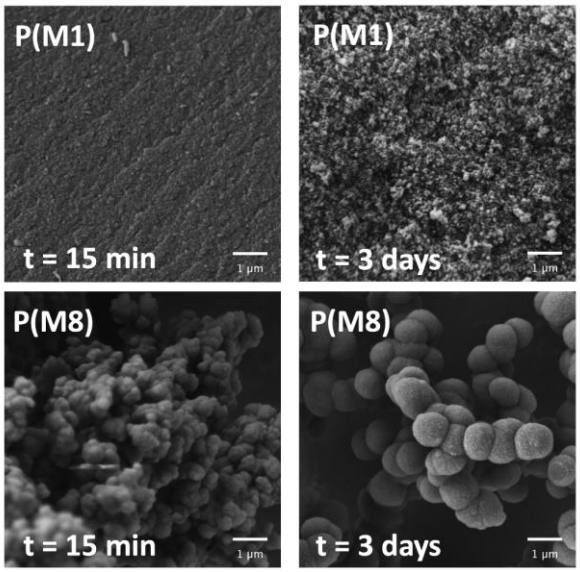

Figure 7 SEM images of P(M1) and P(M8) prepared at various reaction times.

Functionalized networks from Table 2 were prepared by atom-economic chain-growth homopolymerization of monomers bearing in one molecule both (i) two polymerization-active

groups and (ii) the univalent heteroatom functional group. The homopolymerization provided networks with a high content of heteroatom functional groups (7.87 mmol/g of hydrocarbon scaffold). From these points of view, the preparation method described by us differs from the majority of methods used in the literature for the direct synthesis of porous networks functionalized with univalent groups. These methods mostly used the less atom-economic step-growth coupling copolymerizations of pairs of complementary comonomers, one of which carried a univalent functional group, and the other served as a cross-linker.[55] For example, microporous poly(aryleneethynylene) type networks with -NH_2, -NO_2, -OMe, -CF_3, -COOMe, and -OH groups were prepared by step-growth coupling polymerization of substituted dibromoarenes with 1,3,5-triethynylbenzene cross-linker proceeded under HBr elimination (S_{BET} from 247 to 880 m^2/g). Only part of the aromatic segments was decorated with heteroatom groups in these poly(aryleneethynylene) networks while other aromatic segments served as network knots.[56]

3.2. Adsorption properties of poly(1,3-diethynylbenzene) networks

Newly prepared poly(1,3-diethynylbenzene) networks were tested in the physisorption capture of CO_2, vapours of benzene (non-polar adsorptive) and water (polar adsorptive) to evaluate the influence of their functionalization on the efficiency of these processes. All networks from Table 2 were active in reversible CO_2 adsorption. The adsorption capacities (determined at 100 kPa and 273 K), a_{CO2} (in mg/g), and $a_{CO2/S}$ (in $\mu g/m^2$) are given in Table 4, the CO_2 adsorption isotherms (273 K) are depicted in Figure 8. The a_{CO2} values (ranging from 42 to 77 mg/g) were moderate compared to those published for other microporous polymers [57,58] and were most likely governed by both the magnitude of the specific surface area and the character of the functional groups of the networks. The influence of the functionalization on the ability of the networks to capture CO_2 can be discussed based on $a_{CO2/S}$ values, which are related to the surface area (S_{BET}). We found all functionalized networks to show a higher $a_{CO2/S}$ values than the unsubstituted network P(M1) (Table 4). The halo-substituted networks showed a relatively small increase in $a_{CO2/S}$ over $a_{CO2/S}$ of P(M1). However, the $a_{CO2/S}$ values of networks with -CH_2OH, -NO_2, and -COOH groups were three to four times higher than $a_{CO2/S}$ of P(M1). In the research of microporous polymers, much attention is paid to their potential application in the capture and removal of CO_2 the formation of which accompanies a number of technological processes. Microporous polymers with basic groups and building blocks (amino groups, nitrogen-containing heterocycles, and others) are being developed for these purposes. The increased affinity of these polymers towards CO_2 is due to the high energy of

interactions of their basic groups with CO_2 molecules.[58] Our results showed that also non-basic and even slightly acidic functional groups increased the effectiveness of the porous networks in CO_2 adsorption. The increase in effectiveness occurred even though the functional groups of our networks only slightly affected the heat of CO_2 adsorption. The values of the isosteric heat of adsorption (coverage of 0.5 mmol/g) were in the interval from 22 to 24 kJ/mol for P(M1) and halo-substituted networks, and in the interval from 24 to 26 kJ/mol for the networks with $-COOCH_3$, -COOH, $-CH_2OH$ and $-NO_2$ groups (see Supplementary Material, Table S1 and Figure S3-S10). We, therefore, believe that due to the presence of functional groups, segments of our networks became partially polarized, which may have increased the number of sites in the networks suitable for CO_2 capture. It is worth mentioning that linear CO_2 molecules do have zero permanent dipole moment, but the C=O bonds in CO_2 molecules are quite polar due to the difference in electronegativity between oxygen and carbon atoms.

Table 4 Adsorption capacities of the networks: a_{CO2} at 273 K and CO_2 pressure of 100 kPa, a_{H2O} at 297 K and relative humidity of 90 %, $a_{benzene}$ at room temperature and equilibrium pressure of benzene vapour of 13 kPa.

network code	substituent	a_{CO2} [mg/g]	$a_{CO2/S}$ [µg/m^2]	a_{H2O} [mg/g]	$a_{benzene}$ [mg/g]
P(M1)	-H	59	46	65	739
P(M5)	-F	60	56	64	971
P(M6)	-Cl	60	62	56	673
P(M7)	-Br	42	71	25	689
P(M8)	$-NO_2$	75	154	142	235
P(M9)	$-COOCH_3$	62	99	232	280
P(M10)	$-CH_2OH$	77	171	240	175
P(M11)	-COOH	76	143	314	292

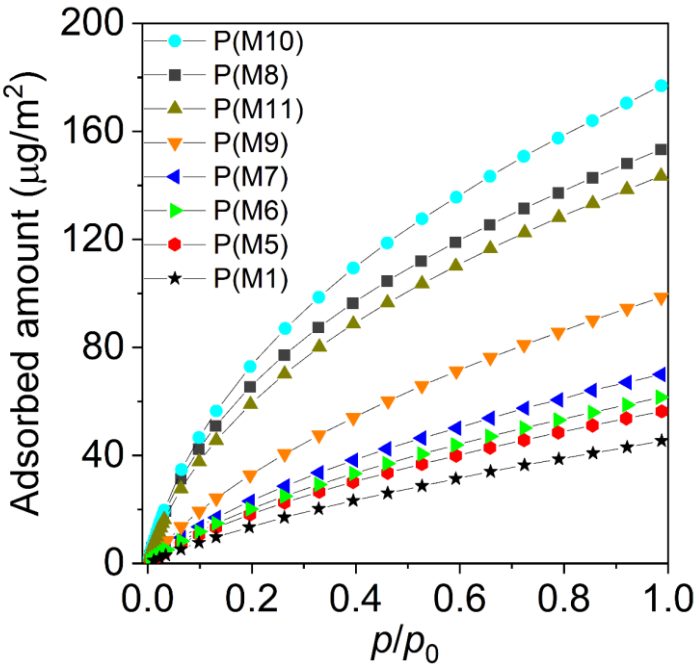

Figure 8 CO_2 adsorption isotherms (273 K) on the networks P(M1), P(M5) - P(M11).

The effectiveness of the networks from Table 2 in the adsorption of benzene vapour was studied at room temperature using a home-made setup (see Experimental Section) in which the networks were exposed to saturated benzene vapour ($p_{benzene}$ = 13 kPa). The adsorption capacities, $a_{benzene}$, were determined gravimetrically after 24 h of exposure (Table 4). Further prolongation of the exposure time did not lead to an increase in $a_{benzene}$ values. Adsorption of benzene vapour was fully reversible, quantitative desorption was always achieved under reduced pressure at room temperature. The unsubstituted network P(M1) and the halo-substituted networks P(M5), P(M6), and P(M7) showed high $a_{benzene}$ values ranging from 673 to 971 mg/g, which corresponded to their hydrophobic character. These networks could be suitable for the removal of non-polar solvent vapours from polluted air. The networks with -NO_2, -COOCH, -CH_2OH, and -COOH groups were less active in benzene physisorption ($a_{benzene}$ values ranged from 175 to 292 mg/g). However, it was interesting that the functionalization with polar groups did not lead to a deeper decrease in $a_{benzene}$ values and that, for example, the P(M11) network containing carboxyl groups still showed a relatively high value of $a_{benzene}$ = 292 mg/g. Therefore, we believe that in the networks with polar oxygen-containing groups, there were non-polarized hydrocarbon segments that interacted with the benzene molecules (most likely by π-π interactions). Due to this, the networks P(M8)-P(M11) partially maintained the efficiency in benzene vapour capture.

The effectiveness of the networks from Table 2 in water vapour capture from the air was studied at 297 K in the relative humidity (RH) range from 0 to 90 % using the gravimetric dynamic vapour sorption (DVS) technique (see Experimental Section). We performed two consecutive cycles of H_2O adsorption/desorption on each network (see adsorption/desorption isotherms in Figure S11 in Supplementary Material). These experiments confirmed that (i) the adsorption and desorption were well reproducible and (ii) H_2O was always completely released from the networks at 297 K simply by reducing the relative humidity to RH = 0 %. The water adsorption capacities, a_{H2O} (297 K, RH = 90 %) significantly depended on the type of functional groups of networks (Table 4). The non-functionalized network P(M1) and the halogenated networks P(M5)-P(M7) were of little interest from the point of view of water vapour capture, as they only showed low values of a_{H2O} = 25 – 65 mg/g. This confirmed the hydrophobic nature of these networks and corresponded well with their high activity in capturing benzene vapour discussed above. Significantly higher and potentially application-interesting values of a_{H2O} (from 232 to 314 mg/g) were obtained for networks with more polar groups -$COOCH_3$, -CH_2OH, and -COOH.[46,59] The adsorption/desorption isotherms of water vapour on these networks [P(M9)-P(M11)] are shown in Figure 9. A common feature of these isotherms was a distinct hysteresis indicating a different mechanism of capture and release of H_2O at higher RH values. Most likely two phenomena contributed to the capture of water vapour on P(M9)-P(M11): (i) adsorption of H_2O on the surface of the network pores occurring from the onset of the experiment (i.e., from low RH values) and (ii) capillary condensation of H_2O in larger pores, which significantly contributed to H_2O capture at RH > 40 %. The surface water adsorption on P(M9)-P(M11) was most likely supported by dipole-dipole interactions or weak hydrogen bonds realized between the functional groups of the networks and the water molecules. However, the energy of these interactions could not be very high because (as already discussed) the quantitative desorption of water from the networks did not require an increase in temperature. Water molecules adsorbed on the surface of the networks at lower RH values were crucial as primary condensation centres ensuring high efficiency of water capture by the capillary condensation mechanism at higher RH values. The mere presence of larger pores in networks was not sufficient for effective capillary condensation of water. The non-functionalized P(M1) showed a high volume of larger pores (Table 2). However, these pores were not effectively involved in the capillary condensation of water vapour, undoubtedly because their surface was not sufficiently covered by water molecules adsorptively trapped at low RH. As a result, the a_{H2O} value achieved on the highly porous but non-functionalized, P(M1) was only 65 mg/g.

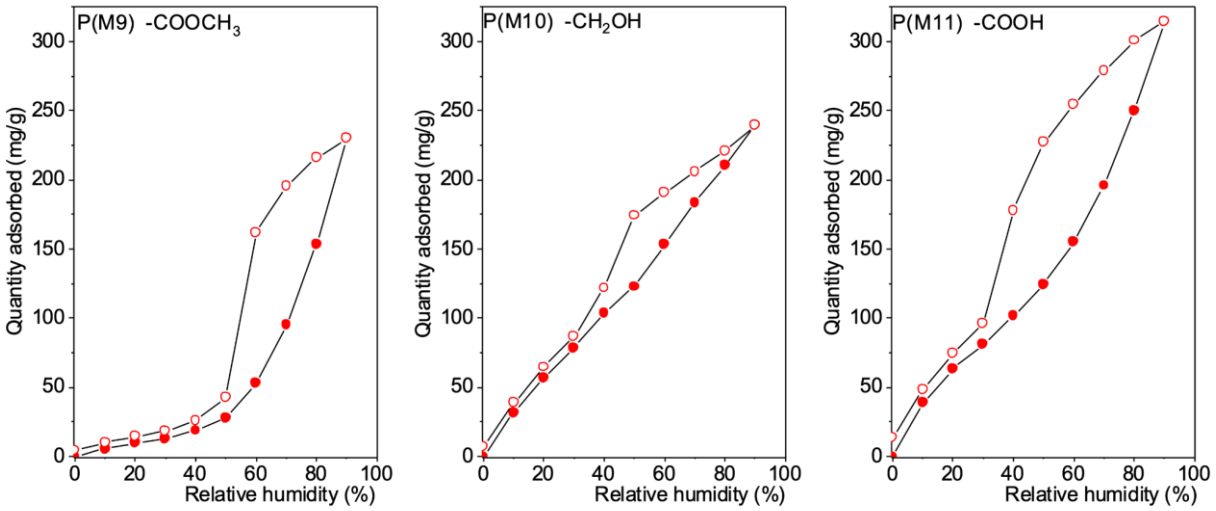

Figure 9 Water adsorption (full points) and desorption (empty points) isotherms (297 K) on P(M9), P(M10) and P(M11).

4. Conclusion

The preparation of functionalized hyper-cross-linked porous polyacetylene networks by one-step chain-growth coordination homopolymerization was described. Substituted 1,3-diethynylbenzenes were used as monomers, which simultaneously ensured both functionalization and hyper-cross-linking of the resulting products. By this atom-economic method, a series of networks with a high content (7.87 mmol/g) of the following univalent functional groups was prepared: -F, -Cl, -Br, -NO_2, -$COOCH_3$, -CH_2OH, and -COOH. The networks showed permanent micro/mesoporosity and high specific surface area (from 450 to 1062 m^2/g). The contribution of mesopores to the total pore volume depended on the character of the functional groups and ranged from 30 % for predominantly microporous networks with NO_2, $COOCH_3$, CH_2OH and COOH groups to 70 % for texturally hierarchical halo-substituted networks. The different nature of the pore size distribution and morphology of individual networks probably reflected the different course of phase separation of the networks during polymerization. The prepared networks were active in the reversible physisorption of CO_2, water vapour, and benzene vapour, while the capture of these adsorptives was controlled by the type of functional groups. CO_2 capture was positively influenced especially by oxygen-containing groups of networks. Halogenated networks showed high benzene vapour capture capacity (up to 971 mg/g) and could be of application interest for the sorption removal of non-polar solvent vapours from the air. Networks with oxygen-containing groups, on the other hand, were effective in capturing water vapour from the air (capture capacity of up to 314 mg/g at room temperature).

Acknowledgement

The authors gratefully acknowledge the financial support from the Czech Science Foundation (Project No. 21-02183S and Project No. 20-01233S) and the Science Foundation of Charles University (Project No. 193223).

Data availability

Data will be made available on request.

Reference

[1] H. Shirakawa, E.J. Louis, A.G. MacDiarmid, C.K. Chiang, A.J. Heeger, Synthesis of electrically conducting organic polymers: halogen derivatives of polyacetylene, J. Chem. Soc., Chem. Commun. (1977) 578–580. https://doi.org/10.1039/C39770000578.

[2] J.W.Y. Lam, Y. Dong, C.C.W. Law, Y. Dong, K.K.L. Cheuk, L.M. Lai, Z. Li, J. Sun, H. Chen, Q. Zheng, H.S. Kwok, M. Wang, X. Feng, J. Shen, B.Z. Tang, Functional disubstituted polyacetylenes and soluble cross-linked polyenes: effects of pendant groups or side chains on liquid crystallinity and light emission of poly(1-phenyl-1-undecyne)s, Macromolecules 38 (2005) 3290–3300. https://doi.org/10.1021/ma048076t.

[3] T. Masuda, Substituted polyacetylenes: synthesis, properties, and functions, Polym. Rev. 57 (2017) 1–14. https://doi.org/10.1080/15583724.2016.1170701.

[4] J. Sedláček, H. Balcar, Substituted polyacetylenes prepared with Rh catalysts: from linear to network-type conjugated polymers, Polym. Rev. 57 (2017) 31–51. https://doi.org/10.1080/15583724.2016.1144207.

[5] F. Freire, E. Quiñoá, R. Riguera, Supramolecular assemblies from poly(phenylacetylene)s, Chem. Rev. 116 (2016) 1242–1271. https://doi.org/10.1021/acs.chemrev.5b00280.

[6] F. Yang, J. Zhang, Q. Zang, T. Shen, J. Ni, H. Zhang, J.Z. Sun, B.Z. Tang, Poly(1-halogen-2-phenylacetylenes) containing tetraphenylethene units: polymer synthesis, unique emission behaviours and application in explosive detection, Mater. Chem. Front. 6 (2022) 368–378. https://doi.org/10.1039/D1QM01490K.

[7] Y. Qiu, Y. Zhang, Q. Jiang, H. Wang, Y. Liao, H. Zhou, X. Xie, Highly specific and sensitive naked-eye fluoride ion recognition via unzipping a helical poly(phenylacetylene), Macromolecules 55 (2022) 9057–9065. https://doi.org/10.1021/acs.macromol.2c01717.

[8] R. Sivkova, O. Trhlíková, J. Zedník, J. Sedláček, Copolymerization of N-(prop-1-yne-3-yl)-4-(piperidine-1-yl)-1,8-naphthalimide with arylacetylenes into fluorescent polyacetylene-type conjugated polymers, Macromol. Chem. Phys. 216 (2015) 2115–2128. https://doi.org/10.1002/macp.201500240.

[9] B.Z. Tang, X. Kong, X. Wan, H. Peng, W.Y. Lam, X.-D. Feng, H.S. Kwok, Liquid crystalline polyacetylenes: synthesis and properties of poly{n-[((4‘-cyano-4-biphenylyl)oxy)carbonyl]-1-alkynes}, Macromolecules 31 (1998) 2419–2432. https://doi.org/10.1021/ma971672l.

[10] Z.-Q. Yu, T.-T. Li, Z. Zhang, J.-H. Liu, W.Z. Yuan, J.W.Y. Lam, S. Yang, E.-Q. Chen, B.Z. Tang, Phase behaviors of side-chain liquid crystalline polyacetylenes with different

length of spacer: Where will the decoupling effect appear?, Macromolecules 48 (2015) 2886–2893. https://doi.org/10.1021/acs.macromol.5b00692.

[11] K. Komaba, M. Otaki, R. Kumai, S. Nimori, H. Goto, Liquid crystal photo-cross-linking phenomenon: synthesis of disubstituted polyacetylenes and emission from liquid crystal, J. Mater. Sci. 58 (2023) 3837–3850. https://doi.org/10.1007/s10853-023-08192-1.

[12] B. Fernández, R. Rodríguez, E. Quiñoá, R. Riguera, F. Freire, Decoding the ECD spectra of poly(phenylacetylene)s: structural significance, ACS Omega 4 (2019) 5233–5240. https://doi.org/10.1021/acsomega.9b00122.

[13] B. Zhao, J. Deng, Emulsion polymerization of acetylenics for constructing optically active helical polymer nanoparticles, Polym. Rev. 57 (2017) 119–137. https://doi.org/10.1080/15583724.2015.1136642.

[14] M. Núñez-Martínez, S. Arias, J. Bergueiro, E. Quiñoá, R. Riguera, F. Freire, The role of polymer–aunp interaction in the stimuli-response properties of PPA–AuNP nanocomposites, Macromol. Rapid. Commun. 43 (2022) 2100616. https://doi.org/10.1002/marc.202100616.

[15] T. Masuda, E. Isobe, T. Higashimura, K. Takada, Poly[1-(trimethylsilyl)-1-propyne]: a new high polymer synthesized with transition-metal catalysts and characterized by extremely high gas permeability, J. Am. Chem. Soc. 105 (1983) 7473–7474. https://doi.org/10.1021/ja00363a061.

[16] Y. Yampolskii, A current position of polyacetylenes among other highly permeable membrane materials, Polym. Rev. 57 (2017) 200–212. https://doi.org/10.1080/15583724.2015.1127960.

[17] M. Chen, G. Hu, T. Shen, H. Zhang, J.Z. Sun, B.Z. Tang, Applications of polyacetylene derivatives in gas and liquid separation, Molecules 28 (2023) 2748. https://doi.org/10.3390/molecules28062748.

[18] W.-E. Lee, D.-C. Han, D.-H. Han, H.-J. Choi, T. Sakaguchi, C.-L. Lee, G. Kwak, Remarkable change in fluorescence emission of poly(diphenylacetylene) film via in situ desilylation reaction: correlation with variations in microporous structure, chain conformation, and lamellar layer distance, Macromol. Rapid. Commun. 32 (2011) 1047–1051. https://doi.org/10.1002/marc.201100073.

[19] Y. Wang, B.S. Ghanem, Z. Ali, K. Hazazi, Y. Han, I. Pinnau, Recent progress on polymers of intrinsic microporosity and thermally modified analogue materials for membrane-based fluid separations, Small Struct. 2 (2021) 2100049. https://doi.org/10.1002/sstr.202100049.

[20] N.B. McKeown, Polymers of Intrinsic Microporosity (PIMs), Polymer (Guildf) 202 (2020) 122736. https://doi.org/10.1016/j.polymer.2020.122736.

[21] Y.-G. Choi, G. Kwak, Viscosity measurement of silicone oils based on diffusion rates in polydiphenylacetylene films, Eur. Polym. J. 110 (2019) 307–312. https://doi.org/10.1016/j.eurpolymj.2018.11.044.

[22] J. Svoboda, M. Bláha, J. Sedláček, J. Vohlídal, H. Balcar, I. Mav-Golež, M. Zigon, New approaches to the synthesis of pure conjugated polymers, Acta Chim. Slov. 53 (2006) 407–416.

[23] Z. Duchoslavová, R. Sivkova, V. Hanková, J. Sedláček, J. Svoboda, J. Vohlídal, J. Zedník, Synthesis and spectral properties of novel poly(disubstituted acetylene)s, Macromol. Chem. Phys. 212 (2011) 1802–1814. https://doi.org/10.1002/macp.201100160.

[24] H. Balcar, J. Sedláček, J. Zedník, V. Blechta, P. Kubát, J. Vohlídal, Polymerization of isomeric N-(4-substituted benzylidene)-4-ethynylanilines and 4-substituted N-(4-ethynylbenzylidene)anilines by transition metal catalysts: preparation and characterization of new substituted polyacetylenes with aromatic Schiff base type pendant groups, Polymer (Guildf) 42 (2001) 6709–6721. https://doi.org/10.1016/S0032-3861(01)00148-3.

[25] M. Goto, Y. Miyagi, M. Minami, F. Sanda, Synthesis and crosslinking reaction of polyacetylenes substituted with benzoxazine rings: Thermally highly stable benzoxazine resins, J. Polym. Sci. A Polym. Chem. 56 (2018) 1884–1893. https://doi.org/10.1002/pola.29076.

[26] O. Lavastre, S. Cabioch, P.H. Dixneuf, J. Sedlacek, J. Vohlídal, New route to conjugated polymer networks: synthesis of poly(4-ethynyl)phenylacetylene and its transformation into a conjugated network, Macromolecules 32 (1999) 4477–4481. https://doi.org/10.1021/ma990024u.

[27] C. Zhang, Y. Zhang, H. Zhang, Y. Hu, X. Zhang, T. Masuda, Synthesis and ion responsiveness of optically active polyacetylenes containing salicylidene Schiff-base moieties, React. Funct. Polym. 87 (2015) 46–52. https://doi.org/10.1016/j.reactfunctpolym.2015.01.003.

[28] Y. Inoue, T. Ishida, N. Sano, T. Yajima, H. Sogawa, F. Sanda, Platinum-mediated reversible cross-linking/decross-linking of polyacetylenes substituted with phosphine ligands: catalytic activity for hydrosilylation, Macromolecules 55 (2022) 5711–5722. https://doi.org/10.1021/acs.macromol.2c00748.

[29] T. Sakaguchi, J. Minami, T. Hashimoto, Synthesis of gas-permeable membranes via crosslinking of poly(diphenylacetylene)s by cationic polymerization and radical coupling of side chains, Polymer (Guildf) 228 (2021) 123893. https://doi.org/10.1016/j.polymer.2021.123893.

[30] V.M. Misin, I.E. Maltseva, M.E. Kazakov, V.A. Volkov, The polymers of diethynylarenes - is selective polymerization at one acetylene bond possible? A review, Polymers (Basel) 15 (2023) 1105. https://doi.org/10.3390/polym15051105.

[31] H. Goto, H.Q. Zhang, E. Yashima, Chiral stimuli-responsive gels: helicity induction in poly(phenylacetylene) gels bearing a carboxyl group with chiral amines, J. Am. Chem. Soc. 125 (2003) 2516–2523. https://doi.org/10.1021/ja029036c.

[32] V.M. Misin, I.E. Maltseva, A.A. Maltsev, Synthesis of homo- and copolymers of para-diethynylbenzene in the presence of the cobalt carbonyl - diphenylbutadiyne complex, ChemistrySelect 7 (2022) e202103612. https://doi.org/10.1002/slct.202103612.

[33] Z. Dong, Z. Ye, Synthesis of hyperbranched poly(phenylacetylene)s containing pendant alkyne groups by one-pot Pd-catalyzed copolymerization of phenylacetylene with diynes, Macromolecules 45 (2012) 5020–5031. https://doi.org/10.1021/ma3007569.

[34] V. Hanková, E. Slováková, J. Zedník, J. Vohlídal, R. Sivkova, H. Balcar, A. Zukal, J. Brus, J. Sedláček, Polyacetylene-type networks prepared by coordination polymerization of diethynylarenes: new type of microporous organic polymers, Macromol. Rapid. Commun. 33 (2012) 158–163. https://doi.org/10.1002/marc.201100599.

[35] E. Slováková, A. Zukal, J. Brus, H. Balcar, L. Brabec, D. Bondarev, J. Sedláček, Transition-metal-catalyzed chain-growth polymerization of 1,4-diethynylbenzene into microporous crosslinked poly(phenylacetylene)s: the effect of reaction conditions, Macromol. Chem. Phys. 215 (2014) 1855–1869. https://doi.org/10.1002/macp.201400198.

[36] L. Sekerová, M. Lhotka, E. Vyskočilová, T. Faukner, E. Slováková, J. Brus, L. Červený, J. Sedláček, Hyper-cross-linked polyacetylene-type microporous networks decorated with terminal ethynyl groups as heterogeneous acid catalysts for acetalization and esterification reactions, Chem. Eur. J. 24 (2018) 14742–14749. https://doi.org/10.1002/chem.201802432.

[37] L. Tan, B. Tan, Hypercrosslinked porous polymer materials: design, synthesis, and applications, Chem. Soc. Rev. 46 (2017) 3322–3356. https://doi.org/10.1039/C6CS00851H.

[38] A. Giri, S. Biswas, M.D.W. Hussain, T.K. Dutta, A. Patra, Nanostructured hypercrosslinked porous organic polymers: morphological evolution and rapid separation of polar organic micropollutants, ACS Appl. Mater. Interfaces 14 (2022) 7369–7381. https://doi.org/10.1021/acsami.1c24393.

[39] S. Bhunia, B. Banerjee, A. Bhaumik, A new hypercrosslinked supermicroporous polymer, with scope for sulfonation, and its catalytic potential for the efficient synthesis of biodiesel at room temperature, Chem. Commun. 51 (2015) 5020–5023. https://doi.org/10.1039/C4CC09872B.

[40] R. Castaldo, G. Gentile, M. Avella, C. Carfagna, V. Ambrogi, Microporous hyper-crosslinked polystyrenes and nanocomposites with high adsorption properties: A Review, Polymers (Basel) 9 (2017) 651. https://doi.org/10.3390/polym9120651.

[41] D. Taylor, S.J. Dalgarno, Z. Xu, F. Vilela, Conjugated porous polymers: incredibly versatile materials with far-reaching applications, Chem. Soc. Rev. 49 (2020) 3981–4042. https://doi.org/10.1039/C9CS00315K.

[42] D. Bondarev, R. Sivkova, P. Šuly, M. Polášková, O. Krejčí, R. Křikavová, Z. Trávníček, A. Zukal, M. Kubů, J. Sedláček, Microporous conjugated polymers via homopolymerization of 2,5-diethynylthiophene, Eur. Polym. J. 92 (2017) 213–219. https://doi.org/10.1016/j.eurpolymj.2017.04.042.

[43] A. Hašková, B. Bashta, Š. Titlová, J. Brus, A. Vagenknechtová, E. Vyskočilová, J. Sedláček, Microporous hyper-cross-linked polymers with high and tuneable content of pyridine units: synthesis and application for reversible sorption of water and carbon dioxide, Macromol. Rapid. Commun. 42 (2021) 2100209. https://doi.org/10.1002/marc.202100209.

[44] B. Bashta, A. Hašková, T. Faukner, M.A. Elsawy, D. Šorm, J. Brus, J. Sedláček, Microporous hyper-cross-linked polyacetylene networks: Covalent structure and texture modification by reversible Schiff-base chemistry, Eur. Polym. J. 136 (2020) 109914. https://doi.org/10.1016/j.eurpolymj.2020.109914.

[45] S. Stahlová, E. Slováková, P. Vaňkátová, A. Zukal, M. Kubů, J. Brus, D. Bondarev, R. Moučka, J. Sedláček, Chain-growth copolymerization of functionalized ethynylarenes with 1,4-diethynylbenzene and 4,4′-diethynylbiphenyl into conjugated porous networks, Eur. Polym. J. 67 (2015) 252–263. https://doi.org/10.1016/j.eurpolymj.2015.03.070.

[46] L. Havelková, B. Bashta, A. Hašková, A. Vagenknechtová, E. Vyskočilová, J. Brus, J. Sedláček, Combining polymerization and templating toward hyper-cross-linked poly(propargyl aldehyde)s and poly(propargyl alcohol)s for reversible H2O and CO2 capture and construction of porous chiral networks, Polymers (Basel) 15 (2023) 743. https://doi.org/10.3390/polym15030743.

[47] D. Šorm, B. Bashta, J. Blahut, I. Císařová, L. Dolejšová Sekerová, E. Vyskočilová, J. Sedláček, Porous polymer networks cross-linked by novel copper Schiff base complex: From synthesis to catalytic activity, Eur. Polym. J. 184 (2023) 111772. https://doi.org/10.1016/j.eurpolymj.2022.111772.

[48] L. Sekerová, P. Březinová, T.T. Do, E. Vyskočilová, J. Krupka, L. Červený, L. Havelková, B. Bashta, J. Sedláček, Sulfonated hyper-cross-linked porous polyacetylene networks as versatile heterogeneous acid catalysts, ChemCatChem 12 (2020) 1075–1084. https://doi.org/10.1002/cctc.201901815.

[49] E. Slováková, M. Ješelnik, E. Žagar, J. Zedník, J. Sedláček, S. Kovačič, Chain-growth insertion polymerization of 1,3-diethynylbenzene high internal phase emulsions into reactive π-conjugated foams, Macromolecules 47 (2014) 4864–4869. https://doi.org/10.1021/ma501142d.

[50] M.-A. MacDonald, R.J. Puddephatt, G.P.A. Yap, Angular arenediethynyl complexes of gold(I), Organometallics 19 (2000) 2194–2199. https://doi.org/10.1021/om0000461.

[51] L. Shu, M. Mayor, Shape-persistent macrocycle with a self-complementary recognition pattern based on diacetylene-linked alternating hexylbenzene and perfluorobenzene rings, Chem. Commun. (2006) 4134–4136. https://doi.org/10.1039/B609004D.

[52] J. Brus, Heating of samples induced by fast magic-angle spinning, Solid State Nucl. Magn. Reson. 16 (2000) 151–160. https://doi.org/10.1016/S0926-2040(00)00061-8.

[53] A. Zukal, E. Slováková, H. Balcar, J. Sedláček, Polycyclotrimers of 1,4-diethynylbenzene, 2,6-diethynylnaphthalene, and 2,6-diethynylanthracene: preparation and gas adsorption properties, Macromol. Chem. Phys. 214 (2013) 2016–2026. https://doi.org/10.1002/macp.201300317.

[54] O. Trhlíková, J. Zedník, H. Balcar, J. Brus, J. Sedláček, [Rh(cycloolefin)(acac)] complexes as catalysts of polymerization of aryl- and alkylacetylenes: Influence of cycloolefin ligand and reaction conditions, J. Mol. Catal. A Chem. 378 (2013) 57–66. https://doi.org/10.1016/j.molcata.2013.05.022.

[55] J.-S.M. Lee, A.I. Cooper, Advances in conjugated microporous polymers, Chem. Rev. 120 (2020) 2171–2214. https://doi.org/10.1021/acs.chemrev.9b00399.

[56] R. Dawson, A. Laybourn, R. Clowes, Y.Z. Khimyak, D.J. Adams, A.I. Cooper, Functionalized conjugated microporous polymers, Macromolecules 42 (2009) 8809–8816. https://doi.org/10.1021/ma901801s.

[57] L. Shao, M. Liu, Y. Sang, J. Huang, One-pot synthesis of melamine-based porous polyamides for CO2 capture, Microporous and Mesoporous Mater. 285 (2019) 105–111. https://doi.org/10.1016/j.micromeso.2019.05.005.

[58] R. Dawson, A.I. Cooper, D.J. Adams, Chemical functionalization strategies for carbon dioxide capture in microporous organic polymers, Polym. Int. 62 (2013) 345–352. https://doi.org/10.1002/pi.4407.

[59] Y. Byun, S.H. Je, S.N. Talapaneni, A. Coskun, Advances in porous organic polymers for efficient water capture, Chem. Eur. J. 25 (2019) 10262–10283. https://doi.org/10.1002/chem.201900940.

Supplementary Material

Functionalized hyper-cross-linked porous homopolymers of ring-substituted 1,3-diethynylbenzenes and their physisorption activity

Lucie Havelková[1,*], *Bogdana Bashta*[1], *Michaela Vaňková*[1], *Jiří Zedník*[1], *Jiří Brus*[2], *Alice Vagenknechtová*[3], *Jan Sedláček*[1,*]

1 Department of Physical and Macromolecular Chemistry, Faculty of Science, Charles University, Hlavova 2030, Prague 2, 128 43, Czech Republic

2 Institute of Macromolecular Chemistry, Czech Academy of Sciences, Heyrovský Sq. 2, Prague 6, 162 00, Czech Republic

3 Department of Gaseous and Solid Fuels and Air Protection, University of Chemistry and Technology in Prague, Technická 5, Prague 6, 166 28 Czech Republic

* Correspondence: lucie.havelkova@natur.cuni.cz, jan.sedlacek@natur.cuni.cz

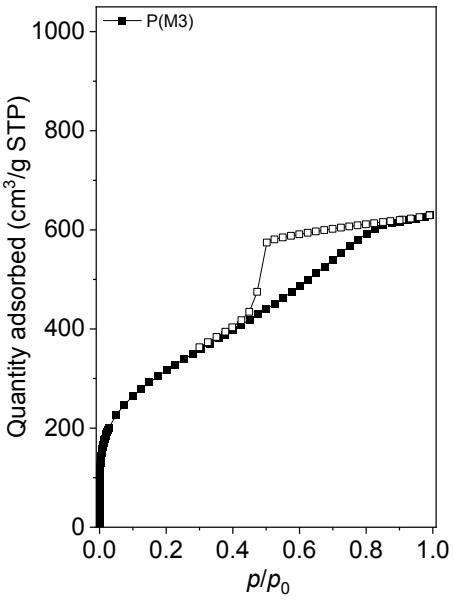

Figure S1. N_2 adsorption (full points) and desorption (empty points) isotherms (77 K) on P(M3).

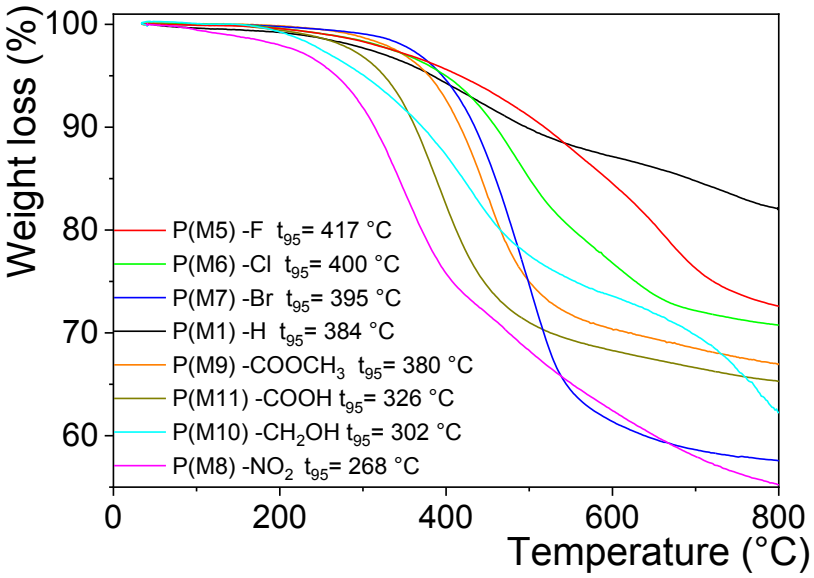

Figure S2. Thermogravimetric analysis of the prepared networks.

Table S1 Isosteric heats of the CO_2 adsorption on the networks, Q_{st}, at the coverage of 0.5 mmol(CO_2)/g.

Network code	Substituent	Q_{st} [kJ/mol]
P(M1)[a)]	-H	22.3
P(M5)[a)]	-F	23.7
P(M6)[a)]	-Cl	23.7
P(M7)[a)]	-Br	22.3
P(M8)[a)]	$-NO_2$	26.4
P(M9)[a)]	$-COOCH_3$	23.6
P(M10)[b)]	$-CH_2OH$	24.4
P(M11)[b)]	-COOH	24.4

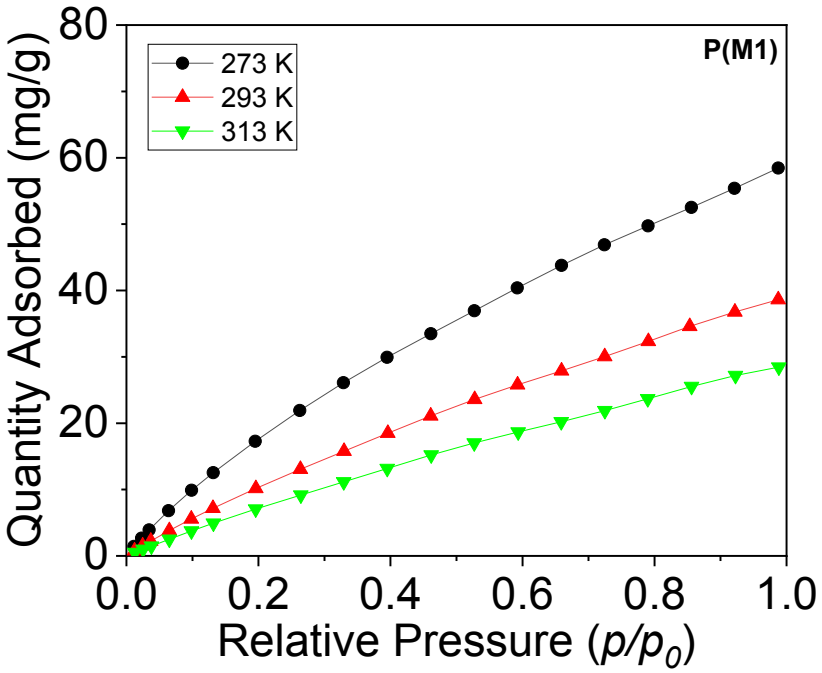

Figure S3 CO_2 adsorption isotherms on P(M1) at 273, 293, and 313 K.

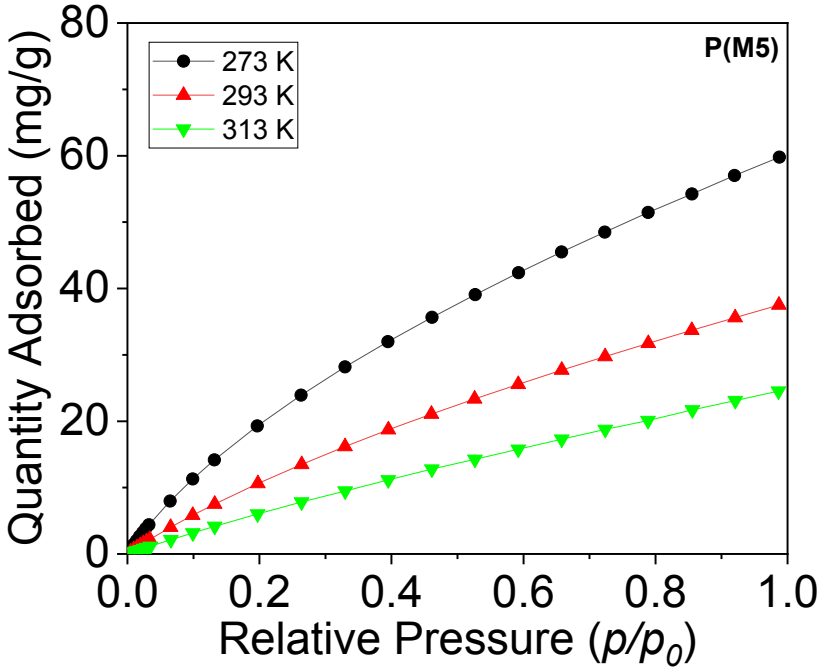

Figure S4 CO_2 adsorption isotherms on P(M5) at 273, 293, and 313 K.

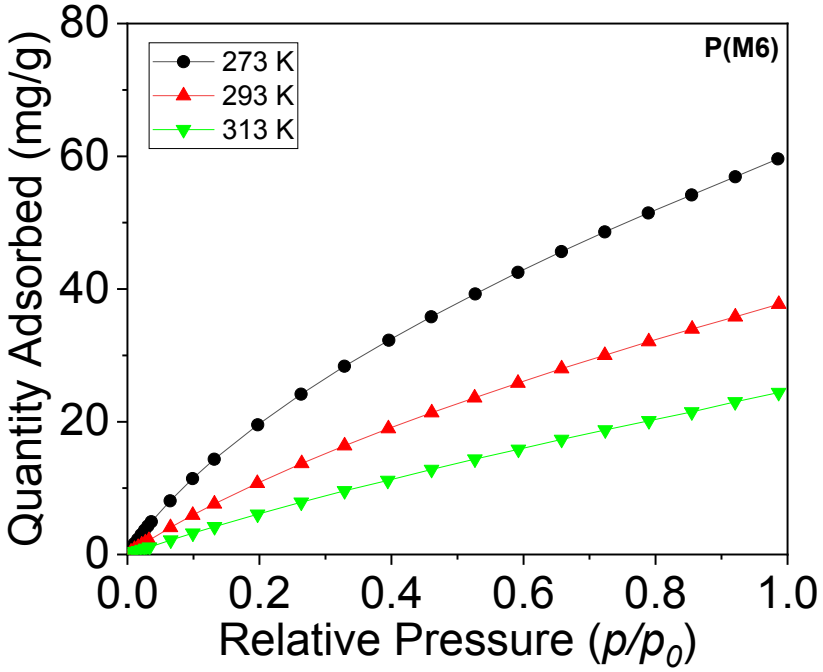

Figure S5 CO_2 adsorption isotherms on P(M6) at 273, 293, and 313 K.

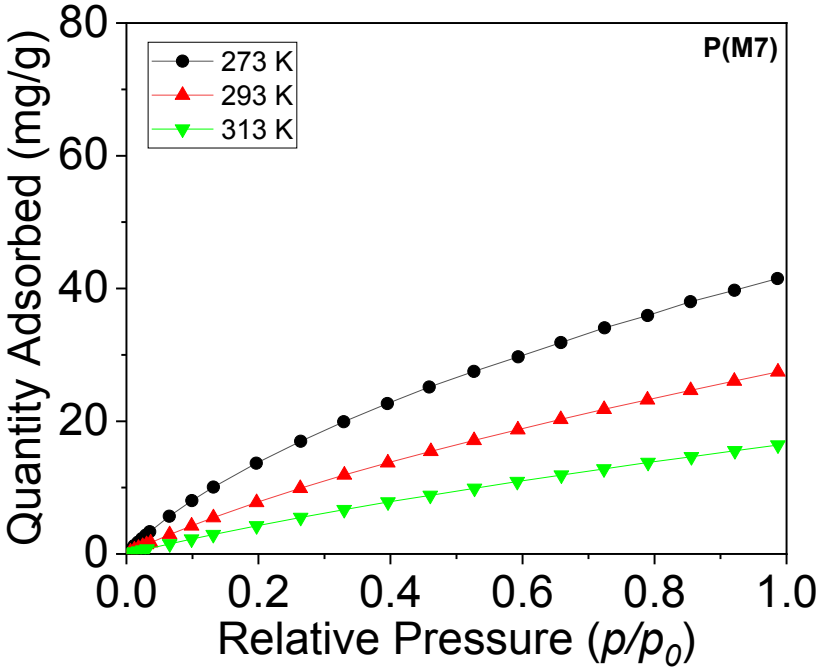

Figure S6 CO_2 adsorption isotherms on P(M7) at 273, 293, and 313 K.

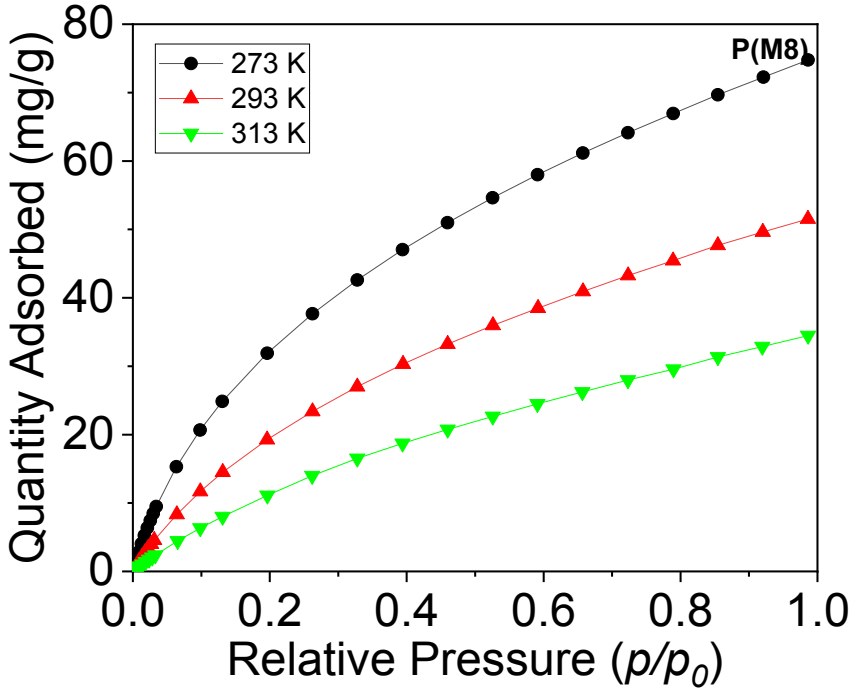

Figure S7 CO_2 adsorption isotherms on P(M8) at 273, 293, and 313 K.

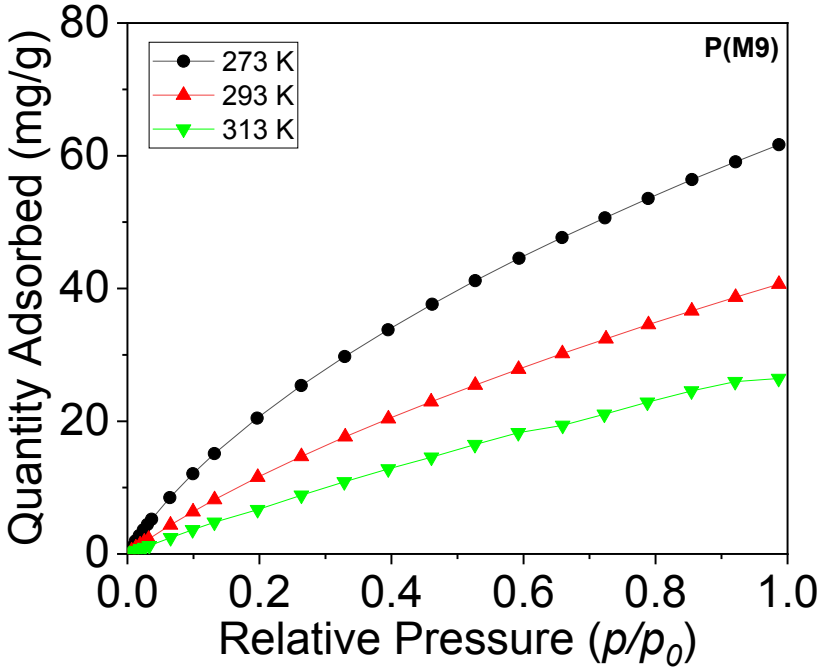

Figure S8 CO_2 adsorption isotherms on P(M9) at 273, 293, and 313 K.

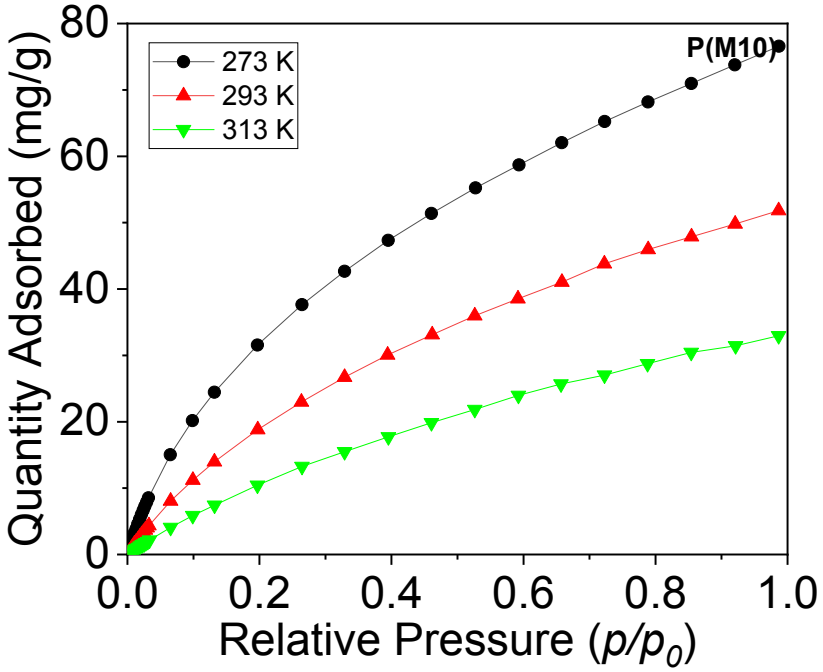

Figure S9 CO_2 adsorption isotherms on P(M10) at 273, 293, and 313 K.

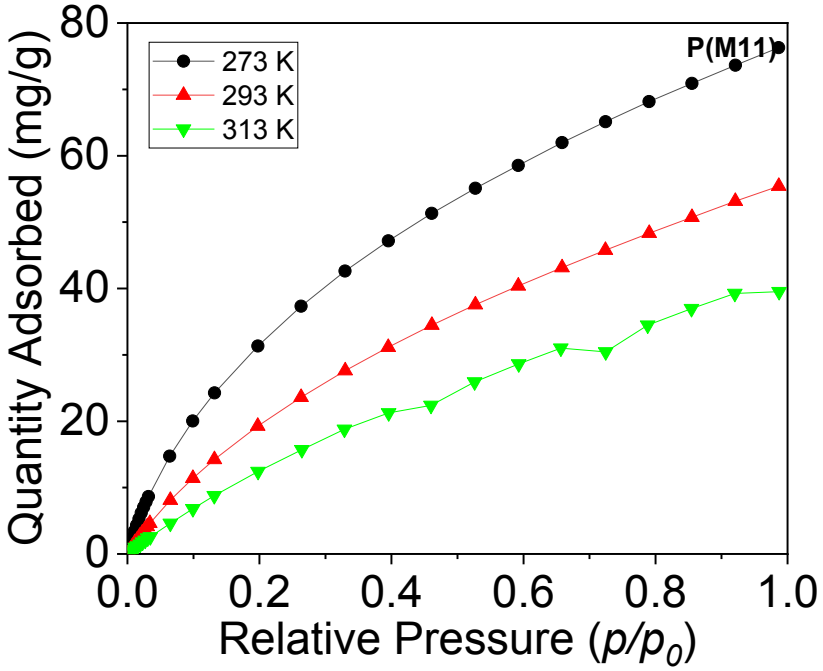

Figure S10 CO_2 adsorption isotherms on P(M11) at 273, 293, and 313 K.

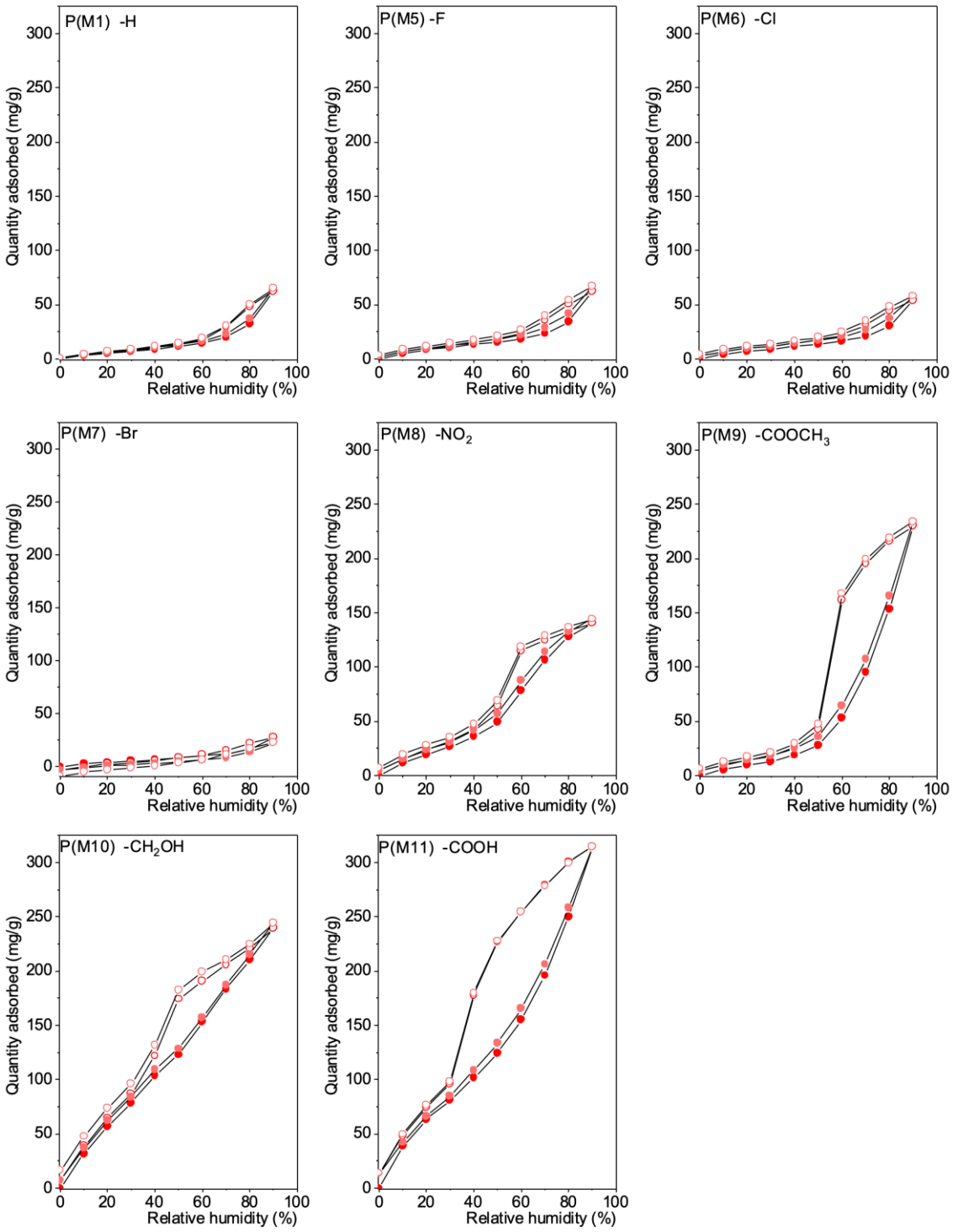

Figure S11 Water adsorption (full points) and desorption (empty points) isotherms (297 K) on prepared networks. Two consecutive measurements.

II.

L. Havelková, A. Hašková, B. Bashta, J. Brus, M. Lhotka, E. Vrbková, M. Kindl, E. Vyskočilová, J. Sedláček: Synthesis of hyper-cross-linked microporous poly(phenylacetylene)s having aldehyde and other groups and their chemisorption and physisorption ability, *European Polymer Journal,* **2019**, *114*, 279.

European Polymer Journal 114 (2019) 279–286

Contents lists available at ScienceDirect

European Polymer Journal

journal homepage: www.elsevier.com/locate/europolj

Synthesis of hyper-cross-linked microporous poly(phenylacetylene)s having aldehyde and other groups and their chemisorption and physisorption ability

Lucie Havelková[a], Alena Hašková[a], Bogdana Bashta[a], Jiří Brus[b], Miloslav Lhotka[c], Eva Vrbková[d], Martin Kindl[d], Eliška Vyskočilová[d,*], Jan Sedláček[a,*]

[a] Department of Physical and Macromolecular Chemistry, Faculty of Science, Charles University in Prague, Hlavova 2030, 128 43 Prague 2, Czech Republic
[b] Institute of Macromolecular Chemistry, v.v.i., Academy of Sciences of the Czech Republic, Heyrovský Sq. 2, 162 06 Prague 6, Czech Republic
[c] Department of Inorganic Technology, University of Chemistry and Technology in Prague, Technická 5, Prague 6 166 28, Czech Republic
[d] Department of Organic Technology, University of Chemistry and Technology in Prague, Technická 5, Prague 6 166 28, Czech Republic

ARTICLE INFO

Keywords:
Polyacetylene
Hyper-cross-linked
Chemisorption
Porous polymer
CO_2 adsorption

ABSTRACT

The chain-growth homopolymerization of 3,5-diethynylbenzaldehyde proceeding through the transformation of the ethynyl groups of the monomer yields hyper-cross-linked poly(3,5-diethynylbenzaldehyde), P(DEBA), with a high content of carbaldehyde groups (6.5 mmol/g) and specific surface of about 900 m^2/g. The covalent structure of P(DEBA) consists of polyene (polyacetylene) main chains cross-linked with 5-formyl-1,3-phenylene links. P(DEBA) selectively and reversibly chemisorbs alcohols and primary amines (capacity up to 350 mg/g) through binding these solutes in the form of acetal and Schiff base type segments, respectively. The condensation of P(DEBA) carbaldehyde groups with amino groups of ethylenediamine (EDA) gives microporous P(DEBA)/EDA2 extensively decorated with base NH_2 groups. P(DEBA)/EDA2 is effective for physisorption of ibuprofen solute (capacity, 1130 mg/g) and CO_2 gas (capacity, 360 mg/g, 7 bar, 273 K) and is active as a heterogeneous catalyst of aldol condensation of *n*-heptanal with benzaldehyde to jasminaldehyde.

1. Introduction

Polymers with permanent porosity and high specific surface area often referred to as Porous Organic Polymers (POP) or Microporous Organic Polymers (MOP) [1–3] have been of growing interest due to their potential applications in the areas of catalysis [4–6], adsorption and separation of gases and solutes [7–11] and construction of sensors and optoactive devices [12–14]. Most POPs possess the architecture of polymer networks and their porosity results from extensive cross-linking combined with the rigidity of the network building blocks which are prevailingly of hydrocarbon nature. However, many applications of such networks require an appropriate and sufficiently extensive POP functionalization with heteroatom-containing groups or segments. In some cases, the heteroatom-containing groups of POPs are created due to the synthesis as network knots (e.g. triazole knots in POPs prepared by the step-growth copolymerization through "click" reaction between ethynyl and azido groups of respective comonomers) [15]. Controlled functionalization of POPs is mostly achieved by polymerization of monomers carrying, in addition to the polymerizable groups, other functional groups specifically selected for decorating the product. These functional groups should not disturb the polymerization process and should remain unchanged after the polymerization. This concept was well developed particularly for poly(aryleneethynylene) type POPs synthesized by step-growth polymerization through Sonogashira cross-coupling of aromatic comonomers bearing bromo and ethynyl complementary groups [16]. A large series of poly(aryleneethynylene) POPs active as physisorbents of tuneable efficiency and selectivity have been prepared by copolymerization of functionalized dibromoarenes (functional groups or heterocycle segments: F, NO_2, OH, OMe, COOMe, CF_3, NH_2, pyridine, pyrimidine, carbazole) and 1,3,5-triethynylbenzene cross-linker [17,18]. Sonogashira cross-coupling of 1,3,5-triethynylbenzene and organometallic complexes with dibrominated *N*,*N*′-bis(salicylidene)ethylenediamine or 2,2′-bipyridine ligands provided organometallic POPs active as heterogeneous catalysts.[19,20] The chain-growth polymerization approach was also efficient for the synthesis of functionalized POPs [21]. Of particular interest here is the recently described radical self-polymerization of monomers carrying both heteroatomic functional group(s) and several

* Corresponding authors.
E-mail addresses: eliska.vyskocilova@vscht.cz (E. Vyskočilová), jan.sedlacek@natur.cuni.cz (J. Sedláček).

https://doi.org/10.1016/j.eurpolymj.2019.02.039
Received 18 January 2019; Received in revised form 22 February 2019; Accepted 24 February 2019
Available online 25 February 2019
0014-3057/

polymerizable vinyl groups in the molecule. The monomeric units formed from these monomers through chain-growth radical homopolymerization managed both the functionalization and cross-linking of the resulting POPs. For example, the polymerization of bis-1,2-(diphenylphosphino)ethane with one vinyl group on each phenyl ring provided a POP of hyper-cross-linked type suitable for catalytic applications [22]. The POP functionalization can also be achieved by postpolymerization modifications. The functionalization of hydrocarbon POPs was achieved through e.g. sulfonation and thiol-yne reactions [23,24]. Nevertheless, the postpolymerization functionalization proceeding through the reaction of proper heteroatomic groups introduced into the POPs in the preceding polymerization step seems to be smoother and more efficient. For example, Cooper et al. reported the synthesis of poly(aryleneethynylene) decorated with NH_2 groups and subsequent efficient modification of these groups in reaction with carboxylic acid anhydrides under formation of amide-groups containing POPs [25].

The monomers with several carbaldehyde groups per molecule are a popular building block in the synthesis of POPs [3,26]. Polycondenzation of these monomers with aminoarenes has been many times reported to provide structurally diverse POPs with comonomeric units interconnected by either azomethine- [27] or aminal-type [28] links. In some cases, the texture parameters of the POPs were well controlled by selection of the comonomers as it was shown by Wang et al. in copolymerization of 1,3,5,7-tetrakis(4-formylphenyl)adamantane with phenylenediamines.[29] Conversely, the POPs decorated by carbaldehyde groups are rather rare although they could be promising for many applications due to the reactivity of carbaldehyde groups. Liu et al. described polycondensation of triphenylene-2,3,6,7,10,11-hexathiol with 2,3,5,6-tetrafluoroterephthaldehyde under formation of a POP in which the HC═O groups were preserved. The POP was subsequently loaded with (catalytically active) Ag nanoparticles formed by reduction of Tollens' reagent by aldehyde groups of POP.[30] Hedin et al. reported the polycondensation of 1,3,5-tris(4-aminophenyl)benzene with an overstoichiometric amount of benzene-1,3,5-tricarboxaldehyde into a Schiff-base-type POP decorated with some amount of unreacted HC═O groups.[31] A poly(aryleneethynylene) POP possessing HC═O groups was prepared by Sonogashira coupling of 1,3,5-triethynylbenzene and 2,6-dibromo-4-trimethylsilylbenzaldehyde.[32] The postpolymerization modification of POPs from refs[31,32] through reaction of the aldehyde groups with aliphatic di- or triamines gave POPs decorated with amino groups efficient in CO_2 adsorption.

In this paper, we report a hyper-cross-linked POP decorated with carbaldehyde groups prepared from the 3,5-diethynylbenzaldehyde monomer. The chain-growth homopolymerization used as a method of preparation allowed to achieve POP with a high content of carbaldehyde groups. The prepared POP is shown as a readily modifiable multifunctional microporous material suitable for reversible chemisorption and physisorption capture of various adsorptives and for catalytic applications.

2. Experimental section

2.1. Materials

3,5-Diethynylbenzaldehyde (DEBA) (Spectra Group Limited, Inc.), acetylacetonato(norborna-2,5-diene)rhodium(I), ([Rh(nbd)acac]) (TCI Europe), *p*-toluidine, ethylenediamine (EDA), *N*-methylaniline, methanol, ethanol, ibuprofen (IBU), benzaldehyde and *n*-heptanal (all by Sigma-Aldrich) and toluene (Penta) were used as obtained. Dichloromethane (Lachner, Czech Republic) was distilled from P_2O_5.

2.2. Techniques

All ^{13}C CP/MAS (Cross-Polarization Magic Angle Spinning) NMR spectra were measured at 11.7 T using a Bruker Avance III 500 WB/US NMR spectrometer as described previously.[6] The nitrogen adsorption/desorption isotherms on the polymers were measured at 77 K using a Triflex V4.02 apparatus (Micromeritics). The Brunauer-Emmett-Teller specific surface area, S_{BET}, and micropore size distribution by the method of Horvath-Kawazoe are reported. Adsorption isotherms of CO_2 in the temperature range from 273 to 313 K were determined using an ASAP 2050 apparatus (Micromeritics). The isosteric heats of CO_2 adsorption on the polymers were obtained according to the Clausius–Clapeyron equation [9]. Before adsorption experiments, the polymers were outgassed at 333 K (temperature ramp of 1 K/min) until the residual pressure of 0.01 torr was obtained. After further heating at 343 K for 1 h the temperature was increased (temperature ramp of 1 K/min) until the temperature of 353 K was achieved. This temperature was maintained for 24 h. Scanning Electron Microscopy (SEM) analysis was performed using Tescan Lyra3 apparatus (TESCAN Brno, ltd., Czech Republic) at an accelerating voltage of 10 kV.

2.3. Polymerization of DEBA

Polymerization of DEBA was performed in CH_2Cl_2 at 70 °C in a sealed thick-wall ampoule under an argon atmosphere. The [Rh(nbd)acac] complex was used as a polymerization catalyst. The initial concentrations were: $[[Rh(nbd)acac]]_0 = 15\ mmol/dm^3$, $[DEBA]_0 = 0.3\ mol/dm^3$. Polymerization was started by adding the solution of catalyst into the solution of DEBA monomer. The polymerization was finished after 72 h by diluting the reaction mixture (containing the solid polymer) with CH_2Cl_2 in the volume ratio 1:30. The solid polymer, poly(3,5-diethynylbenzaldehyde), P(DEBA) was isolated, mechanically ground, washed by decantation in CH_2Cl_2 and finally dried under vacuum at room temperature to constant weight. Details on the postpolymerization modification of P(DEBA) and application of the parent and modified P(DEBA) s in sorption and catalytic experiments are given in Supplementary Data.

3. Results and discussion

3.1. Poly(3,5-diethynylbenzaldehyde), P(DEBA), preparation

3,5-Diethynylbenzaldehyde (DEBA) was chosen as a monomer for preparing a POP with a high carbaldehyde groups content (Scheme 1). In order to achieve this, it was necessary to transform DEBA monomer by means of homopolymerization (i.e. without the participation of comonomers) performed via reaction of ethynyl groups under preservation of carbaldehyde group of the monomer. Having considered these assumptions, we have selected chain-growth polymerization catalysed by the [Rh(nbd)acac] complex as a method for preparing a DEBA-based POP product. The chain-growth polymerization of alkynes with one ethynyl group per a monomer molecule catalysed with transition metal catalysts and yielding the linear substituted polyacetylenes is known for several decades.[33,34] The ethynyl groups of the monomer molecules are transformed into segments of the linear polyene-type conjugated main chains in this polymerization. In particular, Rh(I) complexes belong to very effective catalysts of alkyne polymerizations. Some of these catalysts, especially the [Rh(nbd)acac] and [Rh(cod)acac] complexes (nbd = norborna-2,5-diene, cod = cycloocta-1,5-diene, acac is deprotonated form of acetylacetone), show increased tolerance to some functional groups of the polymerization system (monomer, solvent).[34–37] We found that Rh(I) catalysts polymerized also monomers with two, three or four ethynyl groups per the monomer molecule [e.g. diethynylbenzenes, 1,3,5-triethynylbenzene, tetrakis(4-ethynylphenyl) methane].[6,38] In this case, the microporous polyacetylene networks of the POP type were formed in which the polyene main chains were cross-linked with arene links. Using this procedure we polymerized now DEBA with [Rh(nbd)acac] catalyst in CH_2Cl_2 under the conditions given in Experimental part (see Scheme 1). The polymerization catalyst and solvent were chosen on the basis of our previous studies carried out with the 1,4-diethynylbenzene and 1,3-diethynylbenzene monomers.

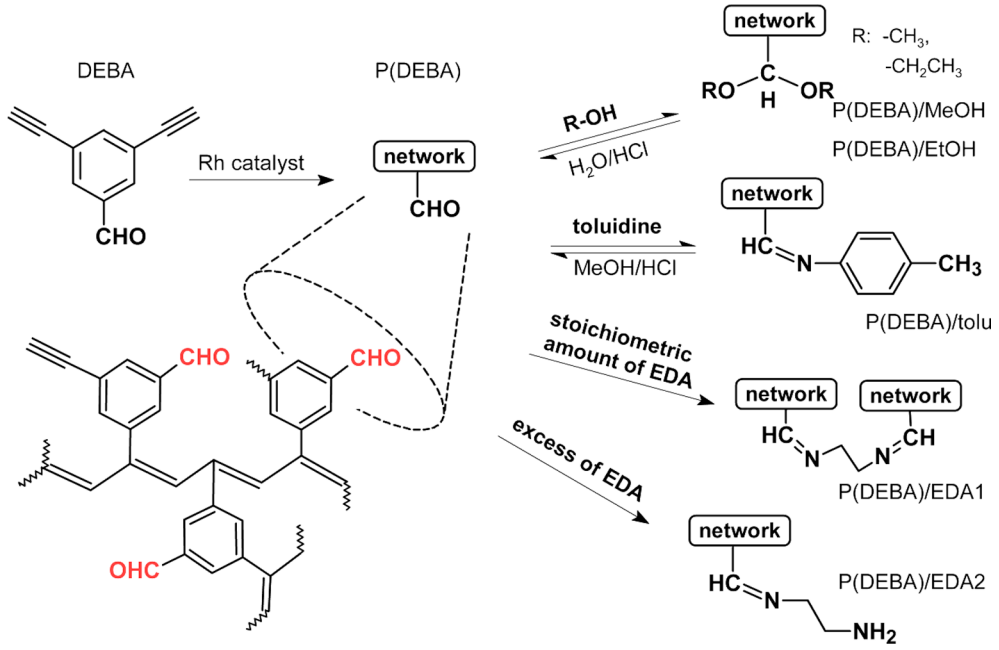

Scheme 1. Chain-growth polymerization of DEBA into microporous network P(DEBA) and subsequent covalent modifications of P(DEBA).

[39,40] The polymerization of DEBA gave quantitative yield of totally insoluble (CH_2Cl_2, methanol, THF, benzene) poly(3,5-diethynylbenzaldehyde), P(DEBA). Fig. 1 shows ^{13}C CP/MAS NMR spectra of DEBA and P(DEBA) together with the signal assignment. It is particularly evident that the signal of carbons of aldehyde groups (δ = 190 ppm) was preserved in the spectrum of P(DEBA). Conversely, the intensity of the signal corresponding to the carbons of ethynyl groups (−*C*≡*C*H, δ = 82 ppm) was substantially diminished in the spectrum of P(DEBA) compared to the spectrum of DEBA monomer. Thus ^{13}C CP/MAS NMR spectroscopy confirmed P(DEBA) to consist of conjugated polyene main chains extensively cross-linked with 5-formyl-1,3-phenylene links. In addition, P(DEBA) contained some amount of linear units in which only one ethynyl group was transformed into a segment of polyene main chain while the second ethynyl group remained non-transformed [see Scheme 1 and also signal of carbons of residual ethynyl groups in ^{13}C CP/MAS NMR spectrum of P(DEBA)].

The nitrogen adsorption/desorption isotherm (77 K) on P(DEBA) (Fig. 2) showed a steep increase in adsorbed amount in the relative pressure (p/p_0) region from 0 to 0.1 (p_0 = 101325 Pa), thus confirming the presence of micropores in P(DEBA). In addition to the micropores, P(DEBA) probably contained also some mesopores as it can be implied from a steep increase in adsorbed amount of N_2 at $p/p_0 > 0.7$ and a slight hysteresis on the adsorption/desorption isotherm. The Brunauer–Emmett–Teller specific surface area, S_{BET}, of P(DEBA) sample further discussed in this article was 916 m^2/g (Table 1). The micropore size distribution of P(DEBA) exhibited a distinct maximum at a width of about 0.70 nm as it is shown in Fig. 2. It should be noted that two other independent DEBA polymerizations gave P(DEBA)s with nearly identical micropore size distributions and values of S_{BET} equal to 894 and 930 m^2/g. Thus, it can be stated that one step [Rh(nbd)acac] catalysed chain-growth homopolymerization of DEBA was a powerful tool for preparing a POP with satisfactory specific surface area and high carbaldehyde group content (6.5 mmol/g).

3.2. Reversible chemisorption of solutes on P(DEBA)

A number of examples of physisorption of solutes (especially dyes) on various POP materials have been described in the literature [17,41]. Conversely, significantly less attention was paid to reversible chemisorption on POPs. Due to the high content of reactive carbaldehyde groups, P(DEBA) appeared to be a promising chemisorbent. So, we examined the possibility of chemisorption of methanol, ethanol, and *p*-toluidine on this material (see Supplementary Data for the details). P(DEBA) was found to bind methanol (captured amount 345 mg/g) and ethanol (170 mg/g) in the form of respective acetals at room temperature (slightly acidified alcohols were submitted for chemisorption). P(DEBA) was modified in this process into poly(3,5-diethylbenzaldehyde dimethyl acetal), P(DEBA)/MeOH and poly(3,5-diethylbenzaldehyde diethyl acetal), P(DEBA)/EtOH, respectively. Most of the carbaldehyde groups of P(DEBA) were consumed through methanol chemisorption, as evidenced by comparing the intensity of signals of (i) the carbon of residual H*C*=O groups (δ = 190 ppm) and (ii) tertiary carbon of the newly formed *C*H(OMe)$_2$ groups (δ = 102 ppm) in ^{13}C CP/MAS NMR spectrum of P(DEBA)/MeOH in Fig. 1. A lower degree of transformation of the carbaldehyde groups of P(DEBA) was achieved in the case of ethanol chemisorption (see the intensity of the signals at δ = 190 ppm and at δ = 100 ppm in ^{13}C CP/MAS NMR spectrum of P(DEBA)/EtOH in Fig. 1). This may reflect the well-known decrease in acetal formation efficiency upon the use of higher alcohols. The chemisorption of alcohols on P(DEBA) was fully reversible: methanol and ethanol were released upon P(DEBA)/MeOH and P(DEBA)/EtOH hydrolysis with H_2O/HCl (100/1; v/v) under simultaneous regeneration of P(DEBA). The ^{13}C CP/MAS NMR spectra of the regenerated P(DEBA) samples were identical with that recorded for the parent P(DEBA). P(DEBA) also efficiently captured *p*-toluidine (captured amount 350 mg/g) by means of its covalent binding through azomethine link (*p*-toluidine dissolved in neutral methanol was submitted for the chemisorption). The ^{13}C CP/MAS NMR spectrum of P(DEBA) with chemisorbed *p*-toluidine, P(DEBA)/tolu, given in Fig. 1, contains the signal of the *C*H$_3$ carbon at 20 ppm and the signal of the carbon of H*C*=N link at 157 ppm. The latter signal evidenced *p*-toluidine to be trapped on P(DEBA) in the form of *N*-benzylidene-*p*-toluidine. Also, the *p*-toluidine chemisorption on P(DEBA) was fully reversible. Upon treating P(DEBA)/tolu with methanol/HCl (100/1; v/v), the HC=N links were hydrolyzed and the chemisorbed *p*-toluidine was released. To regenerate the sorbent completely, the subsequent washing with H_2O/HCl (100/1; v/v) was necessary to release methanol from benzaldehyde dimethyl acetal segments formed due to the reaction of P(DEBA)/tolu with methanol/HCl. The ^{13}C CP/MAS NMR spectrum of the regenerated P(DEBA) was identical with that recorded for the parent P(DEBA).

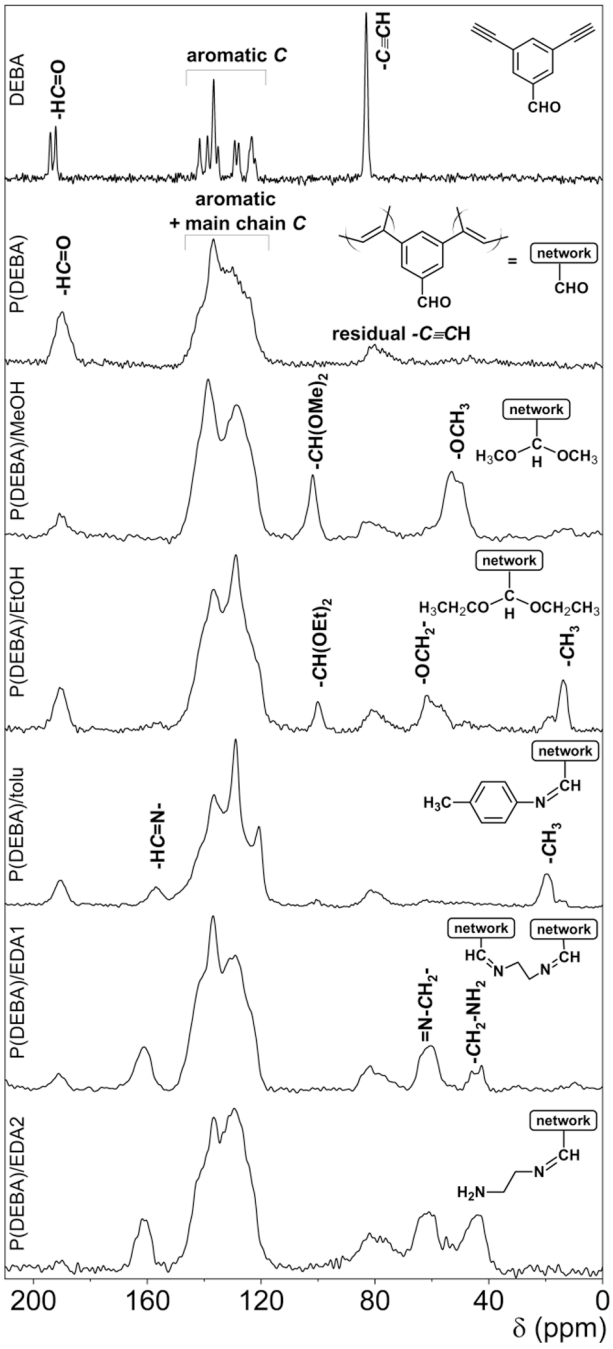

Fig. 1. ^{13}C CP/MAS NMR spectra of the monomer DEBA, parent P(DEBA) polymer and polymers resulting from postpolymerization application and modification of P(DEBA).

Conversely to the ability of P(DEBA) to bind *p*-toluidine, no activity of P (DEBA) was observed if *N*-methylaniline (a positional isomer of *p*-toluidine) was tested as an adsorptive. This further confirmed that *p*-toluidine (primary amine) was chemisorbed on P(DEBA) under the formation of a Schiff base, which could not be achieved with *N*-methylaniline (a secondary amine). It simultaneously indicates that P (DEBA) might be suitable for separating primary amines from secondary and tertiary amines. Table 1 No. 2–7 summarizes the texture characteristics of (i) P(DEBA)s loaded with methanol, ethanol and *p*-toluidine and (ii) P(DEBA)s regenerated through subsequent hydrolytic desorption (sample codes with abbreviation "reg"). Fig. 2 compares N_2 adsorption/desorption isotherms and micropore size distributions of P (DEBA)/EtOH, P(DEBA)/EtOH/reg and parent P(DEBA). The N_2 adsorption/desorption isotherms and micropore size distributions obtained while studying methanol and *p*-toluidine chemisorption are shown in Figs. S1 and S2 in Supplementary Data. It is evident from Table 1 that despite the relatively high amount of solute molecules covalently attached on the pore surface, the materials P(DEBA)/MeOH, P(DEBA)/EtOH and P(DEBA)/tolu retained microporosity: the S_{BET} values decreased by only 23 to 49 percent due to the chemisorption compared to S_{BET} of parent P(DEBA). The preserved porosity of P (DEBA)/MeOH, P(DEBA)/EtOH and P(DEBA)/tolu most probably enabled to achieve high efficiency in the hydrolytic release of chemisorbed molecules from these materials, because it allowed the chemisorbed molecules to be accessed by the hydrolyzing agent. The regeneration of the sorbent via the hydrolytic release of chemisorbed molecules from P(DEBA)/MeOH, P(DEBA)/EtOH and P(DEBA)/tolu led to a certain increase in S_{BET} although the S_{BET} value of the parent P (DEBA) was not fully reached (see Table 1). The chemisorption and subsequent desorption also partly modified the micropore size distribution of the sorbent. The chemisorption resulted in a slight shift of the maximum of the micropore size distribution to the higher values of micropore width most probably due to a partial filling of the smallest micropores of P(DEBA) with the chemisorbed molecules. Upon the desorption, the smallest pores were most probably partly regenerated and the micropore size distributions of P(DEBA)/MeOH/reg, P(DEBA)/EtOH/reg and P(DEBA)/tolu/reg approached to that of the parent P (DEBA).

3.3. Covalently modified P(DEBA)s and their functional properties

The carbaldehyde groups of P(DEBA) can also be used for tuning properties of P(DEBA) via its covalent modifying with proper agents. We used ethylenediamine (EDA) modifier with the aim to introduce base groups to P(DEBA). The reaction of P(DEBA) with EDA performed with a mole ratio of functional groups HC═O/NH_2 = 1/1 provided P (DEBA)/EDA1, a similar reaction performed with HC═O/NH_2 = 1/10 gave P(DEBA)/EDA2 (see Scheme 1 and Supplementary Data for details). ^{13}C CP/MAS NMR spectra of P(DEBA)/EDA1 and P(DEBA)/EDA2 (Fig. 1) contained signal at 161 ppm corresponding to the carbon of H*C*═N link. This confirmed the covalent binding of EDA to P(DEBA) through condensation reaction of aldehyde groups of P(DEBA) and amino groups of EDA. The low intensity of signals of the carbon of residual H*C*═O groups (δ = 190 ppm) in ^{13}C CP/MAS NMR spectra indicated that most carbaldehyde groups were modified by this condensation reaction in P(DEBA)/EDA1 and P(DEBA)/EDA2. The carbons of EDA molecules covalently attached to P(DEBA) were manifested in ^{13}C CP/MAS NMR spectra by the signals at 61 ppm (carbon of ═N*C*H_2− groups) and 44 ppm (carbon of −*C*H_2NH_2 groups). The intensities of these two signals were approximately the same in the case of P(DEBA)/EDA2, which indicated that only one amino group of the EDA molecule was transformed by reaction of EDA with P(DEBA) that led to the formation of −HC═N$CH_2CH_2NH_2$ pendant groups in P(DEBA)/EDA2. Conversely, the ═N*C*H_2− carbon signal was more intense than the *C*H_2NH_2 carbon signal in ^{13}C CP/MAS NMR spectrum of P(DEBA)/EDA1. Evidently, both amino groups were transformed in the course of binding some EDA molecules to P(DEBA) under formation of HC═NCH_2CH_2N═CH cross-links in P(DEBA)/EDA1. This was due to the low EDA amount used for P(DEBA) modification. However, the P(DEBA) additional cross-linking with EDA was not entirely selective and some EDA molecules were incorporated into the parent network as the side −HC═N$CH_2CH_2NH_2$ groups as evidenced by the −*C*H_2NH_2 carbon signal in ^{13}C CP/MAS NMR spectrum of P(DEBA)/EDA1. Nevertheless, the character of the modification of P(DEBA) with EDA was shown to be tuneable to some extent by varying the HC═O/NH_2 ratio in the reaction mixture.

Fig. 3 compares the N_2 adsorption/desorption isotherms and micropore size distribution for P(DEBA) and materials prepared by P (DEBA) modification with EDA. Both modified materials were

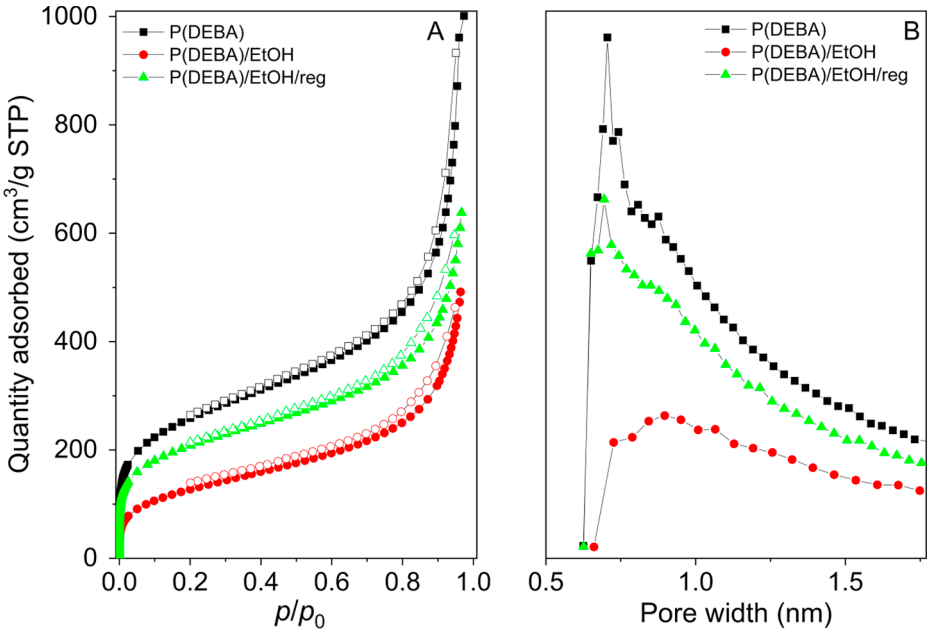

Fig. 2. N_2 adsorption (full points) and desorption (empty points) isotherms (77 K) (A) and micropore size distributions (B) for samples P(DEBA), P(DEBA)/EtOH and P(DEBA)/EtOH/reg.

Table 1
Values of S_{BET} and micropore width, W, (from N_2 adsorption isotherms) for parent P(DEBA) and samples prepared from P(DEBA) through covalent modification.

No.	Sample code	S_{BET} [m^2/g]	W [nm]
1	P(DEBA)	916	0.70
2	P(DEBA)/MeOH	708	0.85
3	P(DEBA)/MeOH/reg	785	0.65
4	P(DEBA)/EtOH	467	0.90
5	P(DEBA)/EtOH/reg	746	0.70
6	P(DEBA)/tolu	582	from 0.80 to 0.90[a)]
7	P(DEBA)/tolu/reg	728	from 0.70 to 0.90[a)]
8	P(DEBA)/EDA1	826	0.65
9	P(DEBA)/EDA2	649	0.90

[a)] Broad distribution.

microporous, the N_2 adsorption/desorption isotherms on P(DEBA)/EDA1, P(DEBA)/EDA2 and parent P(DEBA) showed a similar character. The S_{BET} value of P(DEBA)/EDA2 was 30% lower than that of the parent P(DEBA). Simultaneously, the maximum of micropore size distributions was shifted to the higher values of pore width in P(DEBA)/EDA2 compared to the parent P(DEBA) (see Table 1 and Fig. 3). Most probably, the EDA segments attached to P(DEBA) as the pendant groups partly filled the smallest pores in P(DEBA)/EDA2. Some pores were also probably filled as a result of EDA binding to P(DEBA) in case of P/DEBA)/EDA1. However, due to the cross-linking participating on the modification of P(DEBA) to P(DEBA)/EDA1 (vide supra) (i) the S_{BET} value of P(DEBA)/EDA1 (826 m^2/g) was only slightly lower than that of parent P(DEBA) (916 m^2/g) and (ii) the micropore size distribution of P(DEBA)/EDA1 was not shifted to higher pore width values but, on the contrary, to values slightly lower compared to the parent P(DEBA). Fig. 4 shows SEM images of P(DEBA), P(DEBA)/EDA1 and P(DEBA)/EDA2. It is evident that the modification of P(DEBA) with EDA did not affect the morphology of the materials. All three networks consisted of approximately spherical particles 50–100 nm in diameter.

P(DEBA)/EDA1 and P(DEBA)/EDA2 were used in physisorption of ibuprofen (IBU) dissolved in toluene (6 mg/ml), see Supplementary Data for details. In particular, P(DEBA)/EDA2 has been confirmed to be highly efficient in this process. Under the experimental conditions applied, P(DEBA)/EDA2 had an unexpectedly high capacity of 1.13 g (IBU)/g (compare with e.g. ref.[42]) while the concentration of IBU in the toluene phase decreased to 0.3 mg/ml after 24 h mixing IBU solution with P(DEBA)/EDA2. The time course of the IBU physisorption on P(DEBA)/EDA2 is shown in Supplementary Data, Fig. S3. A lower capacity, 0.49 g(IBU)/g, was found for P(DEBA)/EDA1 under the same conditions. It should be noted that parent P(DEBA) showed no measurable activity in IBU physisorption. The IBU is a slightly acid adsorptive (pK_a = 4.47, Ref. [43]), which explains that the efficiency of the IBU capture increased with increasing content of base NH_2 groups in the sorbents in the order: P(DEBA) ≪ P(DEBA)/EDA1 < P(DEBA)/EDA2.

P(DEBA)/EDA2 with high NH_2 groups content and parent P(DEBA) (free of NH_2 groups) were also used in CO_2 physisorption. The CO_2 adsorption isotherms on these materials measured at various temperatures are given in Supplementary Data, Figs. S4 and S5, the CO_2 adsorption isotherms at 273 K are given in Fig. 5. The CO_2 capture capacities of 240 mg/g and 360 mg/g were determined at 273 K and 7 bar CO_2 pressure for P(DEBA) and P(DEBA)/EDA2, respectively, which represents a 50% increase in capture capacity due to the modification of the sorbent by NH_2 groups. An even higher relative increase in CO_2 capture capacity was observed at higher temperatures (see Table S1 in Supplementary Data), for example at 313 K, the CO_2 capture capacity of P(DEBA)/EDA2 (235 mg/g at 7 bar CO_2) was 75% higher than that of P(DEBA) (135 mg/g at 7 bar CO_2). The isosteric heats of CO_2 physisorption on P(DEBA) and P(DEBA)/EDA2, Q_{st}, (obtained from the temperature dependences of CO_2 adsorption isotherms) are plotted vs. the physisorbed amount in Fig. 5. The heats of CO_2 physisorption at the lowest amount physisorbed, $(Q_{st})_{init}$, were 26 kJ/mol for P(DEBA) and 36 kJ/mol for P(DEBA)/EDA2. The value of 36 kJ/mol ascertained for P(DEBA)/EDA2 is among the higher $(Q_{st})_{init}$ values published in the literature for the CO_2 physisorption on functionalized POPs.[18] It can, therefore, be stated that due to the basicity of the NH_2 groups of P(DEBA)/EDA2 the energy of the CO_2-sorbent interaction was increased. High energy of CO_2-sorbent interaction along with the fact that P(DEBA)/EDA2 contained a high number of base NH_2 groups (about 5.1 mmol/g) was very probably crucial for the observed high efficiency of CO_2 capture on P(DEBA)/EDA2. This finding is consistent with the

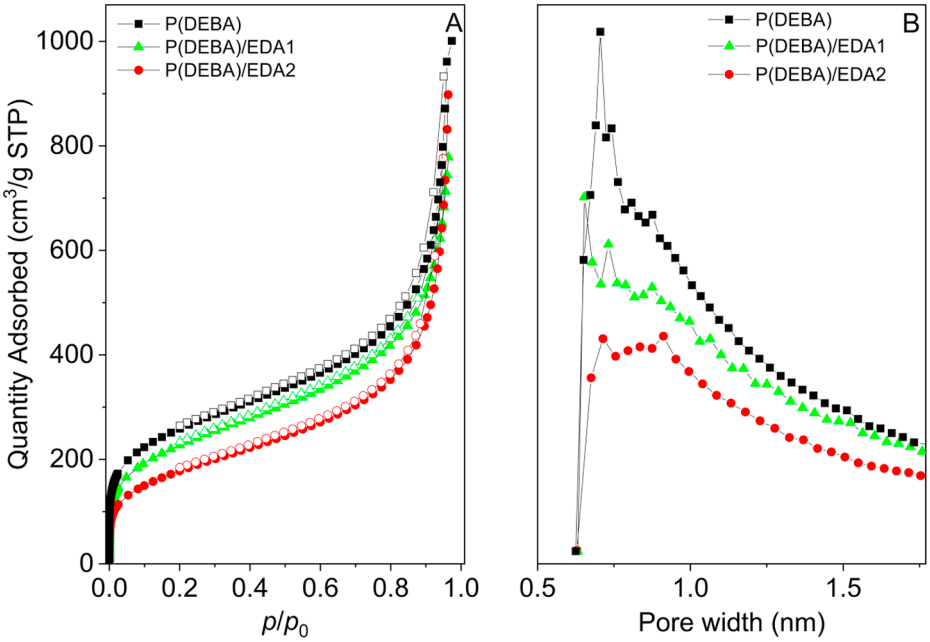

Fig. 3. N_2 adsorption (full points) and desorption (empty points) isotherms (77 K) (A) and pore size distributions (B) for samples P(DEBA), P(DEBA)/EDA1 and P(DEBA)/EDA2.

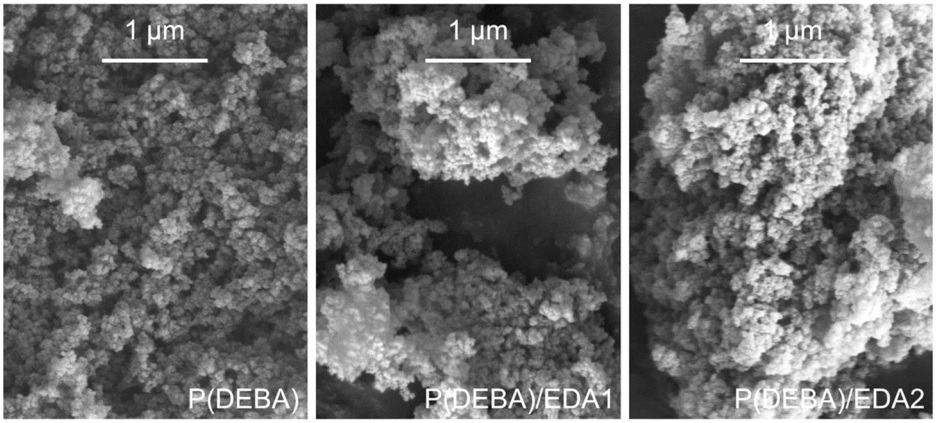

Fig. 4. SEM images of P(DEBA), P(DEBA)/EDA1 and P(DEBA)/EDA2.

opinion of a number of authors (see e.g., Ref. [44]) that to achieve a high CO_2 capture efficiency the functionalization of the sorbent with appropriate base groups is more important than an ultrahigh specific surface area of the sorbents. In this connection, it is worth mentioning that the CO_2 capture capacity of P(DEBA)/EDA2 was significantly higher than the CO_2 capture capacity of parent P(DEBA) despite the fact that the S_{BET} value of P(DEBA)/EDA2 was 30% lower than that of P(DEBA).

The network P(DEBA)/EDA2 was also proved to be active as a heterogeneous catalyst for aldol condensation of benzaldehyde with *n*-heptanal. In principle, this reaction provides two products (see Scheme 2): (i) jasminaldehyde (desired product of cross-condensation) and (ii) 2-pentylnon-2-enal (product of selfcondensation of *n*-heptanal). To suppress the formation of 2-pentylnon-2-enal, benzaldehyde is usually used in excess over *n*-heptanal. Using the mole ratio *n*-heptanal:benzaldehyde = 1:3 and P(DEBA)/EDA2 as a catalyst, the conversion of *n*-heptanal of 61% was achieved within 24 h (80 °C, mole ratio of *n*-heptanal to NH_2 groups of the catalyst = 75). The selectivity to jasminaldehyde was 40%. The catalytic activity and selectivity of P(DEBA)/EDA2 catalyst were similar or slightly higher in comparison to the activity of various oxide-based catalysts applied for this reaction previously [45,46]. The catalytically active centres remained in the solid phase in the course of aldol condensation catalysed with P(DEBA)/EDA2, (the reaction did not proceed further in the liquid phase of the reaction mixture separated by filtration from P(DEBA)/EDA2 in the course of the reaction). Moreover, the GC/MS analysis did not reveal the presence of EDA in the liquid phase of the reaction system. Despite these facts, the catalytic efficiency of P(DEBA)/EDA2 decreased in the second use (*n*-heptanal conversion of 30%, selectivity to jasminaldehyde of 30% under the same conditions). The observed decrease in catalytic efficiency may be due to insufficient removal of reaction products from the active surface of the catalyst (before reusing, P(DEBA)/EDA2 was washed three times with toluene at room temperature). We believe optimization of the catalyst surface regeneration can increase the recycling efficiency of P(DEBA)/EDA.

Nevertheless, it should be noted that P(DEBA) was totally inactive in the studied reaction: no conversion of *n*-heptanal was observed after 24 h of reaction performed in the presence of this polymer network. Evidently, the base NH_2 groups in P(DEBA)/EDA2 were crucial for P(DEBA)/EDA2 to act as a catalyst of the studied aldol condensation.

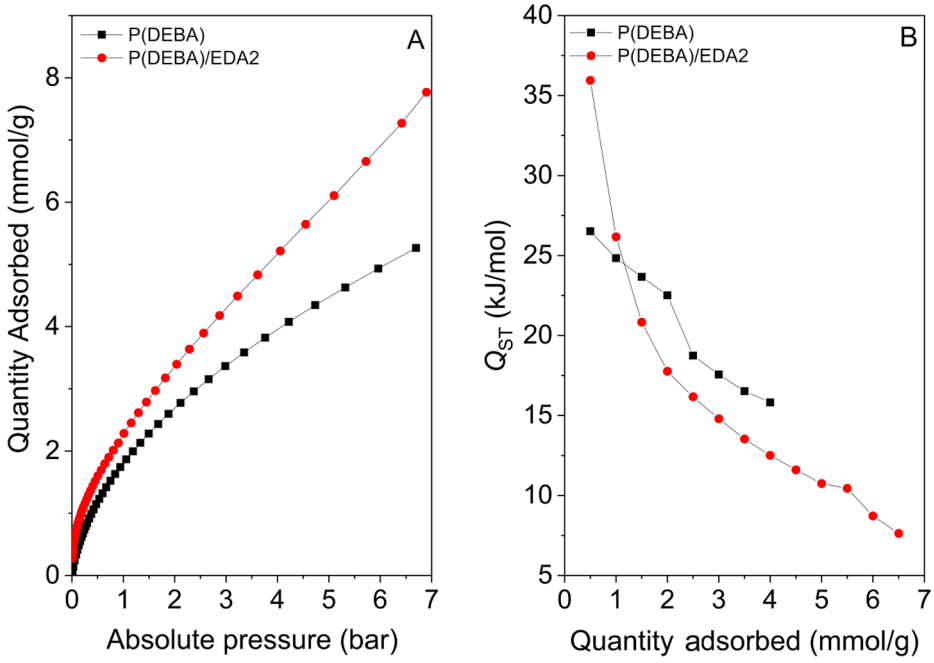

Fig. 5. CO_2 adsorption isotherms (273 K) on P(DEBA) and P(DEBA)/EDA2 (A), isosteric heat of CO_2 physisorption (B).

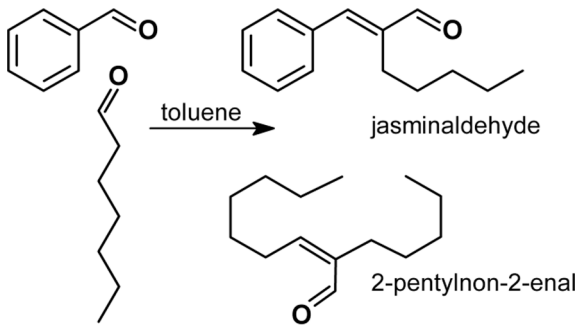

Scheme 2. Condensation of benzaldehyde with *n*-heptanal catalysed with P(DEBA)/EDA2.

4. Conclusion

The polyacetylene-type hyper-cross-linked poly(3,5-diethynylbenzaldehyde), P(DEBA), with a high content of carbaldehyde groups (6.5 mmol/g) and specific surface area of about 900 m^2/g has been prepared by a smooth chain-growth homopolymerization of 3,5-diethynylbenzaldehyde monomer. It has thus been shown that the polymerization method known from the synthesis of linear substituted polyacetylenes can also be an effective tool for the preparation of highly functionalized microporous polymer networks. P(DEBA) has proven to be a multifunctional porous material. Parent P(DEBA) was active in reversible chemisorption of low alcohols and primary amines through binding them in the form of acetals and Schiff bases, respectively. The complete release of chemisorbed compounds was achieved by acid hydrolysis under P(DEBA) regeneration. The covalent modification of P(DEBA) with an excess of ethylene diamine gave microporous network with a high content of primary amino group, P(DEBA)/EDA2. Thanks to the basicity of decorating NH_2 groups, the P(DEBA)/EDA2 was highly efficient in physisorption of ibuprofen and CO_2. P(DEBA)/EDA2 was also active as a heterogeneous catalyst of aldol condensation of *n*-heptanal with benzaldehyde giving desirable jasminaldehyde with moderate selectivity.

Acknowledgements

Financial support from the Czech Science Foundation (Project No. 17-03474S), the Science Foundation of Charles University (A. Hašková, Project No. 88217) is gratefully acknowledged. This work was realized within the Operational Programme Prague – Competitiveness (CZ.2.16/3.1.00/24501) and "National Program of Sustainability" (NPU I LO1613) MSMT-43760/2015. This work has also been supported by Charles University Research Centre program No. UNCE/SCI/014. Authors thank Dr. T. Faukner (Charles University) for valuable discussion.

Data availability

The raw/processed data required to reproduce these findings cannot be shared at this time as the data also forms part of an ongoing study.

Appendix A. Supplementary material

Supplementary data to this article can be found online at https://doi.org/10.1016/j.eurpolymj.2019.02.039.

References

[1] N. Chaoui, M. Trunk, R. Dawson, J. Schmidt, A. Thomas, Trends and challenges for microporous polymers, Chem. Soc. Rev. 46 (11) (2017) 3302–3321.
[2] R. Dawson, A.I. Cooper, D.J. Adams, Nanoporous organic polymer networks, Prog. Polym. Sci. 37 (4) (2012) 530–563.
[3] D. Xu, J.N. Guo, F. Yan, Porous ionic polymers: design, synthesis, and applications, Prog. Polym. Sci. 79 (2018) 121–143.
[4] Q. Sun, Z.F. Dai, X.J. Meng, F.S. Xiao, Porous polymer catalysts with hierarchical structures, Chem. Soc. Rev. 44 (17) (2015) 6018–6034.
[5] S.K. Kundu, A. Bhaumik, Pyrene-based porous organic polymers as efficient catalytic support for the synthesis of biodiesels at room temperature, ACS Sustain. Chem. Eng. 3 (8) (2015) 1715–1723.
[6] L. Sekerová, M. Lhotka, E. Vyskočilová, T. Faukner, E. Slováková, J. Brus, L. Červený, J. Sedláček, Hyper-cross-linked polyacetylene type microporous networks decorated with terminal ethynyl groups as heterogeneous acid catalysts for acetalization and esterification reactions, Chem. Eur. J. 24 (55) (2018) 14742.
[7] J. Germain, F. Svec, J.M.J. Frechet, Preparation of size-selective nanoporous polymer networks of aromatic rings: potential adsorbents for hydrogen storage, Chem. Mat. 20 (22) (2008) 7069–7076.

[8] J.W. Xu, C. Zhang, Z.X. Qiu, Z.Y. Lei, B. Chen, J.X. Jiang, F. Wang, Synthesis and characterization of functional triphenylphosphine-containing microporous organic polymers for gas storage and separation, Macromol. Chem. Phys. 218 (22) (2017) 1700275.
[9] A. Zukal, E. Slováková, H. Balcar, J. Sedláček, Polycyclotrimers of 1,4-diethynylbenzene, 2,6-diethynylnaphthalene, and 2,6-diethynylanthracene: preparation and gas adsorption properties, Macromol. Chem. Phys. 214 (18) (2013) 2016–2026.
[10] Y.Z. Liao, J. Weber, B.M. Mills, Z.H. Ren, C.F.J. Faul, Highly efficient and reversible iodine capture in hexaphenylbenzene-based conjugated microporous polymers, Macromolecules 49 (17) (2016) 6322–6333.
[11] B. Lopez-Iglesias, F. Suárez-García, C. Aguilar-Lugo, A. González Ortega, C. Bartolomé, J.M. Martínez-Ilarduya, J.G. de la Campa, Á.E. Lozano, C. Álvarez, Microporous polymer networks for carbon capture applications, ACS Appl. Mater. Interfaces 10 (31) (2018) 26195–26205.
[12] Q.J. Zhang, Y. Sen, Q. Wang, Q. Xiao, Y. Yue, S.J. Ren, Fluorene-based conjugated microporous polymers: preparation and chemical sensing application, Macromol. Rapid Commun. 38 (23) (2017) 1700445.
[13] J. Sedláček, J. Sokol, J. Zedník, T. Faukner, M. Kubů, J. Brus, O. Trhlíková, Homo- and copolycyclotrimerization of aromatic internal diynes catalyzed with Co-2(CO)(8): a facile route to microporous photoluminescent polyphenylenes with hyperbranched or crosslinked architecture, Macromol. Rapid Commun. 39 (4) (2018) 1700518.
[14] A. Patra, U. Scherf, Fluorescent microporous organic polymers: potential testbed for optical applications, Chem.-Eur. J. 18 (33) (2012) 10074–10080.
[15] J.R. Holst, E. Stockel, D.J. Adams, A.I. Cooper, High surface area networks from tetrahedral monomers: metal-catalyzed coupling, thermal polymerization, and "click" chemistry, Macromolecules 43 (20) (2010) 8531–8538.
[16] U.H.F. Bunz, K. Seehafer, F.L. Geyer, M. Bender, I. Braun, E. Smarsly, J. Freudenberg, Porous polymers based on aryleneethynylene building blocks, Macromol. Rapid Commun. 35 (17) (2014) 1466–1496.
[17] R. Dawson, A. Laybourn, R. Clowes, Y.Z. Khimyak, D.J. Adams, A.I. Cooper, Functionalized conjugated microporous polymers, Macromolecules 42 (22) (2009) 8809–8816.
[18] M.H. Alkordi, R.R. Haikal, Y.S. Hassan, A.H. Emwas, Y. Belmabkhout, Poly-functional porous-organic polymers to access functionality – CO2 sorption energetic relationships, J. Mater. Chem. A 3 (45) (2015) 22584–22590.
[19] Y. Xie, T.T. Wang, X.H. Liu, K. Zou, W.Q. Deng, Capture and conversion of CO2 at ambient conditions by a conjugated microporous polymer, Nat. Commun. 4 (2013) 7.
[20] J.X. Jiang, C. Wang, A. Laybourn, T. Hasell, R. Clowes, Y.Z. Khimyak, J.L. Xiao, S.J. Higgins, D.J. Adams, A.I. Cooper, Metal-organic conjugated microporous polymers, Angew. Chem.-Int. Edit. 50 (5) (2011) 1072–1075.
[21] K. Dong, Q. Sun, X.J. Meng, F.S. Xiao, Strategies for the design of porous polymers as efficient heterogeneous catalysts: from co-polymerization to self-polymerization, Catal. Sci. Technol. 7 (5) (2017) 1028–1039.
[22] Q. Sun, Z.F. Dai, X.L. Liu, N. Sheng, F. Deng, X.J. Meng, F.S. Xiao, Highly efficient heterogeneous hydroformylation over Rh-metalated porous organic polymers: synergistic effect of high ligand concentration and flexible framework, J. Am. Chem. Soc. 137 (15) (2015) 5204–5209.
[23] S. Bhunia, B. Banerjee, A. Bhaumik, A new hypercrosslinked supermicroporous polymer, with scope for sulfonation, and its catalytic potential for the efficient synthesis of biodiesel at room temperature, Chem. Commun. 51 (24) (2015) 5020–5023.
[24] B. Kiskan, J. Weber, Versatile postmodification of conjugated microporous polymers using thiol-yne chemistry, ACS Macro Lett. 1 (1) (2012) 37–40.
[25] T. Ratvijitvech, R. Dawson, A. Laybourn, Y.Z. Khimyak, D.J. Adams, A.I. Cooper, Post-synthetic modification of conjugated microporous polymers, Polymer 55 (1) (2014) 321–325.
[26] S. Mondal, S.K. Kundu, A. Bhaumik, A facile approach for the synthesis of hydroxyl-rich microporous organic networks for efficient CO2 capture and H2 storage, Chem. Commun. 53 (18) (2017) 2752–2755.
[27] C. Xu, N. Hedin, Synthesis of microporous organic polymers with high CO2-over-N2 selectivity and CO2 adsorption, J. Mater. Chem. A 1 (10) (2013) 3406–3414.
[28] M.G. Schwab, D. Crespy, X.L. Feng, K. Landfester, K. Mullen, Preparation of microporous melamine-based polymer networks in an anhydrous high-temperature miniemulsion, Macromol. Rapid Commun. 32 (22) (2011) 1798–1803.
[29] G.Y. Li, B. Zhang, J. Yan, Z.G. Wang, The directing effect of linking units on building microporous architecture in tetraphenyladmantane-based poly(Schiff base) networks, Chem. Commun. 50 (15) (2014) 1897–1899.
[30] J. Liu, J.S. Cui, F. Vilela, J. He, M. Zeller, A.D. Hunter, Z.T. Xu, In situ production of silver nanoparticles on an aldehyde-equipped conjugated porous polymer and subsequent heterogeneous reduction of aromatic nitro groups at room temperature, Chem. Commun. 51 (61) (2015) 12197–12200.
[31] C. Xu, Z. Bacsik, N. Hedin, Adsorption of CO2 on a micro-/mesoporous polyimine modified with tris(2-aminoethyl)amine, J. Mater. Chem. A 3 (31) (2015) 16229–16234.
[32] V. Guillerm, L.J. Weselinski, M. Alkordi, M.I.H. Mohideen, Y. Belmabkhout, A.J. Cairns, M. Eddaoudi, Porous organic polymers with anchored aldehydes: a new platform for post-synthetic amine functionalization en route for enhanced CO2 adsorption properties, Chem. Commun. 50 (16) (2014) 1937–1940.
[33] T. Masuda, Substituted polyacetylenes: synthesis, properties, and functions, Polym. Rev. 57 (1) (2017) 1–14.
[34] J. Sedláček, H. Balcar, Substituted polyacetylenes prepared with Rh catalysts: from linear to network-type conjugated polymers, Polym. Rev. 57 (1) (2017) 31–51.
[35] O. Trhlíková, J. Zedník, H. Balcar, J. Brus, J. Sedláček, [Rh(cycloolefin)(acac)] complexes as catalysts of polymerization of aryl- and alkylacetylenes: influence of cycloolefin ligand and reaction conditions, J. Mol. Catal. A: Chem. 378 (2013) 57–66.
[36] P. Mastrorilli, C.F. Nobile, V. Gallo, G.P. Suranna, G. Farinola, Rhodium(I) catalyzed polymerization of phenylacetylene in ionic liquids, J. Mol. Catal. A: Chem. 184 (1–2) (2002) 73–78.
[37] J. Sedláček, L. Havelková, J. Zedník, R. Coufal, T. Faukner, H. Balcar, J. Brus, Unexpectedly facile Rh(I) catalyzed polymerization of ethynylbenzaldehyde type monomers: synthesis of polyacetylenes bearing reactive and easy transformable pendant Carbaldehyde Groups, Macromol. Rapid Commun. 38 (2017) 1600792.
[38] E. Slováková, M. Ješelnik, E. Žagar, J. Zedník, J. Sedláček, S. Kovačič, Chain-growth insertion polymerization of 1,3-diethynylbenzene high internal phase emulsions into reactive π-conjugated foams, Macromolecules 47 (15) (2014) 4864–4869.
[39] E. Slováková, A. Zukal, J. Brus, H. Balcar, L. Brabec, D. Bondarev, J. Sedláček, Transition-metal-catalyzed chain-growth polymerization of 1,4-diethynylbenzene into microporous crosslinked poly(phenylacetylene)s: the effect of reaction conditions, Macromol. Chem. Phys. 215 (19) (2014) 1855–1869.
[40] V. Hanková, E. Slováková, J. Zedník, J. Vohlídal, R. Sivkova, H. Balcar, A. Zukal, J. Brus, J. Sedláček, Polyacetylene-type networks prepared by coordination polymerization of diethynylarenes: new type of microporous organic polymers, Macromol. Rapid Commun. 33 (2012) 158–163.
[41] Y. Yuan, H.L. Huang, L. Chen, Y.L. Chen, N, N '-Bicarbazole: A versatile building block toward the construction of conjugated porous polymers for CO2 capture and dyes adsorption, Macromolecules 50 (13) (2017) 4993–5003.
[42] C. Charnay, S. Begu, C. Tourne-Peteilh, L. Nicole, D.A. Lerner, J.M. Devoisselle, Inclusion of ibuprofen in mesoporous templated silica: drug loading and release property, Eur. J. Pharm. Biopharm. 57 (3) (2004) 533–540.
[43] Z.X. Huo, Q.H. Wan, L. Chen, Synthesis and evaluation of porous polymethylsilsesquioxane microspheres as low silanol activity chromatographic stationary phase for basic compound separation, J. Chromatogr. A 1553 (2018) 90–100.
[44] R. Dawson, A.I. Cooper, D.J. Adams, Chemical functionalization strategies for carbon dioxide capture in microporous organic polymers, Polym. Int. 62 (3) (2013) 345–352.
[45] E. Vrbková, E. Vyskočilová, L. Červený, Potassium modified alumina as a catalyst for the aldol condensation of benzaldehyde with linear C3–C8 aldehydes, React. Kinet. Mech. Catal. 121 (1) (2017) 307–316.
[46] E. Vrbková, Z. Tišler, E. Vyskočilová, D. Kadlec, L. Červený, Aldol condensation of benzaldehyde and heptanal: a comparative study of laboratory and industrially prepared Mg-Al mixed oxides, J. Chem. Technol. Biotechnol. 93 (1) (2018) 166–173.

Supplementary Data

Synthesis of hyper-cross-linked microporous poly(phenylacetylene)s having aldehyde and other groups and their chemisorption and physisorption ability

Lucie Havelková[a], Alena Hašková[a], Bogdana Bashta[a], Jiří Brus[b], Miloslav Lhotka[c], Eva Vrbková[d], Martin Kindl[d], Eliška Vyskočilová[d]*, Jan Sedláček[a]*

[a]Department of Physical and Macromolecular Chemistry, Faculty of Science, Charles University in Prague, Hlavova 2030, 128 43 Prague 2, Czech Republic
E-mail: jan.sedlacek@natur.cuni.cz

[b]Institute of Macromolecular Chemistry, v.v.i., Academy of Sciences of the Czech Republic, Heyrovský Sq. 2, 162 06 Prague 6, Czech Republic

[c]Department of Inorganic Technology, University of Chemistry and Technology in Prague, Technická 5, Prague 6, 166 28, Czech Republic

[d]Department of Organic Technology, University of Chemistry and Technology in Prague, Technická 5, Prague 6, 166 28, Czech Republic
E-mail: eliska.vyskocilova@vscht.cz

Postpolymerization covalent modification of P(DEBA) with ethylendiamine

The postpolymerization covalent modification of P(DEBA) with ethylenediamine (EDA) was performed in methanol at room temperature under stirring. The reaction time was 14 days. 250 mg of P(DEBA) (1.6 mmol of HC=O) was reacted with 49 mg of EDA (1.6 mmol of NH_2 groups) under formation of modified network P(DEBA)/EDA1. For preparing P(DEBA)/EDA2 modified network, 250 mg of P(DEBA) (1.6 mmol of HC=O) was reacted with 486 mg of EDA (16 mmol of NH_2 groups). Samples of P(DEBA) covalently modified with EDA were separated by filtration, repeatedly washed with methanol to remove physisorbed EDA and dried in vacuum at room temperature to constant weight. Modified samples were subsequently analyzed by ^{13}C CP/MAS NMR to evaluate the character and extent of EDA chemisorption.

Chemisorption of *p*-toluidine and *N*-methylaniline on P(DEBA)

The chemisorption of aromatic amines on P(DEBA) was performed in methanol at room temperature under stirring. In a typical experiment, 250 mg of P(DEBA) was dispersed in 2 ml of methanol and solution of 870 mg of *p*-toluidine in 4 ml methanol was added. An excess of *p*-toluidine (NH_2 groups to HC=O groups mole ratio = 5) was used with the aim to achieve maximum chemisorption capacity of P(DEBA). After 7 days, the P(DEBA) with chemisorbed *p*-toluidine was separated by filtration, repeatedly washed with methanol to remove physisorbed *p*-toluidine and dried under vacuum at room temperature to constant weight. P(DEBA) with chemisorbed *p*-toluidine was subsequently analyzed by ^{13}C CP/MAS NMR to verify the *p*-toluidine chemisorption and to determine the *p*-toluidine loading. The desorption of *p*-toluidine was performed in 50 ml methanol/HCl (100/1; v/v) under stirring for 48 h. After *p*-toluidine desorption, the P(DEBA) chemisorbent was regenerated by washing with H_2O/HCl (100/1; v/v) for 24 h.

Chemisorption of methanol and ethanol on P(DEBA)

The chemisorption of methanol and ethanol on P(DEBA) was performed at room temperature under stirring in neat methanol and ethanol containing HCl (1 vol.%). Neat alcohols were used with the aim to achieve maximum chemisorption capacity of P(DEBA). In a typical experiment, 250 mg of P(DEBA) was dispersed in methanol (50 ml) and the dispersion was mixed for 7 days. The P(DEBA) with chemisorbed methanol was then separated by filtration and dried under vacuum at room temperature to constant weight. P(DEBA) with chemisorbed methanol was subsequently analyzed by ^{13}C CP/MAS NMR to verify the methanol chemisorption and to determine the methanol loading. The desorption of methanol and

regeneration of P(DEBA) chemisorbent was performed in one step in 50 ml H_2O/HCl (100/1; v/v) under stirring for 48 h.

Ibuprofen (IBU) physisorption on polymer networks

In a typical experiment, a polymer network tested as a physisorbent (50 mg) was loaded to 22 ml glass vial and 10 ml of the solution of IBU in toluene (concentration = 6 mg/ml) was added. A vial was closed, assembled to the shaker and shaken at 1500 rpm for the desired time. Samples of liquid phase were taken at certain intervals, filtered through a syringe filter (45 μm) and analyzed using Shimadzu GC 2010 chromatograph fitted with nonpolar column DB-5 (35 m, 0.2 mm diameter, 0.35 μm film) and coupled with quadrupole mass analyzer.

Application of polymer networks as catalysts for aldol condensation of benzaldehyde with *n*-heptanal

In a typical experiment, 25 ml round-bottomed flask was equipped with a condenser and loaded with a polymer network serving as a catalyst (20 mg), toluene (1.5 ml), benzaldehyde (2.17 ml, 21 mmol) and the reaction mixture was heated to 80 °C. Then *n*-heptanal (1 ml, 7 mmol) was added. After 24 h, the reaction mixture was centrifuged and the liquid part was analyzed using Shimadzu GC 17A gas chromatograph fitted with nonpolar column ZB-5 (60 m, 0.32 mm diameter, 0.25 μm film) and FID.

Table S1. CO_2 sorption capacity of P(DEBA) and P(DEBA)/EDA2, a_{CO2}, at various temperatures at 0.1 bar and 7 bar CO_2 pressure.

Sample	a_{CO2} ($mgCO_2/g$)					
	p_{CO2} = 0.1 bar			p_{CO2} = 7 bar		
	T = 273 K	T = 293 K	T = 313 K	T = 273 K	T = 293 K	T = 313 K
P(DEBA)	18	9	5	240	175	135
P(DEBA)/EDA2	33	22	12	360	295	235

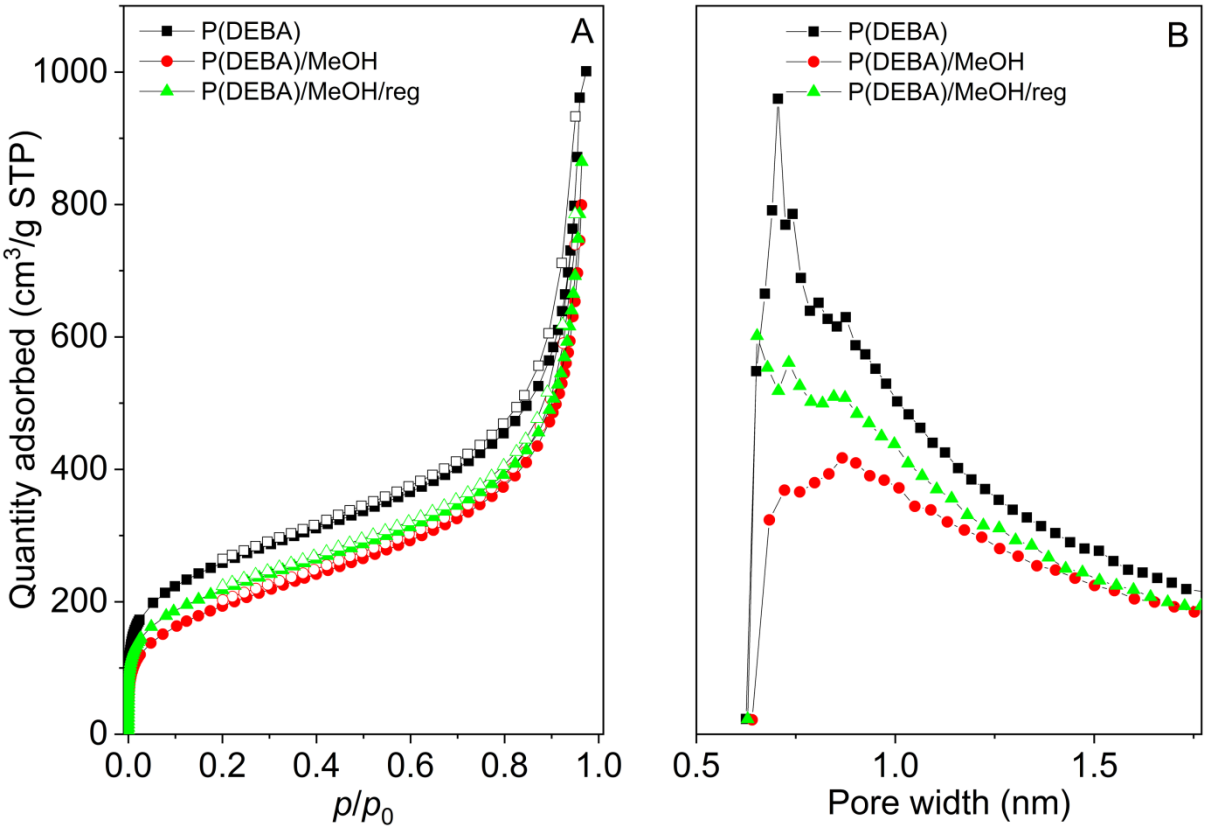

Figure S1 N_2 adsorption (full points) and desorption (empty points) isotherms (77 K) (A) and pore size distributions (B) for samples P(DEBA), P(DEBA)/MeOH, P(DEBA)/MeOH/reg

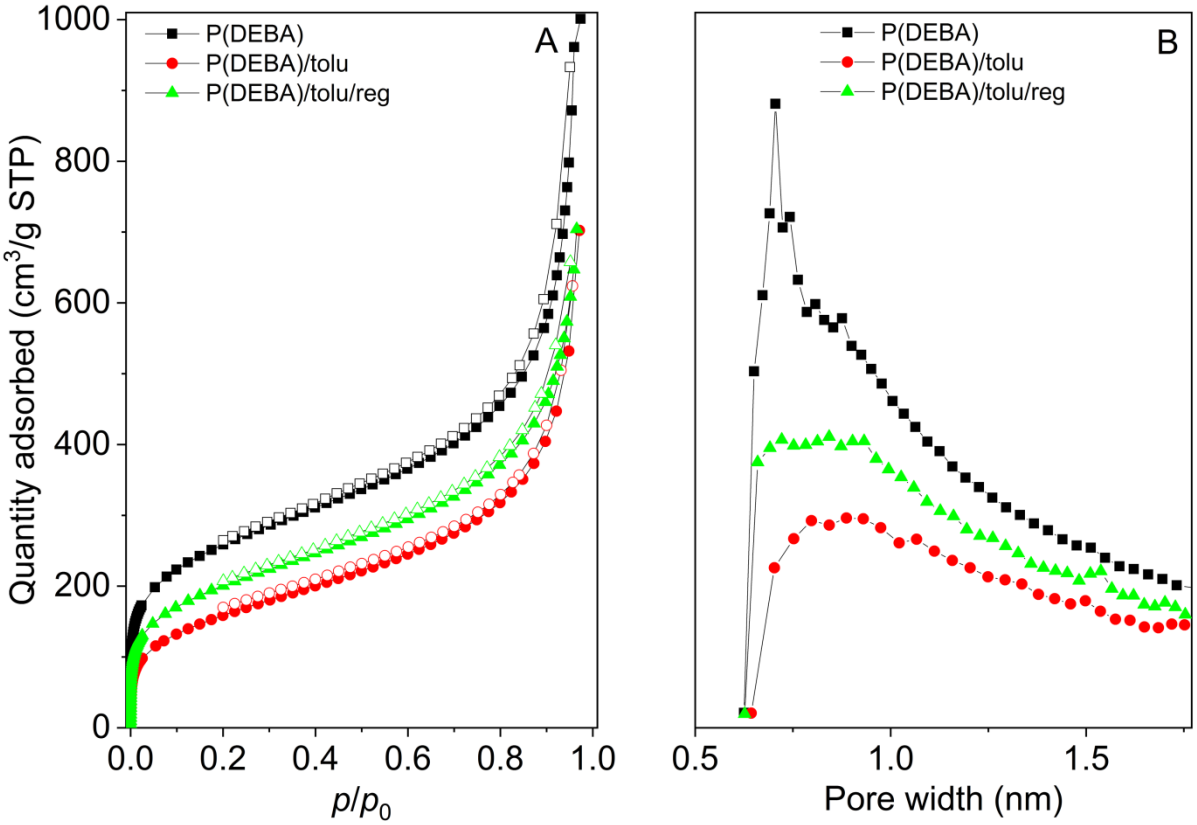

Figure S2 N_2 adsorption (full points) and desorption (empty points) isotherms (77 K) (A) and micropore size distributions (B) for samples P(DEBA), P(DEBA)/tolu and P(DEBA)/tolu/reg

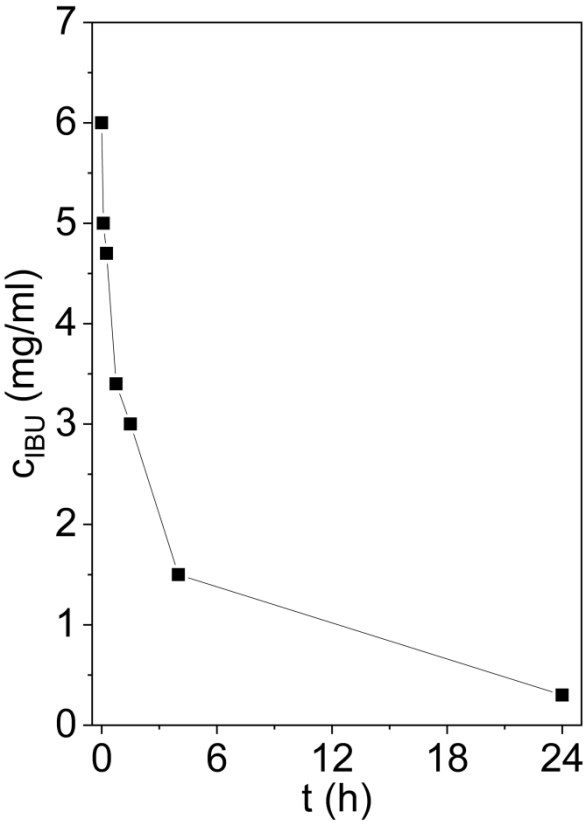

Figure S3 Time course of IBU physisorption on P(DEBA)/EDA2 shown as the time dependence of the concentration of IBU in toluene solution in which P(DEBA)/EDA2 is dispersed. Conditions: 50 mg P(DEBA)/EDA2, initial IBU concentration in toluene = 6.0 mg/ml, 10 ml of IBU solution, room temperature

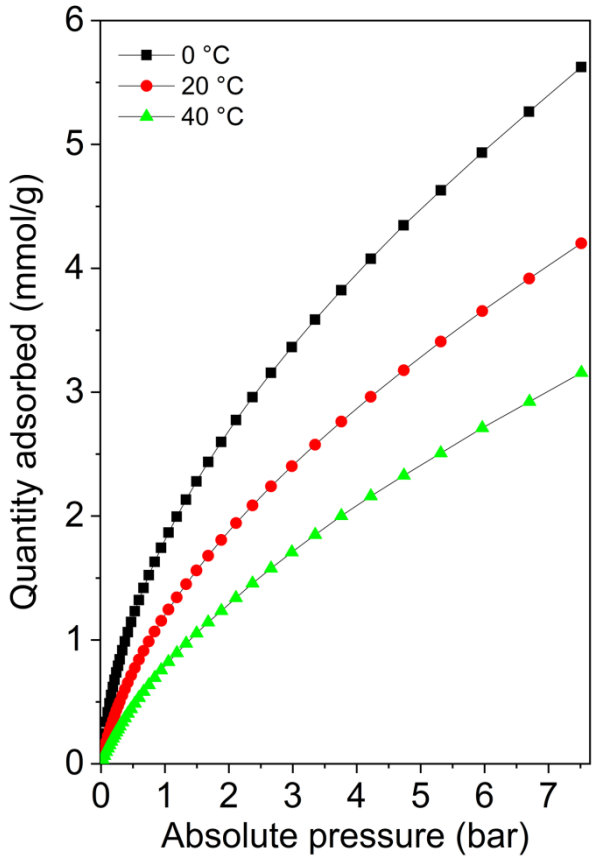

Figure S4 Temperature dependence of CO_2 adsorption isotherms on P(DEBA)

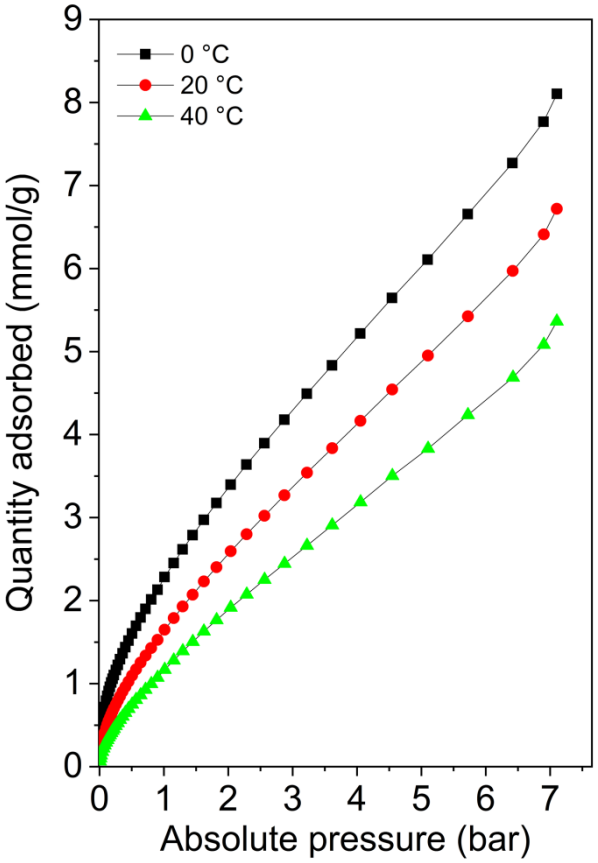

Figure S5 Temperature dependence of CO_2 adsorption isotherms on P(DEBA)/EDA2

III.

L. Havelková, B. Bashta, A. Hašková, A. Vagenknechtová, E. Vyskočilová, J. Brus, J. Sedláček: Combining polymerization and templating toward hyper-cross-linked poly(propargyl aldehyde)s and poly(propargyl alcohol)s for reversible H_2O and CO_2 capture and construction of porous chiral networks, *Polymers*, **2023**, *15*, 743.

polymers

MDPI

Article

Combining Polymerization and Templating toward Hyper-Cross-Linked Poly(propargyl aldehyde)s and Poly(propargyl alcohol)s for Reversible H_2O and CO_2 Capture and Construction of Porous Chiral Networks

Lucie Havelková [1,*], Bogdana Bashta [1], Alena Hašková [1], Alice Vagenknechtová [2], Eliška Vyskočilová [3], Jiří Brus [4] and Jan Sedláček [1,*]

[1] Department of Physical and Macromolecular Chemistry, Faculty of Science, Charles University, Hlavova 2030, 128 43 Prague, Czech Republic
[2] Department of Gaseous and Solid Fuels and Air Protection, University of Chemistry and Technology in Prague, Technická 5, 166 28 Prague, Czech Republic
[3] Department of Organic Technology, University of Chemistry and Technology in Prague, Technická 5, 166 28 Prague, Czech Republic
[4] Institute of Macromolecular Chemistry, Czech Academy of Sciences, Heyrovský Sq. 2, 162 00 Prague, Czech Republic
* Correspondence: lucie.havelkova@natur.cuni.cz (L.H.); jan.sedlacek@natur.cuni.cz (J.S.)

Abstract: Two series of hyper-cross-linked microporous polyacetylene networks containing either -[CH=C(CH=O)]- or -[CH=C(CH_2OH)]- monomeric units are reported. Networks are prepared by chain-growth copolymerization of acetal-protected propargyl aldehyde and acetal-protected propargyl alcohol with a 1,3,5-triethynylbenzene cross-linker followed by hydrolytic deprotection/detemplating. Deprotection not only liberates reactive CH=O and CH_2OH groups in the networks but also modifies the texture of the networks towards higher microporosity and higher specific surface area. The final networks with CH=O and CH_2OH groups attached directly to the polyene main chains of the networks have a specific surface area from 400 to 800 m^2/g and contain functional groups in a high amount, up to 9.6 mmol/g. The CH=O and CH_2OH groups in the networks serve as active centres for the reversible capture of CO_2 and water vapour. The water vapour capture capacities of the networks (up to 445 mg/g at 297 K) are among the highest values reported for porous polymers, making these materials promising for cyclic water harvesting from the air. Covalent modification of the networks with (*R*)-(+)-3-aminopyrrolidine and (*S*)-(+)-2-methylbutyric acid enables the preparation of porous chiral networks and shows networks with CH=O and CH_2OH groups as reactive supports suitable for the anchoring of various functional molecules.

Keywords: porous polymers; hyper-cross-linked; polyacetylenes; chiral modification; water harvesting

Citation: Havelková, L.; Bashta, B.; Hašková, A.; Vagenknechtová, A.; Vyskočilová, E.; Brus, J.; Sedláček, J. Combining Polymerization and Templating toward Hyper-Cross-Linked Poly(propargyl aldehyde)s and Poly(propargyl alcohol)s for Reversible H_2O and CO_2 Capture and Construction of Porous Chiral Networks. *Polymers* **2023**, *15*, 743. https://doi.org/10.3390/polym15030743

Academic Editor: Guipeng Yu

Received: 5 January 2023
Revised: 18 January 2023
Accepted: 29 January 2023
Published: 1 February 2023

1. Introduction

Organic polymer networks with permanent microporosity and high specific surface area, often referred to as porous organic polymers (POP) [1,2], represent an intensively studied group of porous materials, promising for catalytic [3,4], sorption [5–7], separation [8,9], sensing [10], and other applications. The high application potential of POPs reflects the wide variability of texture, composition, and covalent structure that can be achieved with these materials by properly combining and tuning the polymer and organic synthesis procedures used for their preparation. For example, POPs containing various acid and base groups, covalently inbuilt organometallic complexes, and electroactive and photoactive segments were developed for applications in heterogeneous organocatalysis [11,12], organometallic catalysis [13], electrocatalysis [14], and photocatalysis [15]. Texturally and covalently diverse POPs were prepared for reversible CO_2 capture: non-functional POPs

with an ultra-high specific surface area were revealed to be efficient for high-pressure CO_2 capture [16], while functionalized POPs with a significantly lower specific surface area were suitable for the low-pressure CO_2 trapping [17,18]. Several POPs with polar segments were prepared and tested in reversible water vapour capture from the air [19,20]. On the contrary, highly hydrophobic fluorine-rich POPs were also prepared [21,22] and applied to capture the vapour of non-polar hydrocarbons and fluorinated compounds. Application-interesting POPs with ionic [20,23], luminescent [24], chiral [25,26], and other groups [27,28] were also reported in the literature. Unlike inorganic porous materials (zeolites, molecular sieves) or MOF-type materials, POPs are mostly highly stable in an aqueous environment, even in the presence of acids, bases, and salts. Thanks to this, POPs appear to be promising adsorbents for the capture of a wide range of adsorptives and are comparable to COF-type adsorbents.

Functionalization of POPs (crucial for most applications) was mostly achieved by the so-called prepolymerization functionalization approach consisting of the polymerization of monomers bearing heteroatom groups or segments in addition to the polymerization-active groups. Bivalent and trivalent heteroatom segments were inbuilt into POPs, often in the form of networks knots created in the course of polymerization (e.g., triazole [29], imine knots [30]) or in the form of cyclic building blocks [17,31–34]. Univalent functional groups were inbuilt into POPs mostly as substituents (pendant groups) of hydrocarbon aromatic building blocks. For example, Cooper et al. copolymerized 1,3,5-triethynylbenzene with dibromoarenes ring-substituted with various groups (NO_2, OMe, COOMe, CF_3, NH_2, OH) via Sonogashira cross-coupling under elimination of HBr and formation of functionalized poly(aryleneethynylene) type POPs. The functional groups were preserved in the resulting POPs [35]. This concept was adopted by many other authors, and POPs with various univalent functional groups were prepared by step-growth polymerizations using coupling [36], cyclotrimerization [37], knitting [36,38], and other reactions. The chain-growth polymerization approach was also efficient for the synthesis of functionalized POPs. Radical polymerizations of vinyl comonomers and cross-linkers into functionalized POPs were well reviewed in ref. [39]. Our group described the preparation of functionalized polyacetylene POPs by chain-growth coordination and spontaneous polymerizations of ring-functionalized arylacetylenes [9,40,41].

The microporosity of POP is created during polymerization due to the rigidity of the building blocks of POPs and their extensive cross-linking, which prevents tight packing of the network segments. As a result, POPs contain unoccupied space forming micropores. Micropores can be accompanied by larger mesopores in POPs. Mesopores are believed to be formed by the covalent interconnecting of small particles of the microporous network in the later stages of polymerization. In some cases, the porosity of POPs was successfully modified by templating approach. Seo et al. used readily hydrolyzable polylactides as a template to introduce mesopores into hyper-cross-linked POPs prepared by a combination of radical polymerization and knitting reaction [42,43]. A combination of polymerization and high internal phase emulsion templating was efficient for preparing POPs containing both micropores and macropores [44,45]. Huang et al. used radical copolymerization of mixtures of monomers (di-*tert*-butyl-4,4′-stilbene dicarboxylate, *tert*-butyl 4-maleimidobenzoate, *tert*-butyl 4-vinylbenzoate, and divinylbenzene cross-linker) to prepare microporous POPs. The postpolymerization thermal or chemical modification led to the removal of *tert*-butyl groups accompanied by an increase in the micropore volume and the specific surface area of these POPs [46]. We recently reported hyper-cross-linked polyacetylene networks with aromatic template segments covalently attached to the scaffold via azomethine links. The postpolymerization hydrolysis of these links and the removal of template molecules led to a significant modification of the micropore size distribution and the specific surface area of the POPs [47,48]. In some cases, even non-porous networks were modified into POPs with a specific surface area of about 500 m^2/g by this templating approach [48].

In this paper, we report POPs of hyper-cross-linked polyacetylene-type with CH=O and CH_2OH groups attached directly (without any spacer) to the rigid polyacetylene main chains. Acetal-protected aliphatic monomers and chain-growth copolymerization followed

by deprotection and detemplating were used for the synthesis. Prepared POPs with a tuneable content of functional groups and texture were highly active in reversible water vapour capture and were demonstrated as supports for covalent anchoring of various functional molecules, e.g., chiral molecules, under preservation of porosity. The functional properties of POPs are discussed in relation to pore size distribution and the content of functional groups.

2. Materials and Methods

2.1. Materials

(Acetylacetonato)(norbornadiene)rhodium(I), [Rh(nbd)acac], (>98%), 1,3,5-triethynylbenzene, (TEB) (98%), propargylaldehyde diethyl acetal, (M1) (>97%), pent-1-yne (>98%) (all TCI Europe N.N., Zwijndrecht, Belgium), and acetaldehyde ethyl propargyl acetal, (M2) (98%, Acros Organics, Geel, Belgium) were used as obtained. Dichloromethane (99.95%, Lach-Ner Ltd., Neratovice, Czech Republic) was distilled with P_2O_5.

The following chemicals for the modifications were used as received: dansyl hydrazine (>97%), (*R*)-(+)-3-aminopyrrolidine (>98%) (all TCI Europe N.N., Zwijndrecht, Belgium), (*S*)-(+)-2-methylbutyric acid (98%, Sigma Aldrich Ltd., Prague, Czech Republic), *p*-toluenesulfonic acid (monohydrate, p.a., Lachema, Neratovice, Czech Republic), methanol (99.99% Lach-Ner Ltd., Neratovice, Czech Republic), benzene (anhydrous, 99.8%, Sigma Aldrich Ltd., Prague, Czech Republic).

2.2. Copolymerization

Copolymerizations of protected monomers M1 and M2 with 1,3,5-triethynylbenzene (TEB) were performed in CH_2Cl_2 at 75 °C in a sealed thick-wall ampoule under an argon atmosphere using [Rh(nbd)acac] as a polymerization catalyst. The overall initial concentration of monomers was 0.3 mol/dm^3; the concentration of [Rh(nbd)acac] was 15 mmol/dm^3. The mole ratios of the comonomers in the copolymerization feed were either M1 or M2:TEB = 1:1 for P(M1/TEB 1:1) and P(M2/TEB 1:1) networks, respectively, or M1 or M2:TEB = 3:1 concerning P(M1/TEB 3:1) and P(M2/TEB 3:1) networks, respectively. The polymerizations were started by adding the catalyst solution to the solution of monomers. The polymerizations were finished after 7 days by diluting the reaction mixture (containing the solid copolymer) with an excess of CH_2Cl_2. The solid copolymer network was separated, repeatedly washed with CH_2Cl_2, dried under vacuum at room temperature for 2 days to constant weight, and finally mechanically ground. The yield was determined gravimetrically. All polymerizations proceeded with quantitative yield.

2.3. Deprotection of Parent Networks

Typically, 400 mg of the parent copolymer network with protecting acetal groups were kept under stirring in deionized water (100 mL) containing HCl for up to 2 weeks at room temperature. The mole ratio of HCl to protecting groups was 10:1. Then the detemplated copolymer product was thoroughly washed to neutral pH with deionized water and dried under vacuum for 2 days at room temperature.

Details on the postpolymerization modification of P(M1/TEB 1:1)H and P(M2/TEB 1:1)H are given in Supplementary Material.

2.4. Techniques

2.4.1. NMR

All ^{13}C cross-polarization magic angle spinning (CP/MAS) NMR spectra were measured at 11.7 T using a Bruker Avance III 500 WB/US NMR spectrometer (Bruker Corporation, Billerica, MA, USA), as described elsewhere [17].

2.4.2. N_2 and CO_2 Adsorption

The adsorption/desorption isotherms of nitrogen (at 77 K) and CO_2 (at a range from 273 to 333 K) were measured at a Triflex V4.02 apparatus (Micromeritics Instrument

Corporation, Norcross, GA, USA). Prior to the sorption measurements, all the samples were degassed using Micromeritics SmartVacPrep instrument as described previously [17].

The Brunauer–Emmett–Teller specific surface area, S_{BET}, total pore volume, V_{tot}, and micropore volume V_{mi} are reported. The V_{mi} and V_{tot} values were determined according to the N_2 amount trapped at $p/p_0 = 0.1$ and $p/p_0 = 0.97$, respectively. The micropore size distribution was determined by the semi-empirical method of Horvath–Kawazoe. A model for the slit pore geometry (original Horvath–Kawazoe) with carbon–graphite adsorbent was used for the calculation of the size of the pores.

2.4.3. TGA

Thermogravimetric analysis (TGA) was performed on the Setsys Evolution apparatus (Seteram, Caluire-et-Cuire, France) under a nitrogen atmosphere using a heating rate 10 °C/min in a temperature range from 40 to 800 °C.

2.4.4. DVS

The water vapour sorption was measured using a DVS Advantage 2 instrument (Surface Measurement Systems Ltd., London, UK) at 297 K. The device allows monitoring of moisture adsorption under specified conditions.

Approximately 25 mg of the polymer network was first preheated to 100 °C for 120 min. The adsorption/desorption analysis was performed with a relative humidity (RH) setting of 0%–90%–0%–90%–0% (with intermediate steps of 10% RH) and a setting of 180 min for each step.

2.4.5. SEM

SEM measurements were performed using Tescan Lyra3 apparatus (TESCAN Brno, Ltd., Brno, Czech Republic) at an accelerating voltage of 10 kV.

3. Results and Discussion

3.1. Synthesis and Characterization of the Porous Networks

The synthetic part of this study aimed to prepare porous hyper-cross-linked polyacetylene networks containing carbaldehyde (-CH=O) and hydroxymethyl (-CH_2OH) groups attached (without any spacer) to the carbon atoms of linear vinylene units of the main chains of the networks. The chain-growth polymerization of substituted acetylenes used for the preparation of polyacetylenes is mostly reported to be tolerant to various heteroatom groups of the monomers [49–51]. However, in the case of the polyacetylene networks reported here, it was not possible to use respective acetylenes, prop-2-ynal, HC≡C-CH=O, and prop-2-yn-1-ol, HC≡C-CH_2OH, as starting (co)monomers for their preparation. Prop-2-ynal (propargyl aldehyde) is an extremely unstable compound, as reported in the literature [52,53]. Although prop-2-yn-1-ol (propargyl alcohol) is a stable compound, it is also unsuitable for the preparation of polyacetylene networks. Our preliminary experiments showed a poor polymerizability of this compound, apparently due to the presence of a reactive OH group in the vicinity of the polymerization-active ethynyl group. For the preparation of the discussed networks, we, therefore, proposed (i) to use acetylene monomers with protected carbaldehyde and hydroxymethyl groups, (ii) to incorporate these monomers into networks by means of copolymerizations with a proper ethynylated cross-linker, and finally (iii) to deprotect these (parent) networks under the formation of the final products with desired -[CH=C(CH=O)]- and -[CH=C(CH_2OH)]- monomeric units. Two monomers were used for this purpose (see Scheme 1): propargyl aldehyde diethyl acetal, M1 (i.e., the acetal-protected form of prop-2-ynal) and acetaldehyde ethyl propargyl acetal, M2 (i.e., the acetal-protected form of prop-2-yn-1-ol). Monomers M1 and M2 were (independently) copolymerized with 1,3,5-triethynylbenzene (TEB) serving as a cross-linker. Copolymerizations were catalysed with [Rh(nbd)acac] complex (see Scheme 1). The comonomer mole ratios in the feed, M1(or M2):TEB were 1:1 and 3:1 (see Section 2.2 for the details). All copolymerizations provided quantitative yields of respective

networks, which were labelled as follows: P(M1/TEB 1:1), P(M1/TEB 3:1), P(M2/TEB 1:1), and P(M2/TEB 3:1). The prepared networks were dark brown solids, totally insoluble in water, methanol, dichloromethane, tetrahydrofuran, and benzene. All networks showed no observable swelling in any above solvents.

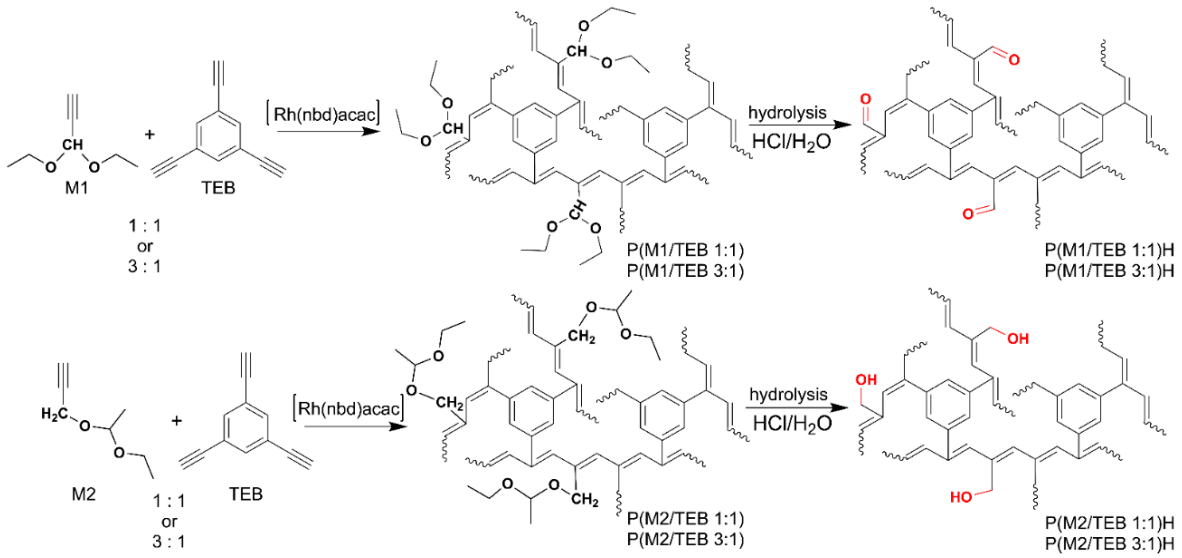

Scheme 1. Preparation of porous networks with CH=O and CH_2OH groups via chain-growth polymerization followed by hydrolytic deprotection.

The ^{13}C CP/MAS NMR spectra of P(M1/TEB 1:1), P(M1/TEB 3:1), P(M2/TEB 1:1), and P(M2/TEB 3:1) are shown in Figure 1. The broad dominating signal in the δ = 120–150 ppm region of all spectra corresponded to the resonance of aromatic carbon atoms of TEB units and polyene main-chain carbon atoms. The signal at δ = 80 ppm in all spectra was due to carbon atoms of unreacted ethynyl groups in the units formed from TEB. Evidently, not all TEB monomer molecules were incorporated into the networks through the polymerization transformation of all three ethynyl groups to form cross-linking units connecting the chains through benzene-1,3,5-triyl segments. Some TEB cross-linking units could contain one unreacted ethynyl group (cross-linking through benzene-1,3-diyl segments), and some TEB molecules could be incorporated into the networks as linear units possessing two unreacted ethyl groups (see ref. [54] for more details). The ^{13}C CP/MAS NMR spectra of P(M1/TEB 1:1) and P(M1/TEB 3:1) contained the distinct signals of carbaldehyde diethyl acetal pendant groups of the M1-type monomeric units. The sharp signal at δ = 14 ppm corresponded to the carbon atoms of methyl groups, the signal at δ = 62 ppm corresponded to carbons of -OCH_2- groups, and the signal at δ = 100 ppm was due to the -$CH(OEt)_2$ carbon atoms. Similarly, the ^{13}C CP/MAS NMR spectra of P(M2/TEB 1:1) and P(M2/TEB 3:1) contained signals characteristic of acetaldehyde ethyl methyl acetal pendant groups of the M2-type monomeric units. Partly distinguished signals at δ = 15 ppm and δ = 20 ppm belonged to carbon atoms of two different methyl groups of M2-type monomeric units (see Scheme 1). The signal at δ = 62 ppm corresponded to the resonance of carbon atoms of -OCH_2- groups and the signal at δ = 100 ppm was due to the carbon atoms of -O-$CH(CH_3)$-O- groups. As evident from Figure 1, the signals of carbon atoms of acetal groups were more pronounced in the spectra of P(M1/TEB 3:1), and P(M2/TEB 3:1) than in the spectra of P(M1/TEB 1:1), and P(M2/TEB 1:1). This corresponded well with the fact that P(M1/TEB 3:1), and P(M2/TEB 3:1) were richer in acetal groups containing units than P(M1/TEB 1:1) and P(M2/TEB 1:1). The above discussed ^{13}C CP/MAS NMR spectra of P(M1/TEB 1:1), P(M1/TEB 3:1), P(M2/TEB 1:1), and P(M2/TEB 3:1) networks were in good agreement with the structure of the networks given in Scheme 1. Prepared polymer networks consisted of polyacetylene (polyvinylene) main chains cross-linked with benzene linkers formed from

TEB. The linear units of the networks were decorated with acetal-protected carbaldehyde or hydroxymethyl groups. The spectra confirmed that no significant deprotection (detectable by ^{13}C CP/MAS NMR spectroscopy) occurred during the synthesis of the networks.

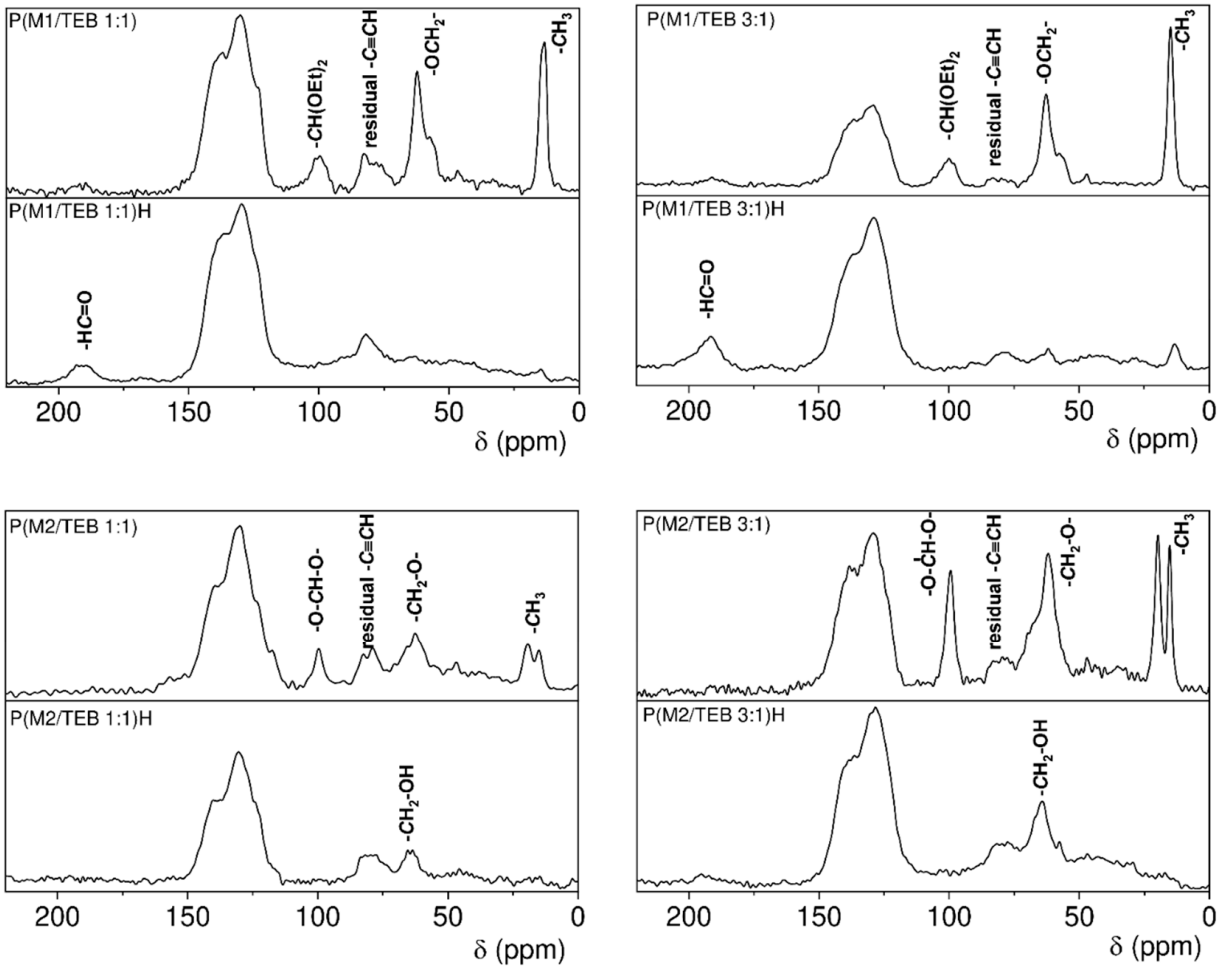

Figure 1. ^{13}C CP/MAS NMR spectra of prepared networks.

Networks P(M1/TEB 1:1), P(M1/TEB 3:1), P(M2/TEB 1:1), and P(M2/TEB 3:1) were subsequently submitted to the hydrolysis in HCl/H_2O (for details see Section 2.3) in order to decompose their acetal pendant groups and remove the low-molecular-weight products of the hydrolysis from the networks. Optimization of the hydrolysis procedure showed that a long reaction time (two weeks at room temperature) was required to ensure the quantitative extent of this process. The hydrolytic deprotection resulted in polymer networks labelled as follows: P(M1/TEB 1:1)H, P(M1/TEB 3:1)H, P(M2/TEB 1:1)H, and P(M2/TEB 3:1)H. ^{13}C CP/MAS NMR spectroscopy confirmed that the hydrolytic deprotection was highly effective, both in the case of networks with M1-type units and in the case of networks with M2-type units. This is evident from Figure 1, in which the ^{13}C CP/MAS NMR spectra of hydrolyzed networks P(M1/TEB 1:1)H, P(M1/TEB 3:1)H, P(M2/TEB 1:1)H, and P(M2/TEB 3:1)H are compared with the ^{13}C CP/MAS NMR spectra of parent networks P(M1/TEB 1:1), P(M1/TEB 3:1), P(M2/TEB 1:1), and P(M2/TEB 3:1). The ^{13}C CP/MAS NMR signals of aliphatic carbon atoms of acetal protecting groups were either absent or very weak in the spectra of all hydrolyzed networks. At the same time, ^{13}C CP/MAS NMR spectroscopy confirmed that the hydrolysis of the parent networks resulted in networks with the required carbaldehyde and hydroxymethyl groups. The ^{13}C CP/MAS NMR spectra of P(M1/TEB 1:1)H and P(M1/TEB 3:1)H contained a well-resolved signal of carbon atoms of -CH=O

groups at δ = 190 ppm. The presence of CH_2OH groups in P(M2/TEB 1:1)H and P(M2/TEB 3:1)H was manifested by a signal at δ = 62 ppm in ^{13}C CP/MAS NMR spectra (see Figure 1).

The covalent structure of the studied networks (rigid polyene main chains hyper-cross-linked with rigid aromatic linkers) was designed so that these networks could exhibit permanent porosity. The nitrogen adsorption/desorption measurements at 77 K confirmed this assumption: both parent and hydrolyzed networks exhibited a micro/mesoporous texture, as evident from the N_2 adsorption/desorption isotherms shown in Figure 2. The presence of the micropores in the networks was manifested by sharp N_2 uptake at low relative pressures. An increase in the adsorbed amount of N_2 at higher relative pressures and a hysteresis on the adsorption/desorption isotherms indicated the presence of mesopores and/or interparticle void volume in the networks. The values of texture parameters of the networks ascertained from the N_2 adsorption isotherms, i.e., Brunauer–Emmett–Teller specific surface area (S_{BET}), micropore volume (V_{mi}), and total pore volume (V_{tot}), are summarized in Table 1. The texture parameters of the parent networks depended on the type and content of linear units. The values of S_{BET}, V_{mi}, and V_{tot} decreased with increasing content of the M1- and M2-type units in the networks. It is obvious that the pendant groups of M1- and M2-type units, due to their flexibility, did not contribute to the formation of porosity and, on the contrary, could partly occupy the potential pores in the networks. Nevertheless, even in the case of P(M1/TEB 3:1) and P(M2/TEB 3:1), micro/mesoporosity and S_{BET} of 314 and 149 m^2/g, respectively, were achieved. Parent networks containing M1-type linear monomeric units generally showed higher values of S_{BET}, V_{mi}, and V_{tot} than parent networks with M2-type linear monomeric units. For example, the S_{BET} of 832 m^2/g was achieved for P(M1/TEB 1:1) while P(M2/TEB 1:1) exhibited a specific surface area roughly 50% lower (S_{BET} = 393 m^2/g). The reason could be the higher symmetry of the pendant groups of the M1-type units, thanks to which these groups might occupy less space in the network. The N_2 adsorption/desorption measurements further clearly proved that the above-described hydrolytic deprotection of M1- and M2-type linear units of parent networks was accompanied by an increase in the S_{BET} and V_{mi} values of the networks. All the hydrolyzed networks, i.e., P(M1/TEB 1:1)H, P(M1/TEB 3:1)H, P(M2/TEB 1:1)H, and P(M2/TEB 3:1)H had higher S_{BET} and V_{mi} values than their parent counterparts. (see Table 1 and Figure 2). The increase in S_{BET} due to hydrolytic deprotection was particularly significant in the case of networks containing M2-type units: compared to the parent networks P(M2/TEB 1:1) and P(M2/TEB 3:1), the hydrolyzed networks P(M2/TEB 1:1)H and P(M2/TEB 3:1)H showed more than twice higher specific surface area values (Table 1). The increase in the micropore volume due to the hydrolysis was also significant in these networks. Parent networks P(M2/TEB 1:1) and P(M2/TEB 3:1) showed V_{mi} of 0.13 and 0.05 cm^3/g, respectively, while the V_{mi} values of their hydrolyzed counterparts were 0.29 cm^3/g (P(M2/TEB 1:1)) and 0.17 cm^3/g (P(M2/TEB 3:1)). Moreover, the hydrolysis of the networks containing M1-type units was accompanied by an increase in S_{BET} and V_{mi} value although this increase was less pronounced. The S_{BET} values increased from 832 to 911 m^2/g due to the transformation of P(M1/TEB 1:1) to P(M1/TEB 1:1)H, the transformation of P(M1/TEB 3:1) to P(M1/TEB 3:1)H was accompanied by an increase in S_{BET} from 313 to 534 m^2/g. Figure 3 compares the micropore size distributions of the parent and hydrolyzed networks. The values of micropore width corresponding to the maxima of the distributions (D_{mi}) are given in Table 1. In the case of all networks, the micropore size distribution was shifted towards lower values of micropore width as a result of hydrolytic deprotection. The D_{mi} values of the parent networks P(M1/TEB 1:1), P(M1/TEB 3:1), P(M2/TEB 1:1), and P(M2/TEB 3:1) ranged from 0.9 to 1.1 nm while D_{mi} = 0.7 nm was determined for all hydrolyzed networks (Table 1). The hydrolytic deprotection of the parent networks proceeded through the decomposition of acetal groups, followed by the removal of aliphatic low-molecular-weight hydrolytic products from the networks. It should be noted that this process was not accompanied by a collapse of the hyper-cross-linked scaffold of the networks. On the contrary, the void volume occupied by the aliphatic protecting groups in the parent networks was emptied

under the formation of new micropores in the hydrolyzed networks. This led in parallel to an increase in S_{BET} values. Figure 4 shows scanning electron microscopy (SEM) images of the parent and hydrolyzed networks. The SEM method did not show any morphological changes due to the deprotection of the networks. Figure S1 of the Supplementary Materials shows the results of thermogravimetric analysis (TGA). The weight loss of all deprotected networks was less than 2% at 200 °C. The temperature values at which a weight loss of 5% was detected were as follows: 241 °C, P(M1/TEB 3:1)H, 248 °C, P(M2/TEB 3:1)H, 264 °C, P(M1/TEB 1:1)H, and 275 °C P(M2/TEB 1:1)H. Thus, the hydrolyzed networks showed relatively high temperature stability.

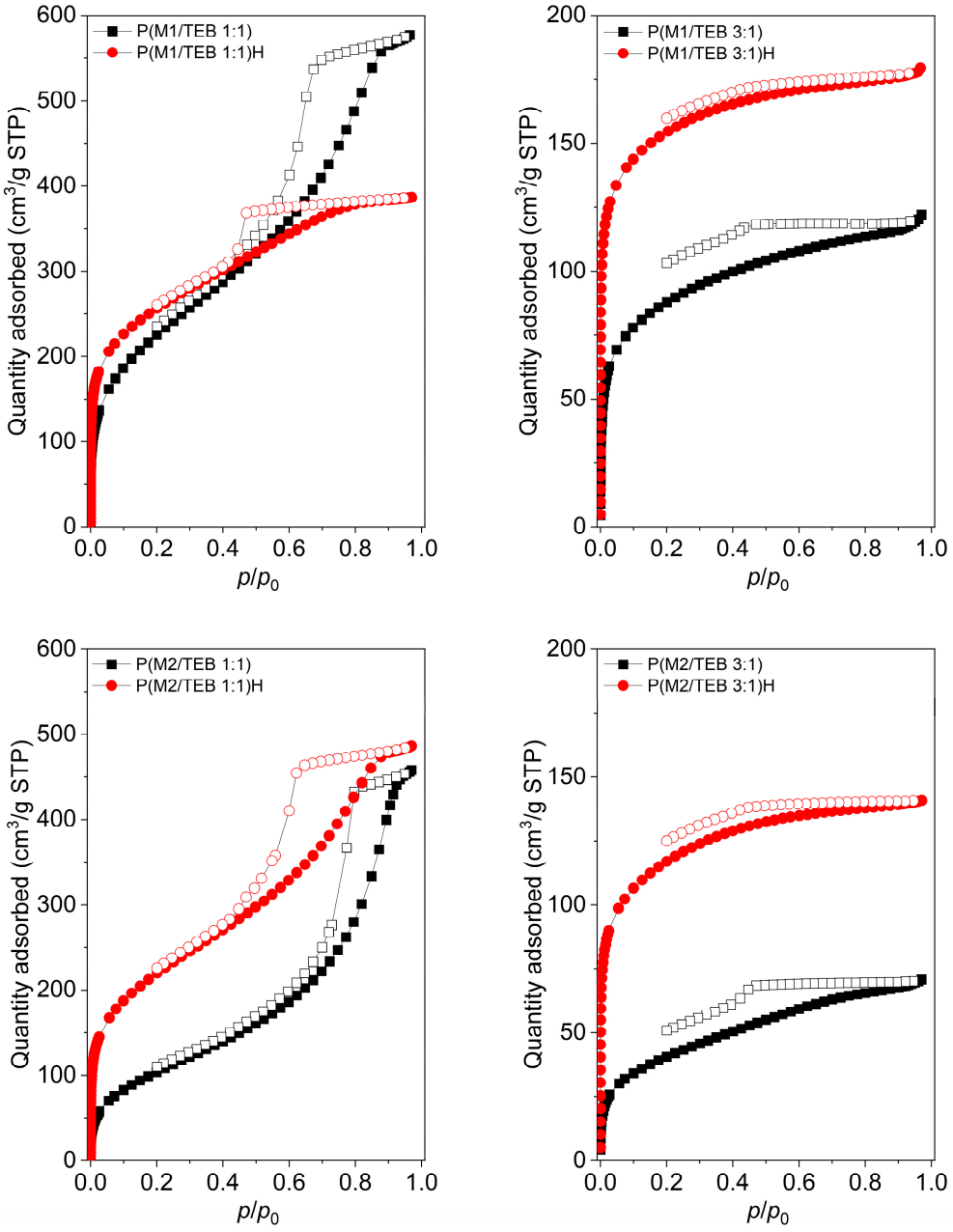

Figure 2. N_2 adsorption (full points) and desorption (empty points) isotherms (77 K) on the prepared networks.

Table 1. Specific surface area (S_{BET}), micropore volume (V_{mi}), total pore volume (V_{tot}), and micropore diameter (D_{mi}) (from N_2 adsorption isotherms) of prepared networks.

Network Code	S_{BET} (m^2/g)	V_{mi} (cm^3/g)	V_{tot} (cm^3/g)	D_{mi} (nm)
P(M1/TEB 1:1)	832	0.29	0.90	0.9
P(M1/TEB 1:1)H	911	0.35	0.60	0.7
P(M1/TEB 3:1)	313	0.12	0.19	1.1
P(M1/TEB 3:1)H	534	0.22	0.28	0.7
P(M2/TEB 1:1)	393	0.13	0.71	1
P(M2/TEB 1:1)H	794	0.29	0.76	0.7
P(M2/TEB 3:1)	149	0.05	0.11	1.1
P(M2/TEB 3:1)H	409	0.17	0.22	0.7

As discussed above, the hydrolytic deprotection of the parent networks was primarily aimed at obtaining networks with reactive carbaldehyde and hydroxymethyl groups. From the point of view of the texture of the networks, the performed deprotection can be considered at the same time as a detemplating process positively modifying the texture of the networks. The applied synthesis combining chain polymerization and deprotection/detemplating thus enabled the preparation of porous networks with a high content of CH=O and CH_2OH groups (up to 9.6 mmol/g) and a satisfactory specific surface area (S_{BET} from 400 to 800 m^2/g) suitable for various applications, as described in the following subsections.

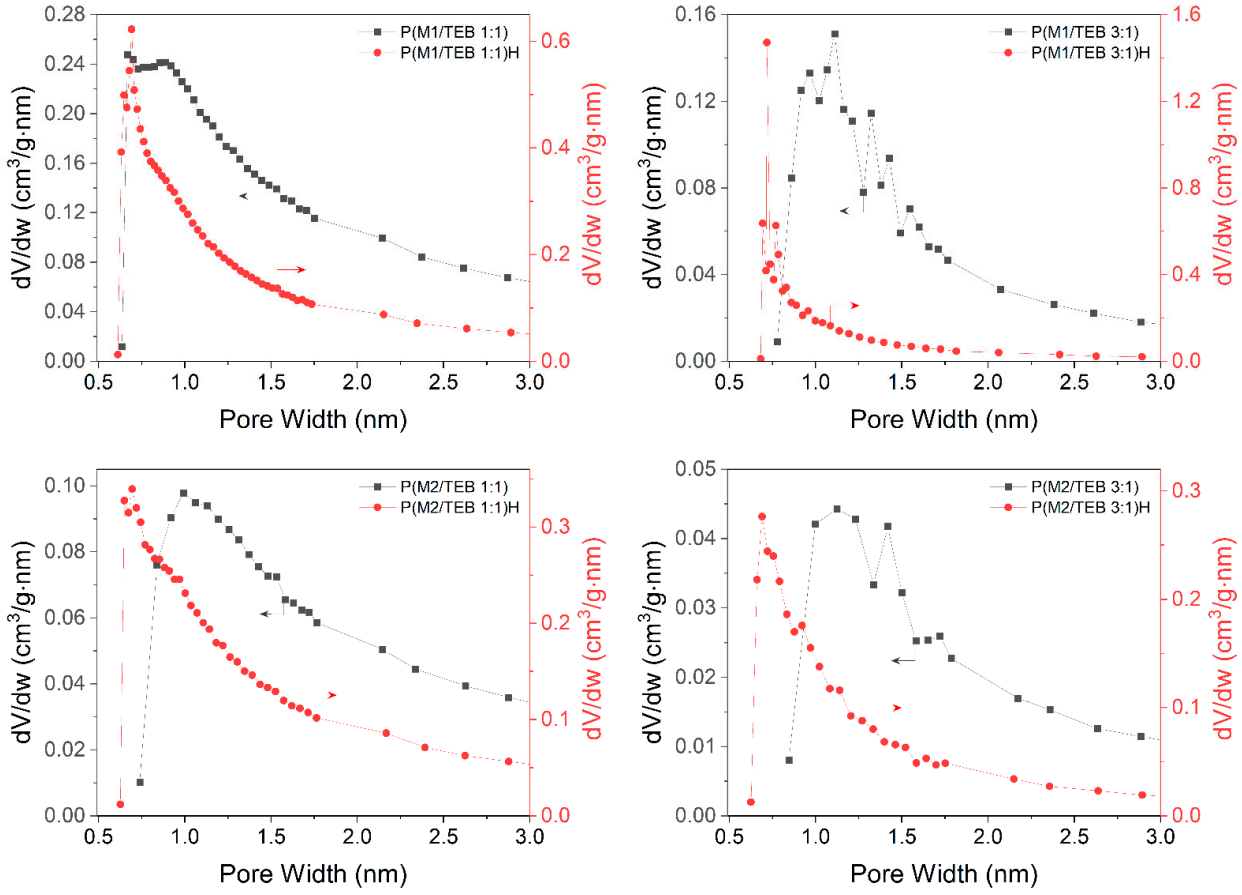

Figure 3. Micropore size distribution of prepared networks.

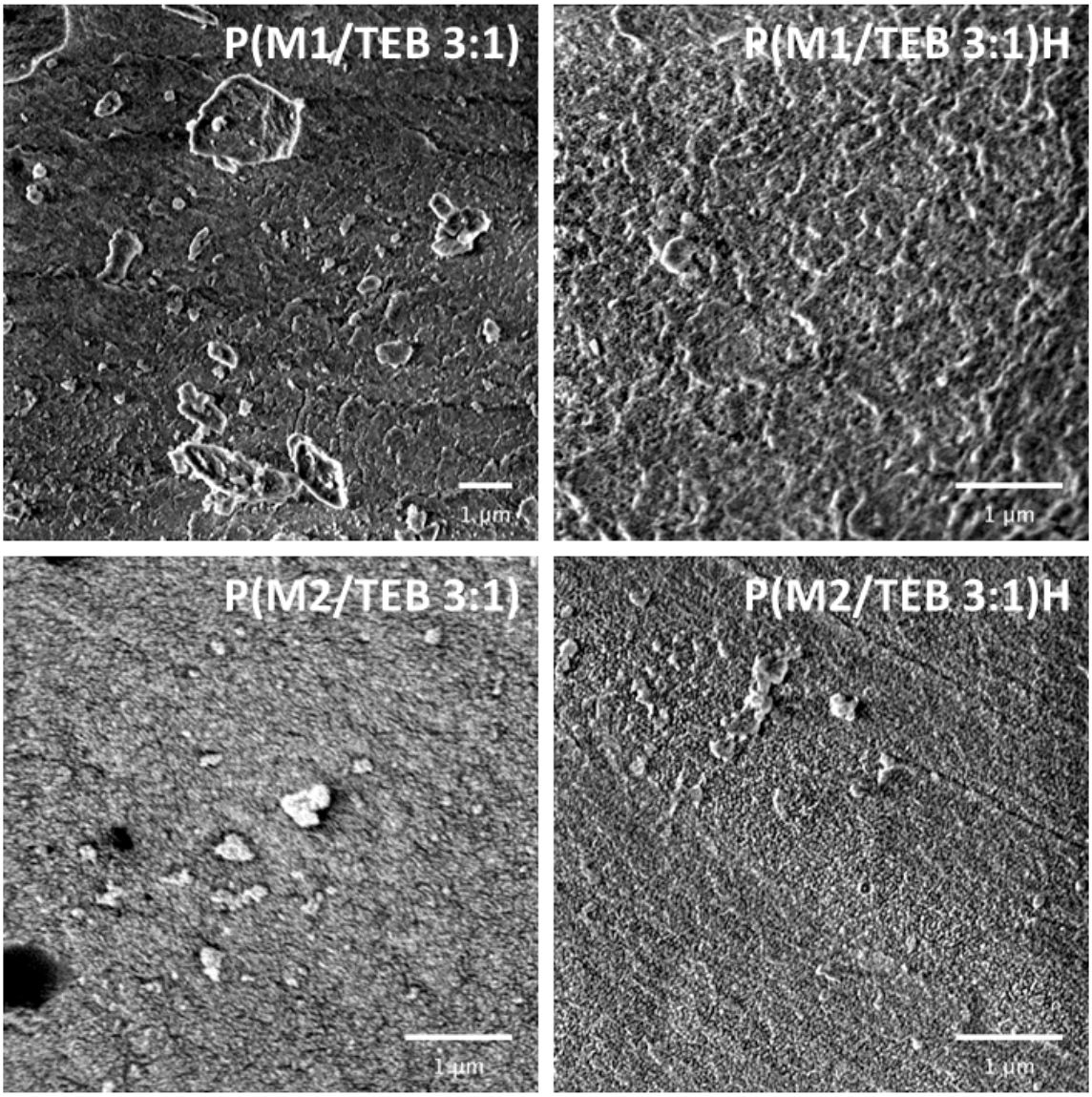

Figure 4. SEM images of the parent and hydrolyzed networks.

3.2. Water Vapour and Carbon Dioxide Capture

In order to evaluate the effect of CH=O and CH_2OH groups of P(M1/TEB 1:1)H, P(M1/TEB 3:1)H, P(M2/TEB 1:1)H and P(M2/TEB 3:1)H on the efficiency of these networks in capturing H_2O and CO_2 a heteroatom-free network was prepared as a comparison sample. Copolymerization of 1-pentyne with TEB cross-linker (3:1 in the feed) provided a P(pentyne/TEB 3:1) network containing -[CH=C($CH_2CH_2CH_3$)]- linear units and showing the following texture parameters: S_{BET} = 810 m^2/g, V_{mi} = 0.28 cm^3/g, and V_{tot} = 1.69 cm^3/g. Details on the synthesis and characterization of P(pentyne/TEB 3:1) are given in Supplementary Materials (Scheme S1, Table S1, Figures S2–S4).

The efficiency of the networks in capturing and releasing water vapour was investigated at 297 K (see Section 2.4.4 for detail). The H_2O adsorption/desorption isotherms are given in Figure 5. The corresponding time course of H_2O adsorption/desorption is shown in Figure S5 of the Supplementary Materials. Table 2 summarizes the capture capacities of the networks for H_2O (i) at relative humidity (RH) of 90% ($a_{H2ORH90}$) and (ii) at RH = 40% ($a_{H2ORH40}$). It is evident that the polar CH=O and CH_2OH groups in the prepared networks dramatically increased the efficiency of these materials in capturing water vapour in comparison to the hydrocarbon network P(pentyne/TEB 3:1). The values

of $a_{H2ORH90}$ ranged from 272 to 445 mg/g for CH=O and CH_2OH groups containing networks while $a_{H2ORH90}$ was only 36 mg/g for P(pentyne/TEB 3:1). The data in Table 2 and the character of the isotherms in Figure 5 indicated that two processes were most likely involved in the capture of water vapour in the functionalized networks: (i) adsorption of H_2O molecules on the surface of pores accompanied by trapping of H_2O in narrow micropores and (ii) capillary condensation of water in larger pores [55] (see Scheme 2). At lower RH values, the adsorption and filling of narrow micropores prevailed. The efficiency of these processes increased with the increasing content of polar groups in the networks. This is evident from Table 2, showing an increase in the value of $a_{H2ORH40}$ in parallel with an increase in the content of CH=O and CH_2OH groups in the networks in the following series: P(M1/TEB 1:1)H < P(M1/TEB 3:1)H and P(M2/TEB 1:1)H < P(M2/TEB 3:1)H. We assume that the CH=O and CH_2OH groups served in the networks as adsorption centres interacting with H_2O molecules via dipole–dipole interactions or weak hydrogen bonding. At higher RH values, the process of capillary condensation of H_2O in the larger pores most probably prevailed and thus significantly contributed to the values of capture capacities reached when RH = 90%, $a_{H2ORH90}$. The values of $a_{H2ORH90}$ increased in the series: P(M1/TEB 3:1)H < P(M1/TEB 1:1)H and P(M2/TEB 3:1)H < P(M2/TEB 1:1)H. This increase did not follow an increase in the extent of functionalization of the networks, but it correlated with an increase in V_{tot} values (see Table 2). We assume that the size of the pore volume available for capillary condensation (volume localized in mesopores or larger micropores) was an important or decisive factor in the efficiency of this process [56]. It is worth noting that in the case of P(M1/TEB 3:1)H and P(M2/TEB 3:1)H, the volume of water captured when RH = 90% roughly corresponded to the total pore volume of these networks determined by N_2 adsorption (see Table 2). It should, however, be emphasized that water capture by capillary condensation did not occur with the hydrocarbon network P(pentyne/TEB 3:1), despite its high V_{tot} value (1.69 cm^3/g). For effective capture of water by capillary condensation, prior coverage of the pore surface with water trapped by adsorption was evidently necessary.

Table 2. H_2O adsorption capacities $a_{H2ORH40}$ (at RH = 40%) and $a_{H2ORH90}$ (at RH = 90%) of the networks at 297 K. V_{tot} values were obtained from N_2 adsorption isotherms at 77 K.

Network Code	Polar Group Content (mmol/g)	V_{tot} (cm^3/g)	$a_{H2ORH40}$ (mg/g)	$a_{H2ORH90}$ (mg/g)
P(M1/TEB 1:1)H	4.90	0.60	100	445
P(M1/TEB 3:1)H	9.61	0.28	139	272
P(M2/TEB 1:1)H	4.85	0.76	56	422
P(M2/TEB 3:1)H	9.42	0.22	98	286
P(pentyne/TEB 3:1)	0	1.69	14	36

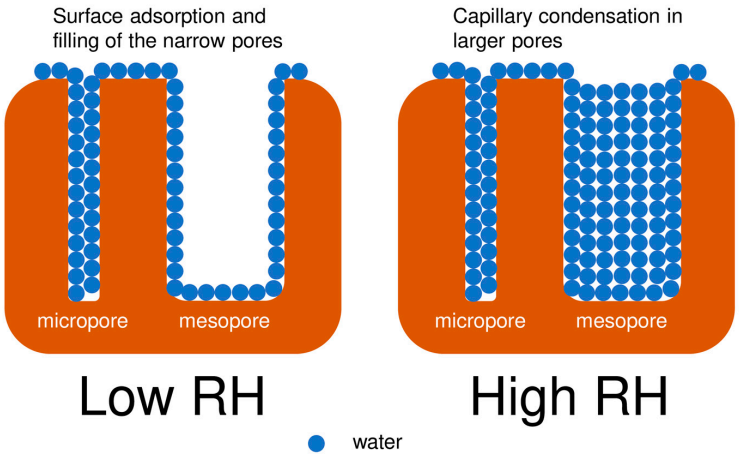

Scheme 2. Schematic mechanism of H_2O capture in networks.

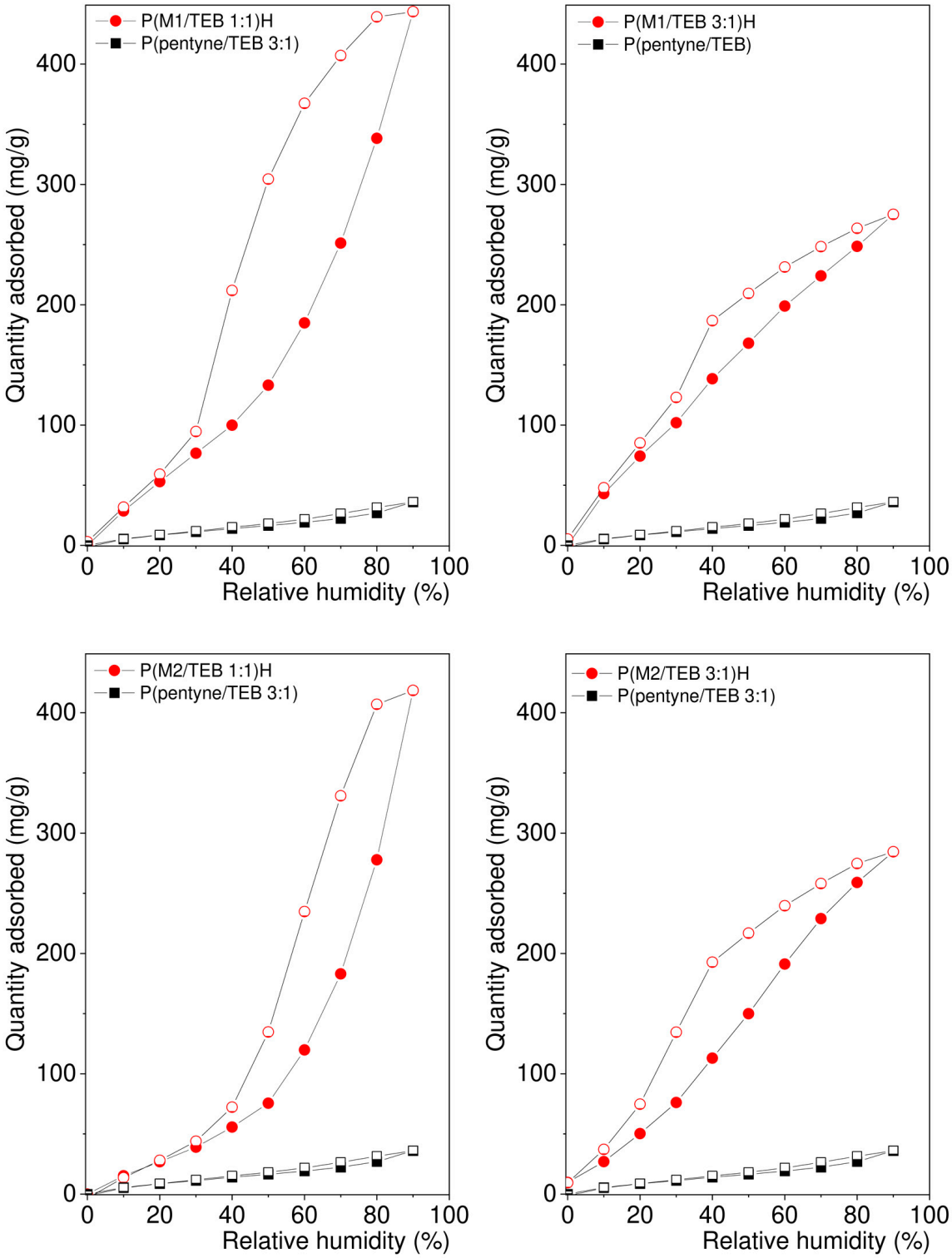

Figure 5. Water adsorption (full points) and desorption (empty points) isotherms (297 K) on the prepared networks.

The participation of capillary condensation in water capture on functionalized networks corresponded with the hysteresis loops on the adsorption/desorption isotherms given in Figure 5. The hysteresis loops were closed in the case of P(M1/TEB 1:1)H, P(M1/TEB 3:1)H, and P(M2/TEB 1:1)H when RH ≈ 20%, and the complete desorption of water from these networks was achieved by isothermal reduction of RH without the

need to increase the temperature. In the case of network P(M2/TEB 3:1)H, the hysteresis loop did not completely close even when RH = 0% (equilibration time 180 min). Nevertheless, the amount of water remaining in the network under these conditions was only 9 mg/g. The water adsorption/desorption isotherms on functionalized networks were well reproducible, as evident from Figure S6 in Supplementary Materials showing the isotherms for two consecutive H_2O adsorption/desorption cycles. Water capture capacities when RH = 90% of P(M1/TEB 1:1)H and P(M2/TEB 1:1)H, $a_{H2ORH90}$ = 445 mg/g and $a_{H2ORH90}$ = 422 mg/g, respectively, corresponded to the highest values reported for sorbents of the porous polymer-type [19,55]. For example, polyphenylene-type POPs functionalized with NH_2 and NO_2 groups exhibited water capture capacities from 290 to 350 mg/g (RH = 97%, 297 K) [37]. Values of $a_{H2ORH90}$ up to 420 mg/g (297 K) were achieved on POPs with epoxy functional groups [57]. Pyridine containing hyper-cross-linked POPs reported recently by our group exhibited $a_{H2ORH90}$ up to 376 mg/g [17]. Water capture capacity of about 550 mg/g, (RH = 90%, 297 K) was reported for ionic POPs with quaternized 1,4-diazabicyclo[2.2.2]octane-type units [20]. Water capture capacities of P(M1/TEB 1:1)H and P(M2/TEB 1:1)H were comparable with capacities reported for various COF-type materials (e.g., COFs with functionalized aromatic building blocks, $a_{H2ORH90}$ up to 700 mg/g [58] and COFs with imine links, $a_{H2ORH90}$ up to 300 mg/g [59]). However, it should be mentioned that COFs showed water capture activity only at higher RH values (mostly RH > 30%). The final synthesis stage of P(M1/TEB 1:1)H and P(M2/TEB 1:1)H was carried out in an aqueous environment, which confirms the high resistance of these materials to water. P(M1/TEB 1:1)H and P(M2/TEB 1:1)H networks are, therefore, more suitable for repeated water capture than porous materials of the zeolite or MOF types, which can degrade during long-term contact with water. The good reproducibility of water vapour capture and the high $a_{H2ORH90}$ values achieved for P(M1/TEB 1:1)H and P(M2/TEB 1:1)H make these networks promising for so-called cyclic water harvesting from the air [60]. Assume that samples P(M1/TEB 1:1)H and P(M2/TEB 1:1)H would work isothermally at 297 K between RH = 20% and RH = 80% in this process. The amount of reversibly trapped/released water would then be 280 mg/g for P(M1/TEB 1:1)H and 250 mg/g for P(M2/TEB 1:1)H.

The efficiency of the networks in capturing and releasing CO_2 was investigated by means of adsorption/desorption isotherms at 273, 293, 313, and 333 K (see Figure S7, Supplementary Materials). The CO_2 capture on all networks was reversible at all temperatures tested (see Figure S7, Supplementary Materials). Table 3 summarizes the CO_2 adsorption capacities (273 K) at an equilibrium CO_2 pressure of 0.2 and 1 bar (values of a_{CO2} in mg(CO_2)/g(network)). The a_{CO2} values (1 bar 273 K) of networks containing CH=O and CH_2OH groups were roughly twice the a_{CO2} value resulting for hydrocarbon P(pentyne/TEB 3:1) network and corresponded to the capacities most frequently reported for CO_2 capture on various functionalized porous polymers under these conditions [2,18]. The CO_2 capture on the networks proceeded (under the conditions used) via the adsorption of CO_2 molecules on the surface. As the individual networks had different specific surface areas, we also report (Table 3) the CO_2 adsorption capacities related to 1 m^2 of the network surface, $a_{CO2/S}$ [$a_{CO2/S} = a_{CO2}/S_{BET}$].

Table 3. CO_2 adsorption capacities of the networks at an equilibrium CO_2 pressure of 0.2 and 1 bar at 273.15 K (a_{CO2} and $a_{CO2/S}$) and isosteric heats of the CO_2 adsorption, Q_{st}, at the coverage of 10 mg(CO_2)/g. S_{BET} values were obtained from N_2 adsorption isotherms at 77 K.

Network Code	Polar Group Content (mmol/g)	S_{BET} (m^2/g)	0.2 bar		1 bar		Q_{st} (kJ/mol)
			a_{CO2} (mg/g)	$a_{CO2/S}$ (μg/m^2)	a_{CO2} (mg/g)	$a_{CO2/S}$ (μg/m^2)	
P(M1/TEB 1:1)H	4.90	911	38.1	41.8	99.0	108.7	26
P(M1/TEB 3:1)H	9.61	534	42.2	79.0	87.6	164.0	29
P(M2/TEB 1:1)H	4.85	749	26.7	35.6	72.6	96.9	26
P(M2/TEB 3:1)H	9.42	409	32.9	80.4	75.2	184.0	27
P(pentyne/TEB 3:1)	0	810	13.5	16.7	39.2	48.3	23

Figure 6 shows the CO_2 adsorption isotherms ($a_{CO2/S}$ vs. the equilibrium CO_2 pressure) at 273 K for all networks. The values of $a_{CO2/S}$ increased significantly with increasing content of CH=O and CH_2OH groups in the networks in the order: P(pentyne/TEB 3:1) < P(M2/TEB 1:1)H~P(M1/TEB 1:1)H < P(M1/TEB 3:1)H~P(M2/TEB 3:1)H. It is clearly visible that the CH=O and CH_2OH groups significantly enhanced the efficiency of the networks in CO_2 capture. The CH=O and CH_2OH groups had a very similar effect, and the CO_2 capture efficiency was influenced by the content of these groups rather than their type. To evaluate the influence of the CH=O and CH_2OH groups of the networks on the efficiency of CO_2 capture at different stages of this process, we used the ratios of the $a_{CO2/S}$ values determined for P(M1/TEB 3:1)H and P(M2/TEB 3:1)H and the $a_{CO2/S}$ values for P(pentyne/TEB 3:1) at the same CO_2 pressure and at 273 K. This ratio was defined as $r = a_{CO2/S,P(M1/TEB3:1)H}/a_{CO2/S,P(pentyne/TEB3:1)}$ in the case of P(M1/TEB 3:1)H and $r = a_{CO2/S,P(M2/TEB3:1)H}/a_{CO2/S,P(pentyne/TEB3:1)}$ in the case of P(M2/TEB 3:1)H. The values of r were plotted versus equilibrium CO_2 pressure in Figure 6. It is obvious that r decreased with increasing equilibrium CO_2 pressure (i.e., with increasing coverage of the surface of the networks with CO_2 molecules): while at a CO_2 pressure of 0.05 bar, the r value was about 6, and it decreased to ~3.5 at a CO_2 pressure of 1 bar. Most probably, CO_2 molecules interacted with CH=O and CH_2OH groups of enhanced affinity toward CO_2 in the initial stage of adsorption. In the later stages of adsorption, CO_2 was probably also trapped on the hydrocarbon segments of the networks, which had a lower affinity toward CO_2 molecules. The increased affinity of networks with CH=O and CH_2OH towards CO_2 is also evident from the comparison of the values of the isosteric heat of CO_2 adsorption, Q_{st}, determined for the coverage of the networks with CO_2 of 10 mg/g. (Table 3). The Q_{st} values were calculated from the temperature dependences of CO_2 adsorption isotherms. The Q_{st} value of P(pentyne/TEB 3:1) was 23 kJ/mol, while the Q_{st} values of the functionalized networks ranged from 26 to 29 kJ/mol and increased slightly with increasing content of CH=O and CH_2OH groups in the networks. The high adsorption efficiency of networks functionalized with CH=O and CH_2OH groups at a CO_2 pressure in the range of 0–0.2 bar and the reversibility of CO_2 adsorption fit the requirements for adsorbents suitable for the reversible capture of CO_2 from gas mixtures with a low partial pressure of CO_2, for example from flue gas [61].

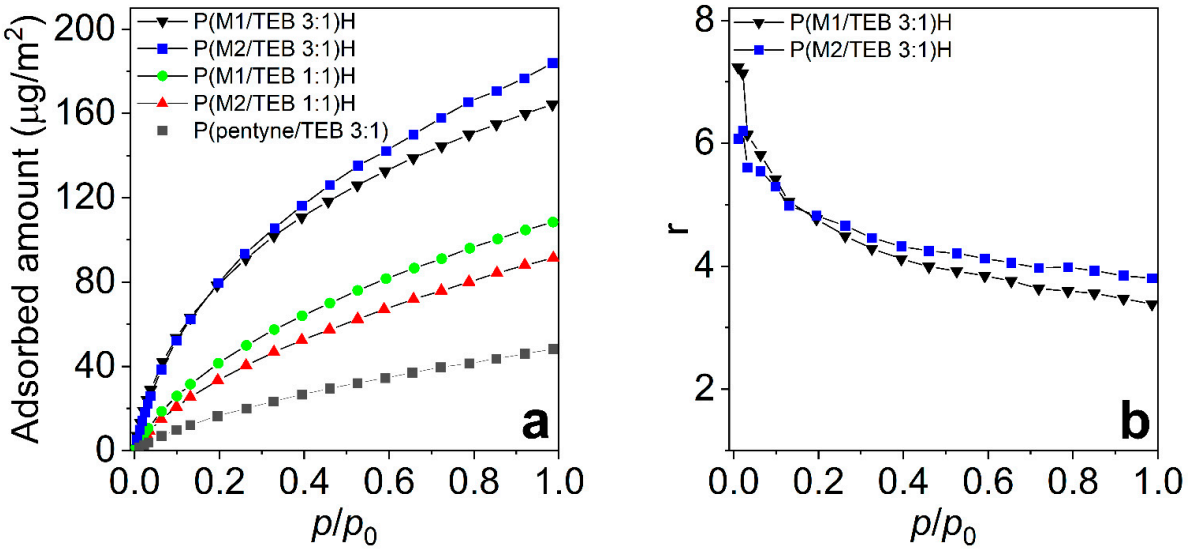

Figure 6. CO_2 adsorption isotherms (273 K) on the networks (**a**), ratio $r = a_{CO2/S,P(M1/TEB3:1)H}/a_{CO2/S,P(pentyne/TEB3:1)}$ and $r = a_{CO2/S,P(M2/TEB3:1)H}/a_{CO2/S,P(pentyne/TEB3:1)}$ versus the equilibrium CO_2 pressure (**b**).

3.3. Covalent Modification of Hydrolyzed Networks

The hydrolyzed networks discussed above represent porous supports whose surfaces could potentially be covalently modified with molecules of various functions. The covalent anchoring of such molecules could proceed via their reaction with reactive CH=O or CH_2OH groups of the networks. We verified this possibility by modifying P(M1/TEB 1:1)H and P(M2/TEB 1:1)H networks with chiral molecules, (*R*)-(+)-3-aminopyrrolidine and (*S*)-(+)-2-methylbutyric acid, respectively (see Supplementary Materials for details). Networks P(M1/TEB 1:1)H and P(M2/TEB 1:1)H were selected for their high S_{BET} values (911 and 794 m^2/g, respectively). The modification of P(M1/TEB 1:1)H with (*R*)-(+)-3-aminopyrrolidine proceeded through the imination reaction of the CH=O groups of the network with the NH_2 groups of the modifying agent and resulted in the network labelled P(M1/TEB 1:1)H-APy in which the chiral pyrrolidine segments were attached to the surface via azomethine links (see Scheme 3). The modification of P(M2/TEB 1:1)H with (*S*)-(+)-2-methylbutyric acid proceeded through the esterification reaction between the OH groups of the network and the COOH groups of the modifying agent and resulted in the network labelled P(M2/TEB 1:1)H-MeBu in which the chiral 2-methylbutyric acid segments were attached to the surface via ester links (see Scheme 3). As expected, the covalent modification partially deteriorated the porosity of the networks: the S_{BET} values of modified P(M1/TEB 1:1)H-APy and P(M2/TEB 1:1)H-MeBu were 348 and 649 m^2/g, respectively, i.e., from 20 to 60% lower than the S_{BET} of the networks before the modification (see Supplementary Materials, Scheme S2, Figures S8 and S9).

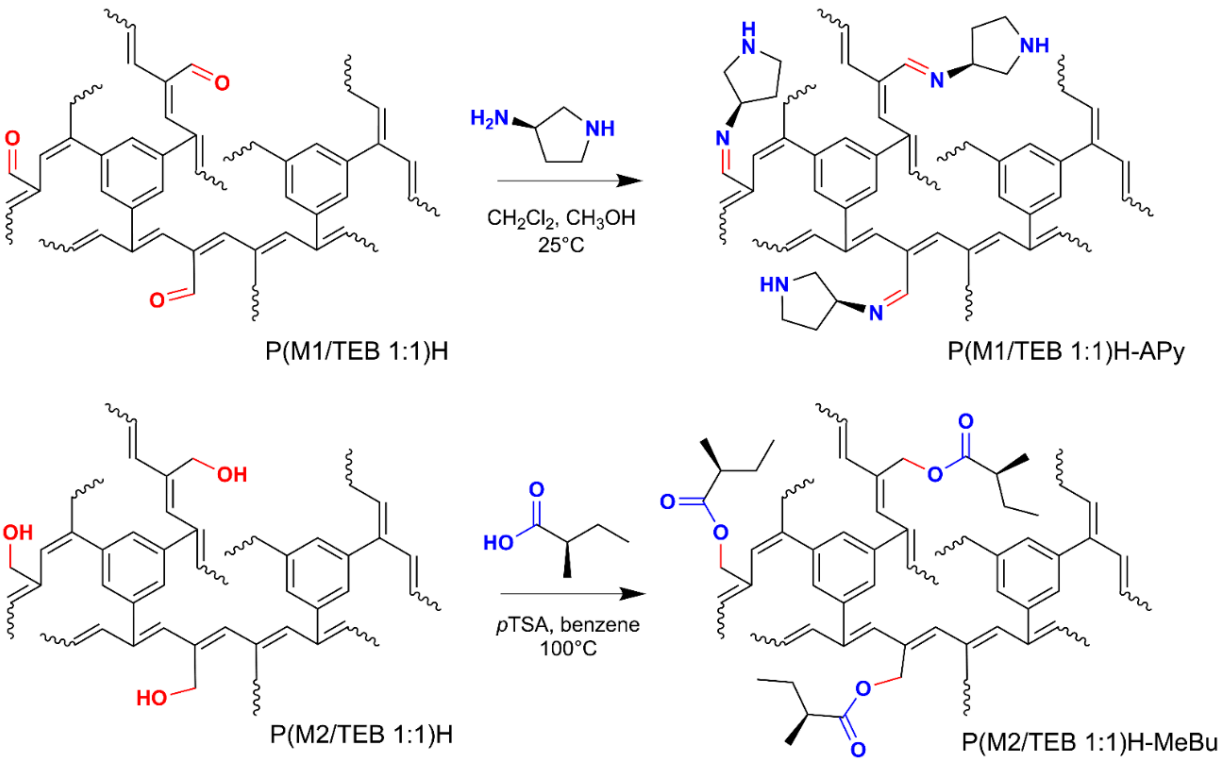

Scheme 3. Postpolymerization covalent modification of the hydrolyzed networks P(M1/TEB 1:1)H and P(M2/TEB 1:1)H by chiral molecules of (*R*)-(+)-3-aminopyrrolidine and (*S*)-(+)-2-methylbutyric acid, respectively. Networks P(M1/TEB 1:1)H-APy and P(M2/TEB 1:1)H-MeBu were prepared.

Figure 7 shows the ^{13}C CP/MAS NMR spectra of the networks before and after covalent modification. The ^{13}C CP/MAS NMR spectra of both modified networks P(M1/TEB 1:1)H-APy and P(M2/TEB 1:1)H-MeBu contained broad partly resolved signals in the aliphatic region, which we ascribed to the sp^3 carbon atoms of pyrrolidine-3-yl and 2-methylbutyl segments, respectively (see Figure 7). The modification of P(M1/TEB 1:1)H

to P(M1/TEB 1:1)H-APy was further accompanied by the disappearance of the signal of carbon atoms of CH=O groups (δ = 190 ppm) in the ^{13}C CP/MAS NMR spectrum of the modified network. This signal was replaced by a weak signal at δ = 163 ppm corresponding to the resonance of the carbon atoms of the newly formed CH=N links. Similarly, the ^{13}C CP/MAS NMR spectrum of P(M2/TEB 1:1)H-MeBu contained a signal at δ = 192 ppm due to the carbon atoms of the newly formed COO links. The extent of the modification of P(M1/TEB 1:1)H to P(M1/TEB 1:1)H-APy was about 75% (based on the ratio of N and C content in the modified network given by elemental analysis). In the modification of P(M2/TEB 1:1)H to P(M2/TEB 1:1)H-MeBu, about 40% of the CH_2OH groups were modified by esterification with (*S*)-(+)-2-methylbutyric acid (based on the intensity of ^{13}C CP/MAS NMR signals of P(M2/TEB 1:1)H-MeBu). Even if the above-discussed modifications were not quantitative, it was possible to introduce chiral groups into the networks in satisfactory amounts: 3.7 mmol/g in the case of P(M1/TEB 1:1)H-APy and 1.9 mmol/g in the case of P(M2/TEB 1:1)H-MeBu.

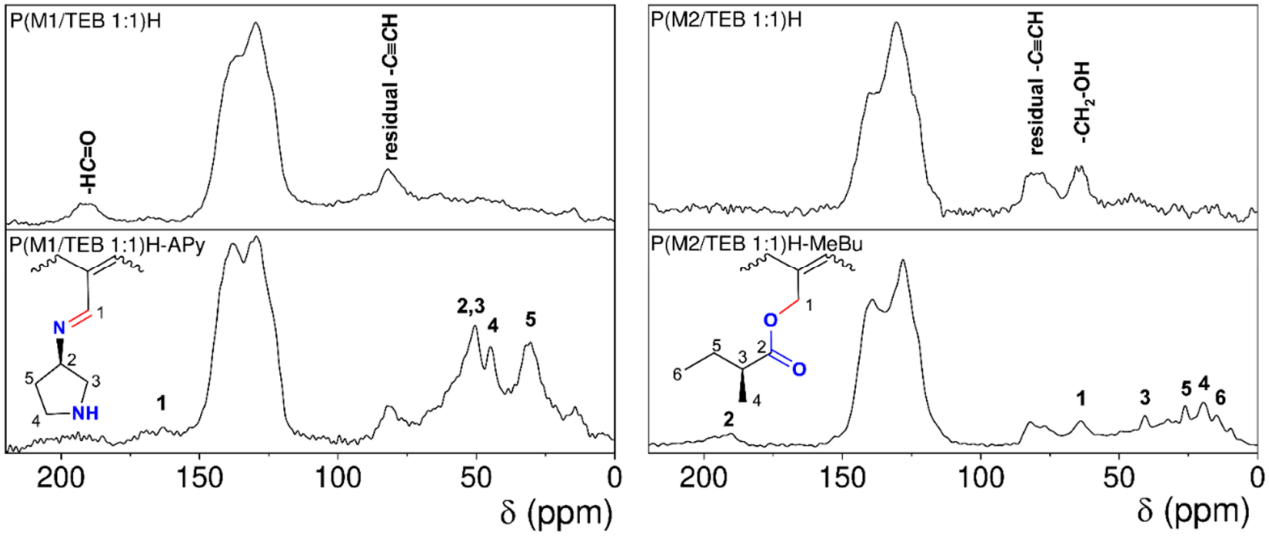

Figure 7. ^{13}C CP/MAS NMR spectra of the hydrolyzed networks P(M1/TEB 1:1)H and P(M2/TEB 1:1)H and modified networks P(M1/TEB 1:1)H-APy and P(M2/TEB 1:1)H-MeBu.

Evidently, the modification of the P(M1/TEB 1:1)H network via imination was more efficient than the esterification modification of P(M2/TEB 1:1)H. It should, however, be mentioned that modification of CH=O groups of P(M1/TEB 1:1)H via Schiff-base chemistry may be limited by the size of the molecules of the modifying agents. Our attempts to modify P(M1/TEB 1:1)H in reaction with dansylhydrazine (under formation of hydrazone links) failed (efficiency < 10%), probably due to sterically hindered penetration of bulky dansylhydrazine molecules ($C_{12}H_{15}N_3O_2S$) into the pores. On the other hand, such a limitation could be useful for the size-controlled separation of mixtures of primary amines (hydrazines) through their chemisorption on P(M1/TEB 1:1)H or other CH=O groups containing POPs.

4. Conclusions

The chain-growth copolymerization of acetal-protected propargyl aldehyde and acetal-protected propargyl alcohol with 1,3,5-triethynylbenzene cross-linker followed by hydrolytic deprotection of the products provided hyper-cross-linked micro/mesoporous polyacetylene networks with CH=O and CH_2OH groups attached without any spacer to the polyacetylene main chains of the networks. These networks can not be prepared by direct copolymerization of unprotected monomers due to the high reactivity of these monomers. The removable acetal segments not only protected the aldehyde and hydroxymethyl groups of the monomers during polymerization but also served as a template

in the parent networks. The hydrolytic removal of these segments thus simultaneously modified the composition of the networks and their texture, which changed towards higher microporosity and higher specific surface area. The reported two-step synthesis thus allowed the preparation of micro/mesoporous networks with a tuneable content of CH=O and CH_2OH groups (up to a high value of 9.6 mmol/g) and a specific surface area ranging from 400 to 800 m^2/g.

The CH=O and CH_2OH groups in the networks served as active centres for the physisorption of CO_2 and water vapour. The networks were highly effective in reversible low-pressure CO_2 adsorption. The networks also exhibited high water vapour capturing and releasing efficiency (capture capacity up to 445 mg/g at 297 K and RH = 90%), making them promising materials for water harvesting from the air. The water vapour capturing efficiency of the networks was controlled by the content of polar groups in the networks (low RH) and the total pore volume (high RH). Thanks to the presence of reactive groups CH=O and CH_2OH, the networks represent supports suitable for the covalent anchoring of functional molecules, as shown by the modification of the networks with (*R*)-(+)-3-aminopyrrolidine and (*S*)-(+)-2-methylbutyric acid under formation of porous networks decorated with chiral moieties.

Supplementary Materials: The following supporting information can be downloaded at: https://www.mdpi.com/article/10.3390/polym15030743/s1, Figure S1: Thermogravimetric analysis of the networks; Scheme S1: Copolymerization of 1-pentyne with triethynylbenzene (TEB) resulting in P(pentyne/TEB 3:1); Table S1: The textural parameters of the P(pentyne/TEB 3:1) network; Figure S2: ^{13}C CP/MAS NMR spectrum of P(pentyne/TEB 3:1); Figure S3: N_2 adsorption and desorption isotherms (77 K) on P(pentyne/TEB 3:1); Figure S4: Micropore size distribution of P(pentyne/TEB 3:1); Figure S5: The time course of adsorption/desorption of water on the networks (297 K) reported as a change in mass vs. time.; Figure S6: H_2O adsorption and desorption isotherms on the networks at 297 K. Two consecutive measurements; Figure S7: CO_2 adsorption and desorption on the networks at 273, 293, 313, and 333 K; Scheme S2: Postpolymerization chemisorption modification of the hydrolyzed networks P(M1/TEB 1:1)H and P(M2/TEB 1:1)H by chiral molecules of (*R*)-(+)-3-aminopyrrolidine and (*S*)-(+)-2-methylbutyric acid.; Figure S8: N_2 adsorption and desorption isotherms (77 K) on the networks P(M1/TEB 1:1)H, P(M2/TEB 1:1)H, P(M1/TEB 1:1)H-Apy, and P(M2/TEB 1:1)H-MeBu; Figure S9: Changes in micropore size distributions due to the modification of the networks with chiral moieties.

Author Contributions: Conceptualization, J.S.; data curation, B.B., A.V. and J.B.; formal analysis, A.V. and J.B.; funding acquisition, E.V. and J.S.; investigation, L.H.; methodology, L.H.; supervision, J.S.; visualization, L.H.; writing—original draft, L.H. and J.S.; writing—review and editing, B.B., A.H. and E.V. All authors have read and agreed to the published version of the manuscript.

Funding: This research was funded by the Czech Science Foundation [Project 21-02183S] and "Grant Schemes at CU" [reg. no. CZ.02.2.69/0.0/0.0/19_073/0016935] (START/SCI/081).

Institutional Review Board Statement: Not applicable.

Data Availability Statement: The data presented in this study are available on request from the corresponding author.

Conflicts of Interest: The authors declare no conflict of interest.

References

1. Dawson, R.; Cooper, A.I.; Adams, D.J. Nanoporous organic polymer networks. *Prog. Polym. Sci.* **2011**, *37*, 530–563. [CrossRef]
2. Taylor, D.; Dalgarno, S.J.; Xu, Z.; Vilela, F. Conjugated porous polymers: Incredibly versatile materials with far-reaching applications. *Chem. Soc. Rev.* **2020**, *49*, 3981–4042. [CrossRef] [PubMed]
3. Zhou, Y.-B.; Zhan, Z.-P. Conjugated Microporous Polymers for Heterogeneous Catalysis. *Chem. Asian J.* **2017**, *13*, 9–19. [CrossRef] [PubMed]
4. Bhanja, P.; Modak, A.; Bhaumik, A. Porous Organic Polymers for CO_2 Storage and Conversion Reactions. *Chemcatchem* **2018**, *11*, 244–257. [CrossRef]
5. Cousins, K.; Zhang, R. Highly Porous Organic Polymers for Hydrogen Fuel Storage. *Polymers* **2019**, *11*, 690. [CrossRef]

6. Chowdhury, A.; Bhattacharjee, S.; Chatterjee, R.; Bhaumik, A. A new nitrogen rich porous organic polymer for ultra-high CO_2 uptake and as an excellent organocatalyst for CO_2 fixation reactions. *J. CO_2 Util.* **2022**, *65*, 102236. [CrossRef]
7. Song, K.S.; Fritz, P.W.; Coskun, A. Porous organic polymers for CO_2 capture, separation and conversion. *Chem. Soc. Rev.* **2022**, *51*, 9831–9852. [CrossRef]
8. Zhou, L.; Hu, Y.; Li, G. Conjugated Microporous Polymers with Built-In Magnetic Nanoparticles for Excellent Enrichment of Trace Hydroxylated Polycyclic Aromatic Hydrocarbons in Human Urine. *Anal. Chem.* **2016**, *88*, 6930–6938. [CrossRef]
9. Havelková, L.; Hašková, A.; Bashta, B.; Brus, J.; Lhotka, M.; Vrbková, E.; Kindl, M.; Vyskočilová, E.; Sedláček, J. Synthesis of hyper-cross-linked microporous poly(phenylacetylene)s having aldehyde and other groups and their chemisorption and physisorption ability. *Eur. Polym. J.* **2019**, *114*, 279–286. [CrossRef]
10. Zhang, Q.; Yu, S.; Wang, Q.; Xiao, Q.; Yue, Y.; Ren, S. Fluorene-Based Conjugated Microporous Polymers: Preparation and Chemical Sensing Application. *Macromol. Rapid Commun.* **2017**, *38*, 1700445. [CrossRef]
11. Debruyne, M.; Van Speybroeck, V.; Van Der Voort, P.; Stevens, C.V. Porous organic polymers as metal free heterogeneous organocatalysts. *Green Chem.* **2021**, *23*, 7361–7434. [CrossRef]
12. Sekerová, L.; Březinová, P.; Do, T.T.; Vyskočilová, E.; Krupka, J.; Červený, L.; Havelková, L.; Bashta, B.; Sedlacek, J. Sulfonated Hyper-cross-linked Porous Polyacetylene Networks as Versatile Heterogeneous Acid Catalysts. *Chemcatchem* **2019**, *12*, 1075–1084. [CrossRef]
13. Zheng, Y.; Wang, X.; Liu, C.; Yu, B.; Li, W.; Wang, H.; Sun, T.; Jiang, J. Triptycene-supported bimetallic salen porous organic polymers for high efficiency CO_2 fixation to cyclic carbonates. *Inorg. Chem. Front.* **2021**, *8*, 2880–2888. [CrossRef]
14. Bonfant, G.; Balestri, D.; Perego, J.; Comotti, A.; Bracco, S.; Koepf, M.; Gennari, M.; Marchiò, L. Phosphine Oxide Porous Organic Polymers Incorporating Cobalt(II) Ions: Synthesis, Characterization, and Investigation of H_2 Production. *ACS Omega* **2022**, *7*, 6104–6112. [CrossRef]
15. Zhang, T.; Xing, G.; Chen, W.; Chen, L. Porous organic polymers: A promising platform for efficient photocatalysis. *Mater. Chem. Front.* **2019**, *4*, 332–353. [CrossRef]
16. Yuan, D.; Lu, W.; Zhao, D.; Zhou, H.-C. Highly Stable Porous Polymer Networks with Exceptionally High Gas-Uptake Capacities. *Adv. Mater.* **2011**, *23*, 3723–3725. [CrossRef]
17. Hašková, A.; Bashta, B.; Titlová, S.; Brus, J.; Vagenknechtová, A.; Vyskočilová, E.; Sedláček, J. Microporous Hyper-Cross-Linked Polymers with High and Tuneable Content of Pyridine Units: Synthesis and Application for Reversible Sorption of Water and Carbon Dioxide. *Macromol. Rapid Commun.* **2021**, *42*, e2100209. [CrossRef]
18. Dawson, R.; Cooper, A.I.; Adams, D.J. Chemical functionalization strategies for carbon dioxide capture in microporous organic polymers. *Polym. Int.* **2013**, *62*, 345–352. [CrossRef]
19. Byun, Y.; Je, S.H.; Talapaneni, S.N.; Coskun, A. Advances in Porous Organic Polymers for Efficient Water Capture. *Chem. A Eur. J.* **2019**, *25*, 10262–10283. [CrossRef] [PubMed]
20. Byun, J.; Patel, H.; Thirion, D.; Yavuz, C. Reversible water capture by a charged metal-free porous polymer. *Polymer* **2017**, *126*, 308–313. [CrossRef]
21. Mukherjee, S.; Zeng, Z.; Shirolkar, M.M.; Samanta, P.; Chaudhari, A.K.; Tan, J.; Ghosh, S.K. Self-Assembled, Fluorine-Rich Porous Organic Polymers: A Class of Mechanically Stiff and Hydrophobic Materials. *Chem. A Eur. J.* **2018**, *24*, 11771–11778. [CrossRef]
22. Zhang, W.; Li, Y.; Wu, Y.; Fu, Y.; Chen, S.; Zhang, Z.; He, S.; Yan, T.; Ma, H. Fluorinated porous organic polymers for efficient recovery perfluorinated electronic specialty gas from exhaust gas of plasma etching. *Sep. Purif. Technol.* **2022**, *287*, 120561. [CrossRef]
23. Ai, C.; Tang, J.; Zhang, Q.; Tang, X.; Wu, S.; Pan, C.; Yu, G.; Yuan, J. A knitting copolymerization Strategy to Build Porous Polytriazolium Salts for Removal of Anionic Dyes and MnO_4^-. *Macromol. Rapid Commun.* **2022**. [CrossRef]
24. Sedláček, J.; Sokol, J.; Zedník, J.; Faukner, T.; Kubů, M.; Brus, J.; Trhlíková, O. Homo- and Copolycyclotrimerization of Aromatic Internal Diynes Catalyzed with $Co_2(CO)_8$: A Facile Route to Microporous Photoluminescent Polyphenylenes with Hyperbranched or Crosslinked Architecture. *Macromol. Rapid Commun.* **2017**, *39*, 1700518. [CrossRef]
25. Monterde, C.; Navarro, R.; Iglesias, M.; Sánchez, F. Adamantyl-BINOL as platform for chiral porous polymer aromatic frameworks. Multiple applications as recyclable catalysts. *J. Catal.* **2019**, *377*, 609–618. [CrossRef]
26. Wu, Z.; Li, T.; Ding, Y.; Hu, A. Synthesis of Chiral Porous Organic Polymers Through Nucleophilic Substitution for Chiral Separation. *ACS Appl. Polym. Mater.* **2020**, *2*, 5414–5422. [CrossRef]
27. Song, W.; Zhang, M.; Huang, X.; Chen, B.; Ding, Y.; Zhang, Y.; Yu, D.; Kim, I. Smart-borneol-loaded hierarchical hollow polymer nanospheres with antipollution and antibacterial capabilities. *Mater. Today Chem.* **2022**, *26*, 101252. [CrossRef]
28. Tang, Y.; Varyambath, A.; Ding, Y.; Chen, B.; Huang, X.; Zhang, Y.; Yu, D.-G.; Kim, I.; Song, W. Porous organic polymers for drug delivery: Hierarchical pore structures, variable morphologies, and biological properties. *Biomater. Sci.* **2022**, *10*, 5369–5390. [CrossRef]
29. Holst, J.R.; Stöckel, E.; Adams, D.J.; Cooper, A.I. High Surface Area Networks from Tetrahedral Monomers: Metal-Catalyzed Coupling, Thermal Polymerization, and "Click" Chemistry. *Macromolecules* **2010**, *43*, 8531–8538. [CrossRef]
30. Xu, C.; Bacsik, Z.; Hedin, N. Adsorption of CO_2 on a micro-/mesoporous polyimine modified with tris(2-aminoethyl)amine. *J. Mater. Chem. A* **2015**, *3*, 16229–16234. [CrossRef]
31. Xiong, S.; Tang, X.; Pan, C.; Li, L.; Tang, J.; Yu, G. Carbazole-Bearing Porous Organic Polymers with a Mulberry-Like Morphology for Efficient Iodine Capture. *ACS Appl. Mater. Interfaces* **2019**, *11*, 27335–27342. [CrossRef]

32. Bondarev, D.; Sivkova, R.; Šuly, P.; Polášková, M.; Krejčí, O.; Křikavová, R.; Trávníček, Z.; Zukal, A.; Kubů, M.; Sedláček, J. Microporous conjugated polymers via homopolymerization of 2,5-diethynylthiophene. *Eur. Polym. J.* **2017**, *92*, 213–219. [CrossRef]
33. Zhang, Q.; Zeng, K.; Wang, C.; Wei, P.; Zhao, X.; Wu, F.; Liu, Z.-R. An imidazole functionalized porous organic polymer for the highly efficient extraction of uranium from aqueous solutions. *New J. Chem.* **2022**, *46*, 9238–9249. [CrossRef]
34. Rodríguez-González, F.E.; Niebla, V.; Velázquez-Tundidor, M.; Tagle, L.H.; Martin-Trasanco, R.; Coll, D.; Ortiz, P.A.; Escalona, N.; Pérez, E.; Jessop, I.A.; et al. A new porous organic polymer containing Tröger's base units: Evaluation of the catalytic activity in Knoevenagel condensation reaction. *React. Funct. Polym.* **2021**, *167*, 104998. [CrossRef]
35. Dawson, R.; Laybourn, A.; Clowes, R.; Khimyak, Y.Z.; Adams, D.J.; Cooper, A.I. Functionalized Conjugated Microporous Polymers. *Macromolecules* **2009**, *42*, 8809–8816. [CrossRef]
36. Wang, T.; Zhao, Y.-C.; Zhang, L.-M.; Cui, Y.; Zhang, C.-S.; Han, B.-H. Novel approach to hydroxy-group-containing porous organic polymers from bisphenol A. *Beilstein J. Org. Chem.* **2017**, *13*, 2131–2137. [CrossRef]
37. Wisser, F.M.; Eckhardt, K.; Wisser, D.; Böhlmann, W.; Grothe, J.; Brunner, E.; Kaskel, S. Tailoring Pore Structure and Properties of Functionalized Porous Polymers by Cyclotrimerization. *Macromolecules* **2014**, *47*, 4210–4216. [CrossRef]
38. Li, H.; Han, X.; Yu, W.; Zhang, L.; Wei, M.; Wang, Z.; Kong, F.; Wang, W. Dimethoxypillar[5]arene knitted porous polymers for efficient removal of organic micropollutants from water. *Chem. Eng. J. Adv.* **2022**, *12*, 100384. [CrossRef]
39. Dong, K.; Sun, Q.; Meng, X.; Xiao, F.-S. Strategies for the design of porous polymers as efficient heterogeneous catalysts: From co-polymerization to self-polymerization. *Catal. Sci. Technol.* **2017**, *7*, 1028–1039. [CrossRef]
40. Stahlová, S.; Slováková, E.; Vaňkátová, P.; Zukal, A.; Kubů, M.; Brus, J.; Bondarev, D.; Moučka, R.; Sedláček, J. Chain-growth copolymerization of functionalized ethynylarenes with 1,4-diethynylbenzene and 4,4′-diethynylbiphenyl into conjugated porous networks. *Eur. Polym. J.* **2015**, *67*, 252–263. [CrossRef]
41. Petrášová, S.; Zukal, A.; Brus, J.; Balcar, H.; Pastva, J.; Zedník, J.; Sedláček, J. New Hyper-Crosslinked Partly Conjugated Networks with Tunable Composition by Spontaneous Polymerization of Ethynylpyridines with Bis(bromomethyl)arenes: Synthesis, Spectral Properties, and Activity in CO_2 Capture. *Macromol. Chem. Phys.* **2013**, *214*, 2856–2866. [CrossRef]
42. Seo, M.; Kim, S.; Oh, J.; Kim, S.-J.; Hillmyer, M.A. Hierarchically Porous Polymers from Hyper-cross-linked Block Polymer Precursors. *J. Am. Chem. Soc.* **2015**, *137*, 600–603. [CrossRef] [PubMed]
43. Lee, J.; Seo, M. Downsizing of Block Polymer-Templated Nanopores to One Nanometer via Hyper-Cross-Linking of High χ–Low *N* Precursors. *ACS Nano* **2021**, *15*, 9154–9166. [CrossRef] [PubMed]
44. Slováková, E.; Ješelnik, M.; Žagar, E.; Zedník, J.; Sedláček, J.; Kovačič, S. Chain-Growth Insertion Polymerization of 1,3-Diethynylbenzene High Internal Phase Emulsions into Reactive π-Conjugated Foams. *Macromolecules* **2014**, *47*, 4864–4869. [CrossRef]
45. Jurjevec, S.; Žerjav, G.; Pintar, A.; Žagar, E.; Kovačič, S. Tunable poly(aryleneethynylene) networks prepared by emulsion templating for visible-light-driven photocatalysis. *Catal. Today* **2020**, *361*, 146–151. [CrossRef]
46. Huang, J.; Zhou, X.; Lamprou, A.; Maya, F.; Svec, F.; Turner, S.R. Nanoporous Polymers from Cross-Linked Polymer Precursors via *tert*-Butyl Group Deprotection and Their Carbon Dioxide Capture Properties. *Chem. Mater.* **2015**, *27*, 7388–7394. [CrossRef]
47. Bashta, B.; Hašková, A.; Faukner, T.; Elsawy, M.A.; Šorm, D.; Brus, J.; Sedláček, J. Microporous hyper-cross-linked polyacetylene networks: Covalent structure and texture modification by reversible Schiff-base chemistry. *Eur. Polym. J.* **2020**, *136*, 109914. [CrossRef]
48. Bashta, B.; Havelková, L.; Sokol, J.; Brus, J.; Sedláček, J. Microporous polymers prepared from non-porous hyper-cross-linked networks by removing covalently attached template molecules. *Microporous Mesoporous Mater.* **2021**, *330*, 111636. [CrossRef]
49. Sedláček, J.; Balcar, H. Substituted Polyacetylenes Prepared with Rh Catalysts: From Linear to Network-Type Conjugated Polymers. *Polym. Rev.* **2016**, *57*, 31–51. [CrossRef]
50. Masuda, T. Substituted Polyacetylenes: Synthesis, Properties, and Functions. *Polym. Rev.* **2016**, *57*, 1–14. [CrossRef]
51. Inoue, Y.; Ishida, T.; Sano, N.; Yajima, T.; Sogawa, H.; Sanda, F. Platinum-Mediated Reversible Cross-linking/Decross-linking of Polyacetylenes Substituted with Phosphine Ligands: Catalytic Activity for Hydrosilylation. *Macromolecules* **2022**, *55*, 5711–5722. [CrossRef]
52. Perlmutter, P. Propargyl Aldehyde. In *Encyclopedia of Reagents for Organic Synthesis*; John Wiley & Sons: Hoboken, NJ, USA, 2001; ISBN 9780470842898. [CrossRef]
53. Zhou, L.; Kaiser, R.I.; Gao, L.G.; Chang, A.H.H.; Liang, M.; Yung, Y.L. Pathways to Oxygen-Bearing Molecules in the Interstellar Medium and in Planetary Atmospheres: Cyclopropenone (c-C_3H_2O) and Propynal (HCCCHO). *Astrophys. J.* **2008**, *686*, 1493–1502. [CrossRef]
54. Sekerová, L.; Lhotka, M.; Vyskočilová, E.; Faukner, T.; Slováková, E.; Brus, J.; Červený, L.; Sedláček, J. Hyper-Cross-Linked Polyacetylene-Type Microporous Networks Decorated with Terminal Ethynyl Groups as Heterogeneous Acid Catalysts for Acetalization and Esterification Reactions. *Chem. A Eur. J.* **2018**, *24*, 14742–14749. [CrossRef]
55. Metrane, A.; Delhali, A.; Ouikhalfan, M.; Assen, A.H.; Belmabkhout, Y. Water Vapor Adsorption by Porous Materials: From Chemistry to Practical Applications. *J. Chem. Eng. Data* **2022**, *67*, 1617–1653. [CrossRef]
56. Chen, Q.; Liu, D.-P.; Zhu, J.-H.; Han, B.-H. Mesoporous Conjugated Polycarbazole with High Porosity via Structure Tuning. *Macromolecules* **2014**, *47*, 5926–5931. [CrossRef]
57. Byun, Y.; Coskun, A. Epoxy-Functionalized Porous Organic Polymers via the Diels-Alder Cycloaddition Reaction for Atmospheric Water Capture. *Angew. Chem. Int. Ed.* **2018**, *57*, 3173–3177. [CrossRef]

58. Karak, S.; Kandambeth, S.; Biswal, B.P.; Sasmal, H.S.; Kumar, S.; Pachfule, P.; Banerjee, R. Constructing Ultraporous Covalent Organic Frameworks in Seconds via an Organic Terracotta Process. *J. Am. Chem. Soc.* **2017**, *139*, 1856–1862. [CrossRef]
59. Nguyen, H.L.; Hanikel, N.; Lyle, S.J.; Zhu, C.; Proserpio, D.M.; Yaghi, O.M. A Porous Covalent Organic Framework with Voided Square Grid Topology for Atmospheric Water Harvesting. *J. Am. Chem. Soc.* **2020**, *142*, 2218–2221. [CrossRef]
60. Lu, H.; Shi, W.; Guo, Y.; Guan, W.; Lei, C.; Yu, G. Materials Engineering for Atmospheric Water Harvesting: Progress and Perspectives. *Adv. Mater.* **2022**, *34*, 2110079. [CrossRef]
61. Singh, G.; Lee, J.; Karakoti, A.; Bahadur, R.; Yi, J.; Zhao, D.; AlBahily, K.; Vinu, A. Emerging trends in porous materials for CO_2 capture and conversion. *Chem. Soc. Rev.* **2020**, *49*, 4360–4404. [CrossRef]

Supplementary Materials

Combining polymerization and templating toward hyper-cross-linked poly(propargyl aldehyde)s and poly(propargyl alcohol)s for reversible H_2O and CO_2 capture and construction of porous chiral networks

Lucie Havelková [1,], Bogdana Bashta [1], Alena Hašková [1], Alice Vagenknechtová [2], Eliška Vyskočilová [3], Jiří Brus [4] and Jan Sedláček [1,*]*

1 Department of Physical and Macromolecular Chemistry, Faculty of Science, Charles University, Hlavova 2030, 12843, Prague, Czech Republic

2 Department of Gaseous and Solid Fuels and Air Protection, University of Chemistry and Technology in Prague, Technická 5, Prague, 166 28 Czech Republic

3 Department of Organic Technology, University of Chemistry and Technology in Prague, Technická 5, Prague, 166 28 Czech Republic

4 Institute of Macromolecular Chemistry, Czech Academy of Sciences, HeyrovskýSq.2,Prague,162 00, Czech Republic

* Correspondence: lucie.havelkova@natur.cuni.cz (L.H.); jan.sedlacek@natur.cuni.cz (J.S.)

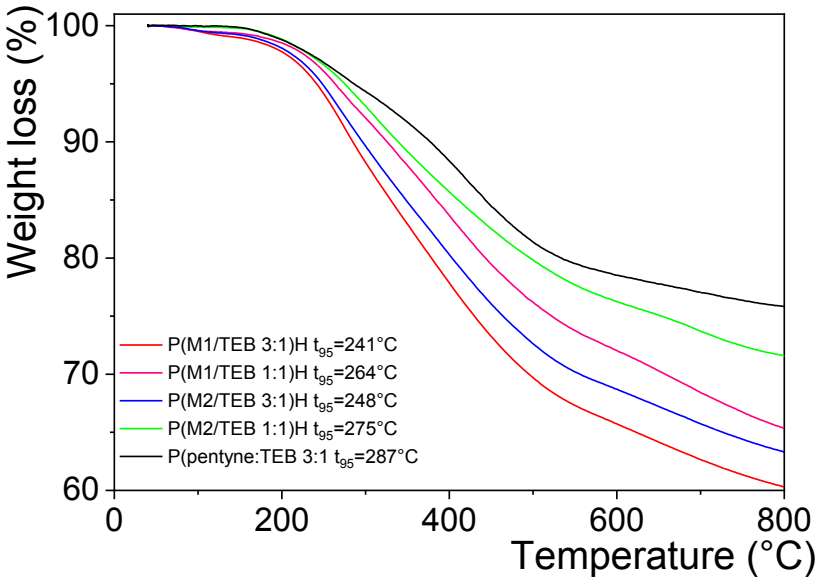

Figure S1. Thermogravimetric analysis of the networks.

Synthesis of P(pentyn/TEB 3:1)

Copolymerization of 1-pentyne with 1,3,5-triethynylbenzene (TEB) was performed in CH_2Cl_2 at 75 °C in a sealed thick-wall ampoule under an argon atmosphere using the [Rh(nbd)acac] complex as a polymerization catalyst. The reaction time was 7 days. The initial concentration of comonomers was 0,3 mol/dm^3 and the concentration of [Rh(nbd)acac] was 15 mmol/dm^3. The comonomer mole ratio in the feed 1-pentyne:TEB was 3:1. 600 mg of 1-pentyne and 441 mg of TEB were dissolved in 35 ml of CH_2Cl_2. A solution of 173 mg of the catalyst in 4 ml of CH_2Cl_2 was added to the solution of comonomers to start the polymerization. After 7 days, the precipitated polymer was separated, repeatedly washed with CH_2Cl_2, and dried under vacuum for 2 days at room temperature. The polymer network P(pentyne/TEB 3:1) was formed in quantitative yield.

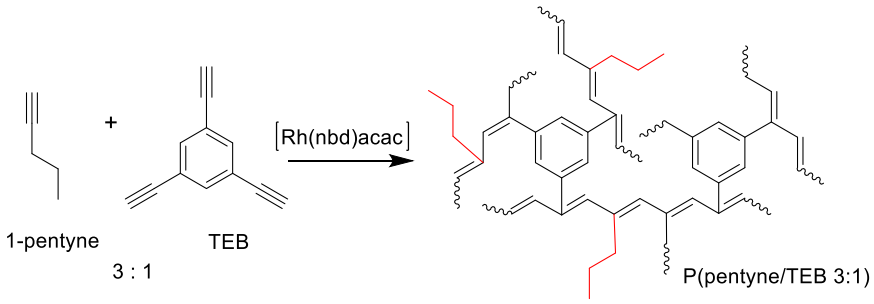

Scheme S1. Copolymerization of 1-pentyne with triethynylbenzene (TEB) resulting in P(pentyne/TEB 3:1).

Table S1. The textural parameters of the P(pentyne/TEB 3:1) network.

Network code	S_{BET} [m^2/g]	V_{mi} [cm^3/g]	V_{tot} [cm^3/g]	D_{mi} [nm]
P(pentyne/TEB 3:1)	810	0.28	1.69	0.9

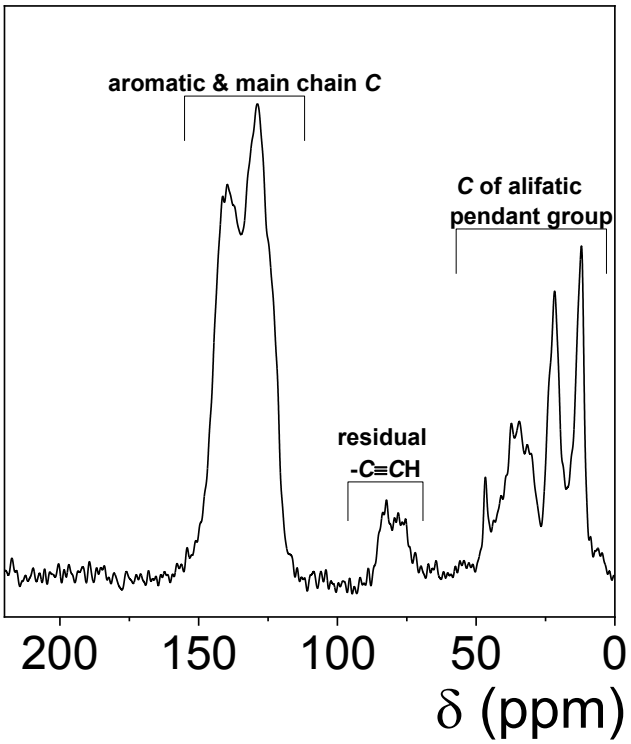

Figure S2. ^{13}C CP/MAS NMR spectrum of P(pentyne/TEB 3:1).

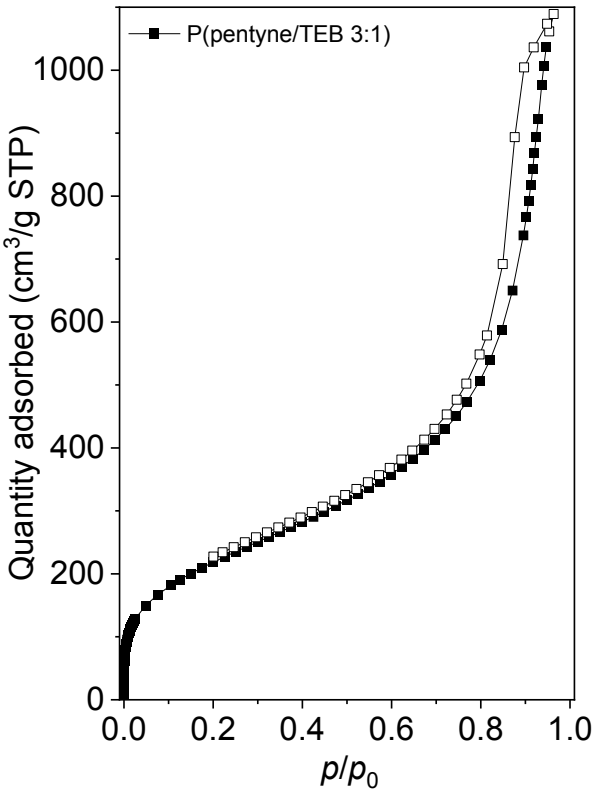

Figure S3. N_2 adsorption (full points) and desorption (empty points) isotherms (77 K) on P(pentyne/TEB 3:1).

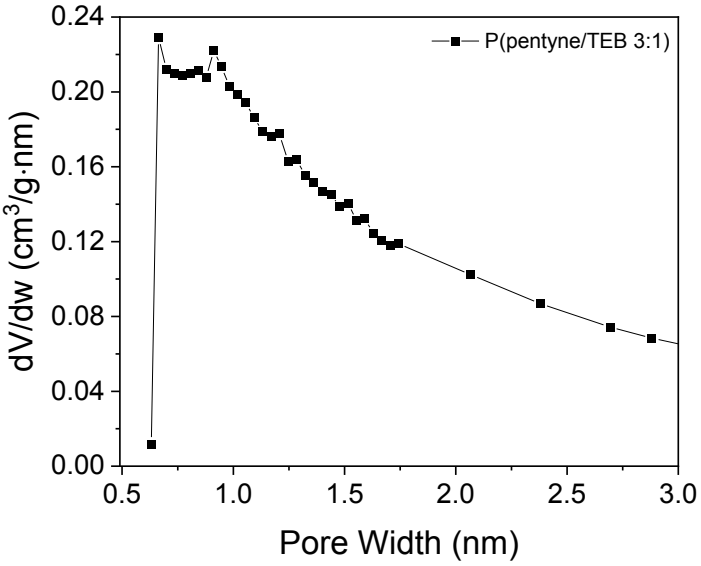

Figure S4. Micropore size distribution of P(pentyne/TEB 3:1).

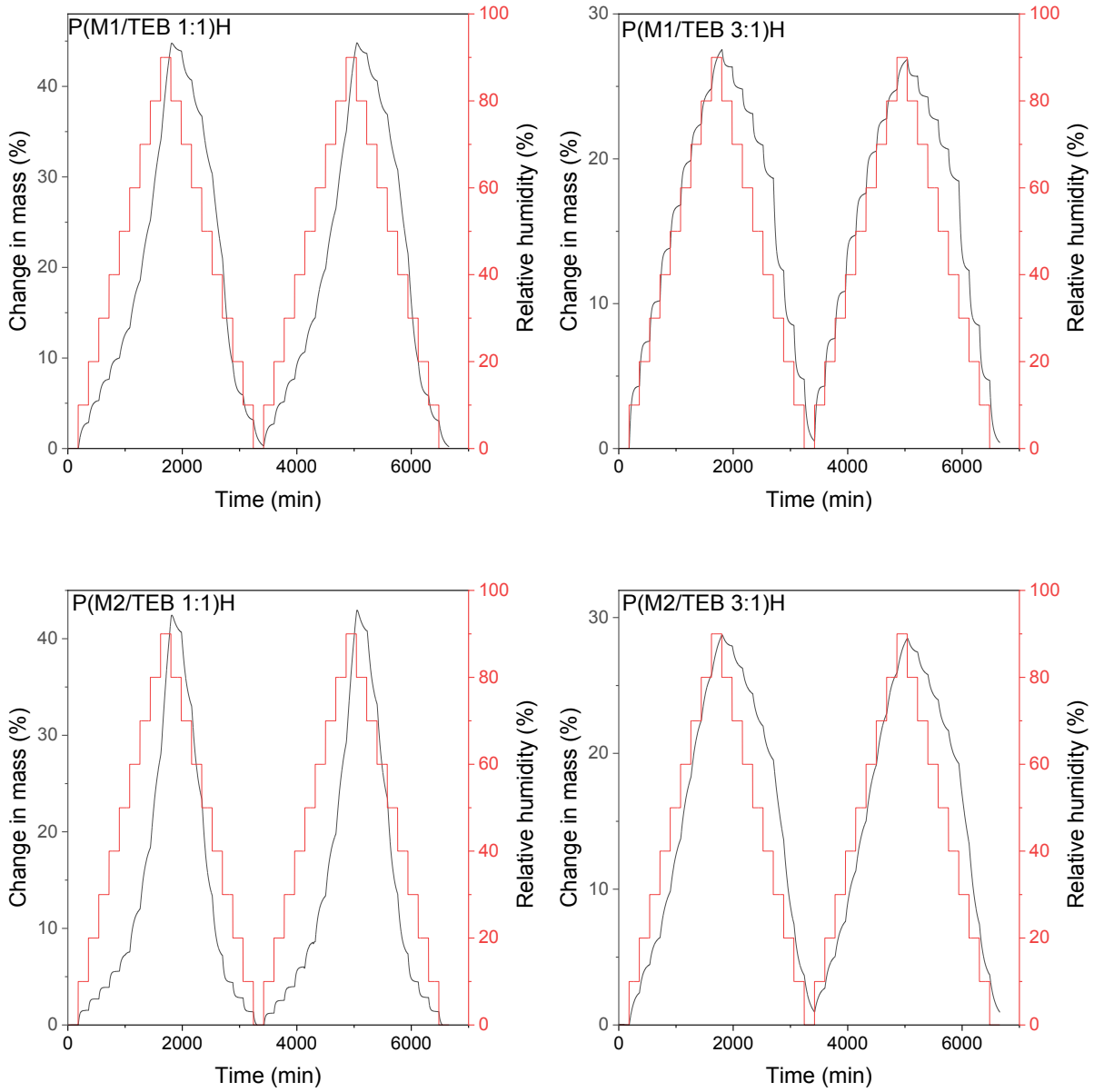

Figure S5. The time course of adsorption/desorption of water on the networks (297 K) reported as a change in mass vs. time (black line). Relative humidity of the gas phase (red line).

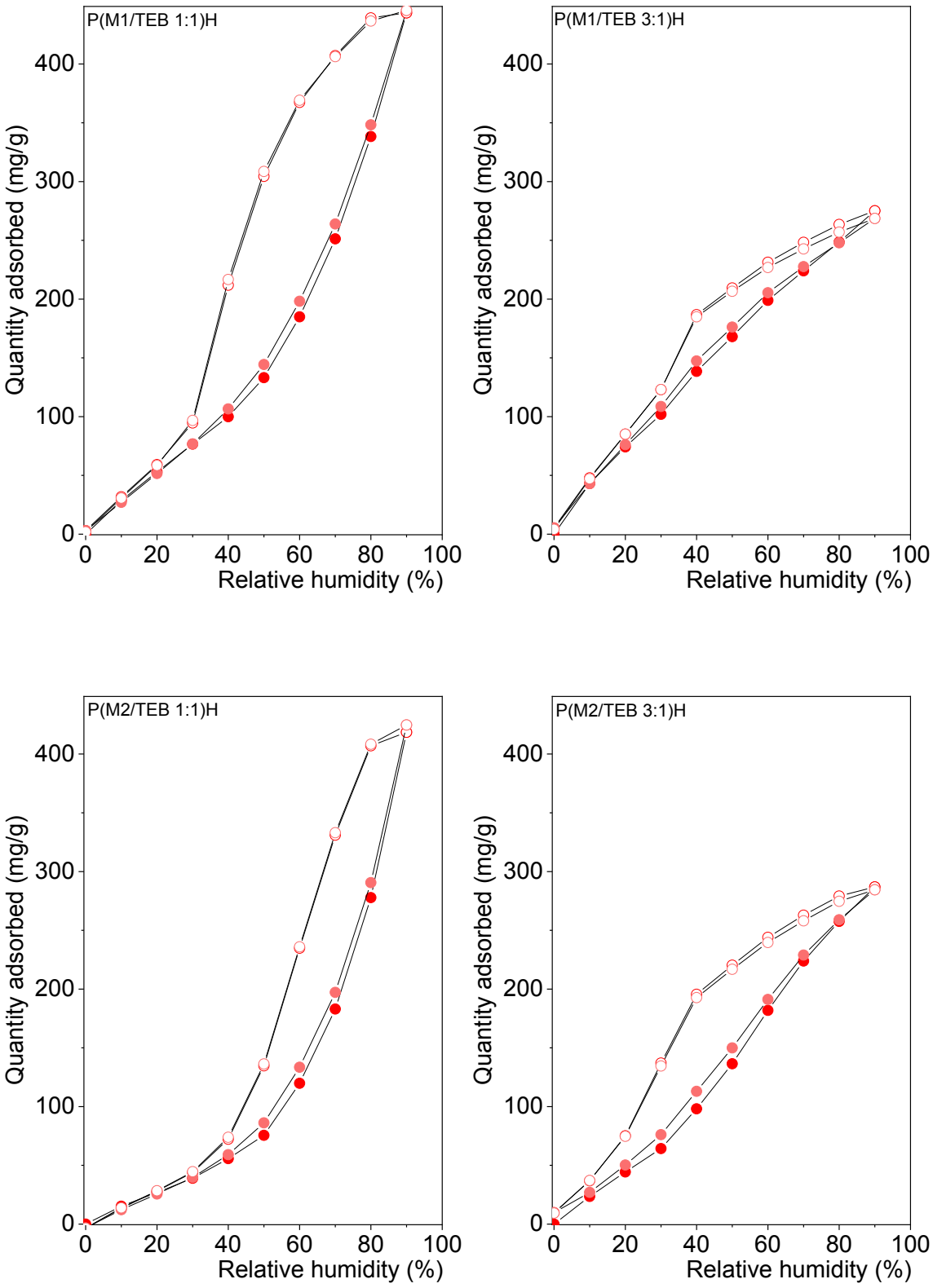

Figure S6. H_2O adsorption (full points) and desorption (empty points) isotherms on the networks at 297 K. Two consecutive measurements.

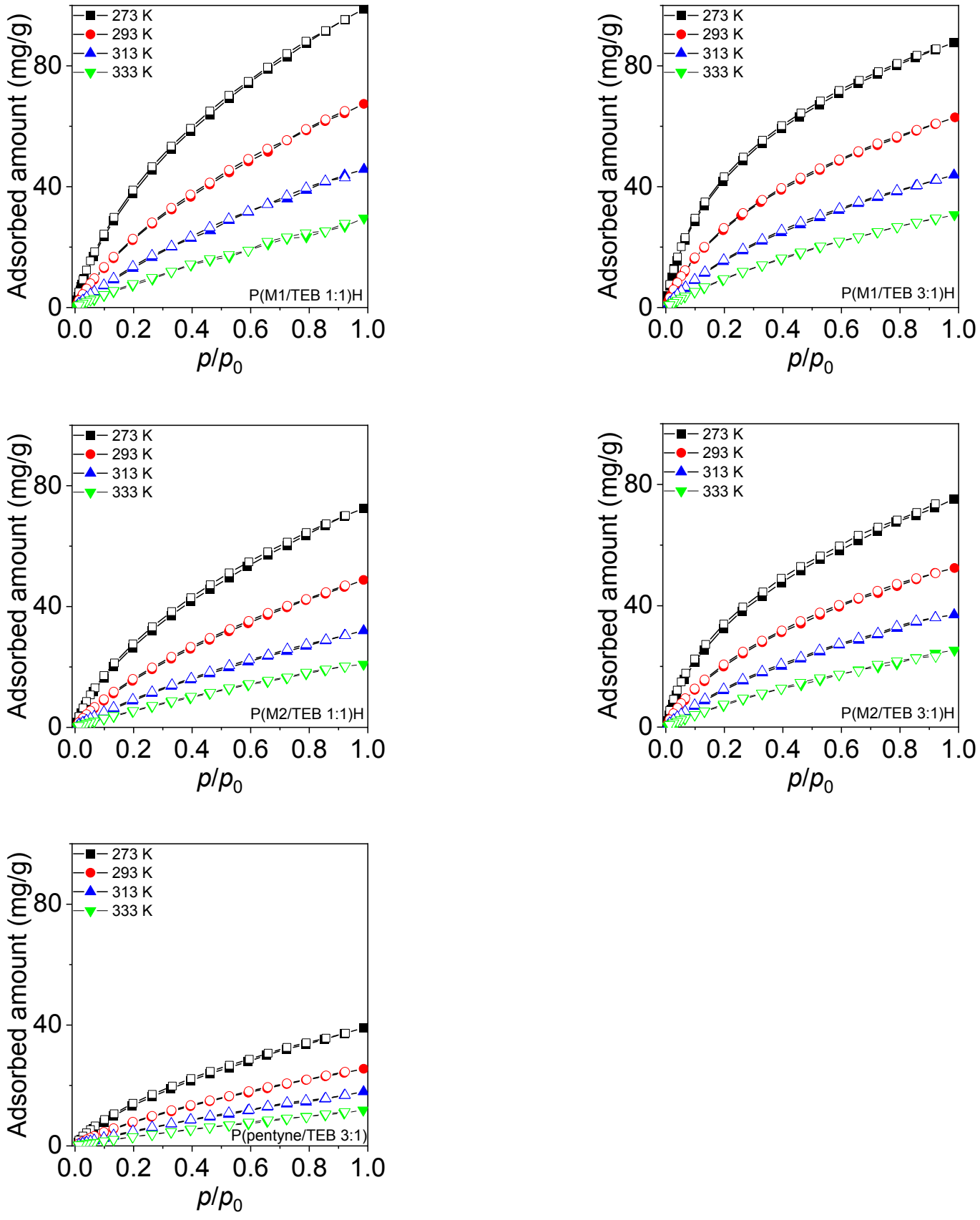

Figure S7. CO_2 adsorption (full points) and desorption (empty points) on the networks at 273, 293, 313 and 333 K.

Postpolymerization modification of P(M1/TEB 1:1)H with (*R*)-(+)-3-aminopyrrolidine

The postpolymerization covalent modification of P(M1/TEB 1:1)H with (*R*)-(+)-3-aminopyrrolidine was performed in the mixture of dichloromethane and methanol (2/1; v/v) at room temperature under stirring. The reaction time was 14 days. In a typical experiment, 180 mg of P(M1/TEB 1:1)H was reacted with 385 mg of (*R*)-(+)-3-aminopyrrolidine. An excess of modifier (NH_2 groups to CHO groups mole ratio = 5) was used to support the modification of CHO groups. The P(M1/TEB 1:1)H network covalently modified with (*R*)-(+)-3-aminopyrrolidine was separated by filtration, repeatedly washed with methanol and dichloromethane to remove physisorbed amine and dried under vacuum at room temperature to constant weight.

Postpolymerization modification of P(M2/TEB 1:1)H with (*S*)-(+)-2-methylbutyric acid

The postpolymerization covalent modification of P(M2/TEB 1:1)H with (*S*)-(+)-2-methylbutyric acid was performed as azeotropic esterification in benzene. In a typical experiment, 500 mg of (*S*)-(+)-2-methylbutyric acid was dissolved in 50 ml of benzene and 23 mg of *p*-toluenesulfonic acid was added and dissolved, then 200 mg of P(M2/TEB 1:1)H was dispersed in this solution. An excess of modifier (COOH groups to OH groups mole ratio = 5) was used to support the modification of OH groups. The mixture was stirred at 100°C for 4 days. The reaction was terminated by adding the excess of benzene (200 ml). The P(M2/TEB 1:1)H network covalently modified with (*S*)-(+)-2-methylbutyric acid was separated by filtration and repeatedly washed with benzene to remove physisorbed carboxylic acid and dried under vacuum at room temperature to constant weight.

Chemisorption of dansyl hydrazine on P(M1/TEB 1:1)H

The chemisorption was performed in the mixture of dichloromethane and methanol (4/1; v/v) at room temperature under stirring. In a typical experiment, 425 mg of dansyl hydrazine (DH) was dissolved in the mixture of 4 ml dichloromethane and 1 ml of methanol and then 100 mg of P(M1/TEB 1:1)H was dispersed in the solution. An excess of chemisorbent (NH_2 groups to CHO groups mole ratio = 3 for DH) was used to achieve maximum chemisorption capacity of P(M1/TEB 1:1)H. After 14 days, P(M1/TEB 1:1)H with chemisorbed DH was repeatedly washed with the mixture of dichloromethane and methanol (4/1; v/v) to removed physisorbed DH, then separated by filtration and dried under vacuum at room temperature to constant weight.

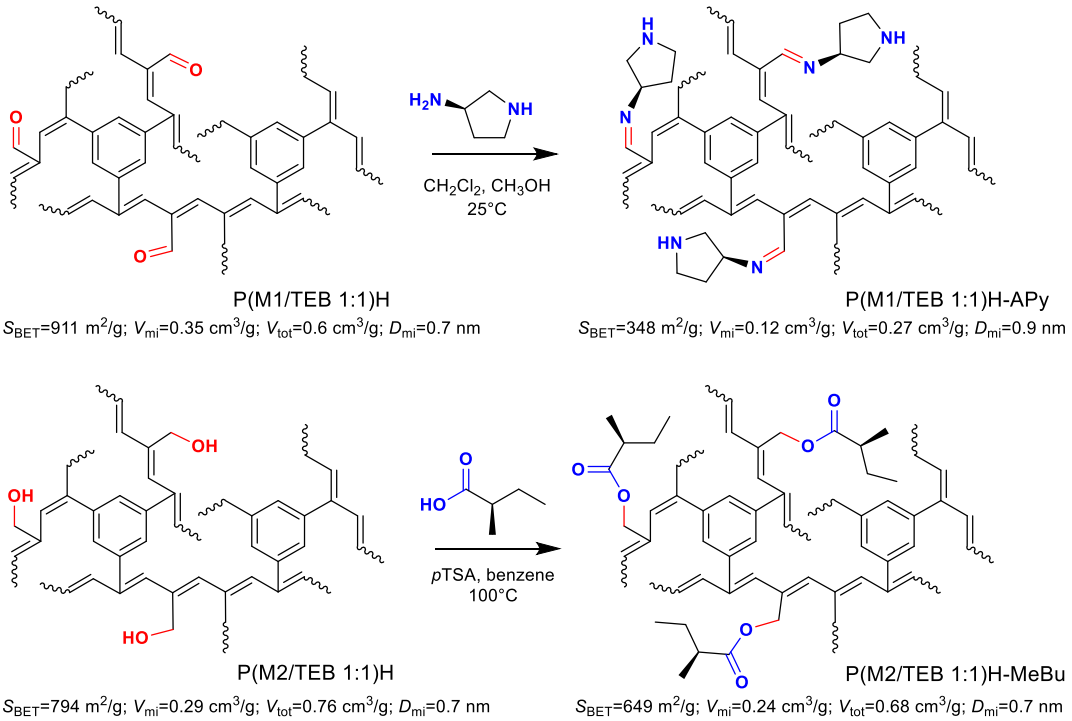

P(M1/TEB 1:1)H

S_{BET}=911 m^2/g; V_{mi}=0.35 cm^3/g; V_{tot}=0.6 cm^3/g; D_{mi}=0.7 nm

P(M1/TEB 1:1)H-APy

S_{BET}=348 m^2/g; V_{mi}=0.12 cm^3/g; V_{tot}=0.27 cm^3/g; D_{mi}=0.9 nm

P(M2/TEB 1:1)H

S_{BET}=794 m^2/g; V_{mi}=0.29 cm^3/g; V_{tot}=0.76 cm^3/g; D_{mi}=0.7 nm

P(M2/TEB 1:1)H-MeBu

S_{BET}=649 m^2/g; V_{mi}=0.24 cm^3/g; V_{tot}=0.68 cm^3/g; D_{mi}=0.7 nm

Scheme S2. Postpolymerization chemisorption modification of the hydrolyzed networks P(M1/TEB 1:1)H and P(M2/TEB 1:1)H by chiral molecules of (R)-(+)-3-aminopyrrolidine and (S)-(+)-2-methylbutyric acid, respectively. Networks P(M1/TEB 1:1)H-APy and P(M2/TEB 1:1)H-MeBu were prepared.

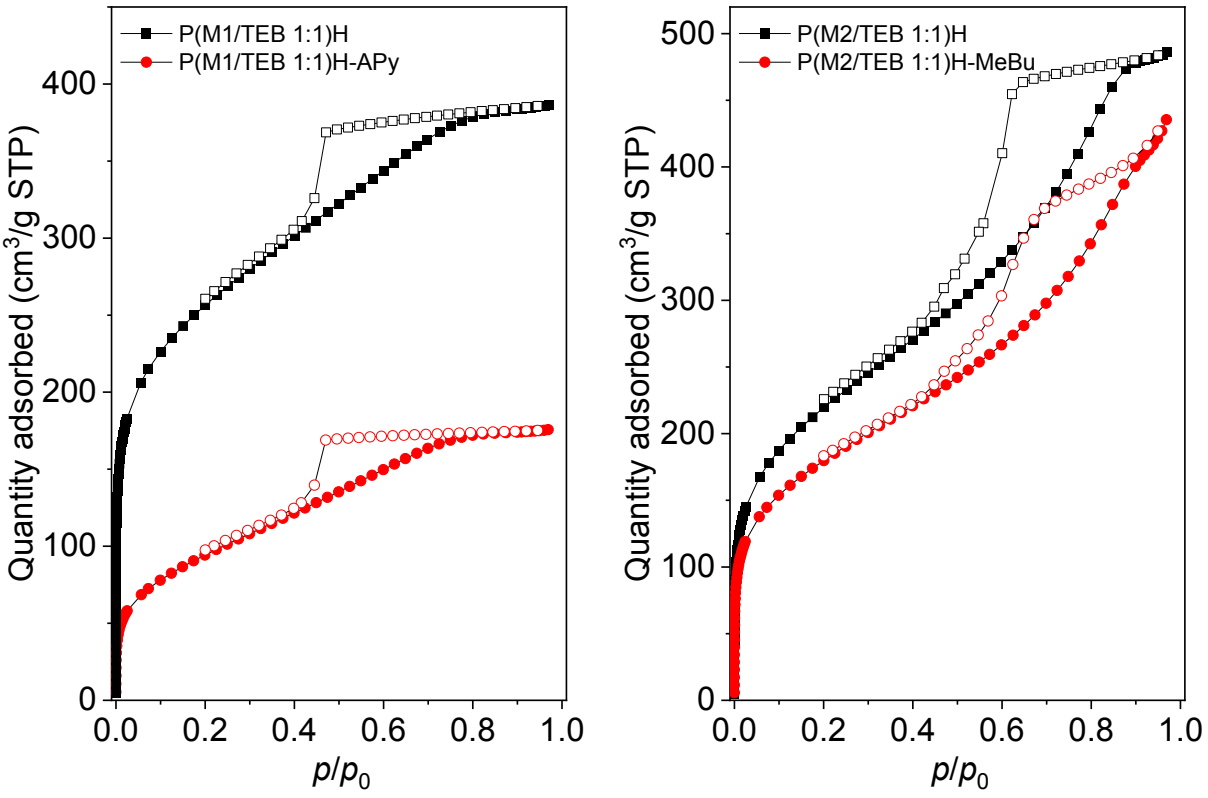

Figure S8. N_2 adsorption (full points) and desorption (empty points) isotherms (77 K) on the networks P(M1/TEB 1:1)H, P(M2/TEB 1:1)H, P(M1/TEB 1:1)H-APy and P(M2/TEB 1:1)H-MeBu.

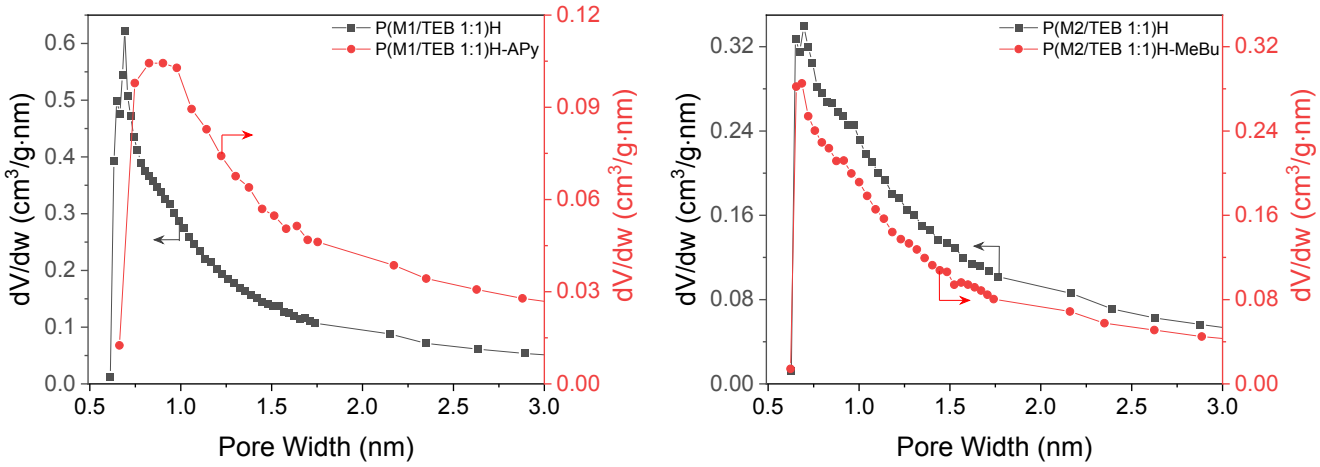

Figure S9. Changes in micropore size distributions due to the modification of the networks with chiral moieties.

IV.

B. Bashta, **L. Havelková**, J. Sokol, J. Brus, J. Sedláček: Microporous polymers prepared from non-porous hyper-cross-linked networks by removing covalently attached template molecules, *Microporous and Mesoporous Materials*, **2022**, *330*, 111636.

Microporous and Mesoporous Materials 330 (2022) 111636

Contents lists available at ScienceDirect

Microporous and Mesoporous Materials

journal homepage: www.elsevier.com/locate/micromeso

Microporous polymers prepared from non-porous hyper-cross-linked networks by removing covalently attached template molecules

Bogdana Bashta [a,*], Lucie Havelková [a], Jiří Sokol [a], Jiří Brus [b], Jan Sedláček [a,**]

[a] Department of Physical and Macromolecular Chemistry, Faculty of Science, Charles University, Hlavova 2030, 12843, Prague 2, Czech Republic
[b] Institute of Macromolecular Chemistry, Czech Academy of Sciences, Heyrovský Sq. 2, Prague 6, 162 06, Czech Republic

ARTICLE INFO

Keywords:
Microporous polymers
Networks
Hyper-cross-linked
Polyacetylenes
Schiff base
Covalent templating
Gas sorption

ABSTRACT

A new method for the formation of permanent micropores in hyper-cross-linked networks is reported. This method is based on a template approach, using small molecules (4-methylaniline and 4-methylbenzaldehyde) as templates. These molecules are covalently attached via azomethine links to parent non-porous hyper-cross-linked polyacetylene networks prepared by chain-growth homo and copolymerization of ethynylated monomers. Highly efficient and well-defined postpolymerization hydrolysis of the networks leads to (i) cleavage of azomethine links and (ii) removal of the template molecules from the networks. Although up to 40 wt % of the mass of the networks are removed via hydrolysis, the hyper-cross-linked scaffold of the networks is not collapsed and micropores are formed in the networks. In this way, the parent non-porous networks are transformed into networks with permanent micropores (diameter ~1 nm) and a specific surface area up to 623 m^2/g^{-1}. Simultaneously with the formation of micropores, functional groups (NH_2, CHO) are introduced into the networks. The prepared microporous networks adsorb the model adsorptives (up to 1.73 mmol CO_2/g and up to 6.53 mmol I_2/g.). The detemplating and micropores formation is confirmed by solid state NMR spectra and N_2 adsorption/desorption isotherms. The reported method of micropores formation could find a wider application for the preparation of microporous polymers with a well-defined texture and surface functionalization. Not only azomethine links but also many other groups with cleavable bonds could potentially be used for templating with covalently attached small molecules.

1. Introduction

After about two decades of intensive research, Porous Organic Polymers (POPs) or Microporous Organic Polymers (MOPs) have gained an important position among porous materials. POPs are organic or organometallic materials with permanent porosity and a high specific surface area in the order of hundreds to several thousand m^2/g [1–5]. Due to the predominantly organic nature of POPs, these materials can be prepared in a variety of covalent structures and with a wide spectrum of different functional groups. Thanks to their covalent and textural diversity, POPs are promising for applications in various areas, especially in (i) gas separation and reversible storage [6–10], (ii) separation of solutes [11–13], (iii) heterogeneous catalysis [14–19], (iv) optoactive materials and sensors construction [20–22], (v) energy transformation and storage [23,24], and (vi) analytical chemistry [25,26].

Most POPs possess the architecture of highly cross-linked polymer networks composed mainly of rigid cyclic and aromatic segments. The rigidity and the high degree of cross-linking prevent tight packing of the network segments, as a result, the networks contain unoccupied space forming micropores (i.e. pores with a diameter <2 nm). Micropores form directly during polymerization. The diameter of the micropores was in some cases controlled by the size and molecular geometry of the monomer molecules used for the synthesis. It was reported, for example, by Cooper et al. in the case of poly(arylenethynylene)-type POPs prepared via coupling polymerization [27] and by Wang et al. in the case POPs with adamantane knots prepared by condensation polymerization [28].

To prepare POPs containing, in addition to micropores, larger mesopores (diameter from 2 to 50 nm) and/or macropores (diameter >50 nm) various templating approaches were applied. In this case, micropores were formed due to polymerization and cross-linking while large pores resulted after removal of the template. Ding et al. hyper-cross-

* Corresponding author.
** Corresponding author.
E-mail addresses: bashtab@natur.cuni.cz (B. Bashta), jan.sedlacek@natur.cuni.cz (J. Sedláček).

https://doi.org/10.1016/j.micromeso.2021.111636
Received 22 September 2021; Received in revised form 25 November 2021; Accepted 8 December 2021
Available online 11 December 2021
1387-1811/

linked phenylmethylsilicone oligomers via Friedel-Crafts knitting reaction into microporous POPs. Postpolymerization decomposition of Si-containing segments led to the formation of mesopores in these POPs [29]. Seo et al. used readily hydrolyzable polylactide as a template to introduce mesopores into hyper-cross-linked POPs prepared by a combination of radical polymerization and Friedel-Crafts knitting reaction [30]. Pore size distribution was controlled by the molar mass of the polylactide template and the covalent composition of POPs [31,32]. A combination of polymerization and High-Internal-Phase-Emulsion templating was efficient for preparing POPs containing both micropores and macropores [33,34].

The template technique was also applied in several cases to modify the microporous texture of POPs. Lee and Seo prepared primary networks by radical copolymerization of 4-(chloromethyl)styrene, 4-(trimethylsilyl)styrene, and divinylbenzene. The secondary (postpolymerization) cross-linking of these networks through the reaction of $ClCH_2$- groups with benzene rings was accompanied by the removal of $(CH_3)_3Si$- side groups. This facilitated the cross-linking process. Simultaneously, the removal of $(CH_3)_3Si$- groups (serving as the low-molecular-weight template) caused the formation of additional voids in POPs. This was manifested by an increase in micropore volume and diameter in comparison with similar POPs prepared from copolymers free of $(CH_3)_3Si$- template groups [35]. Huang et al. used radical copolymerization of mixtures of monomers (di-*tert*-butyl-4, 4′-stilbene dicarboxylate, *tert*-butyl 4-vinylbenzoate, *tert*-butyl 4-maleimidobenzoate, and divinylbenzene cross-linker) to prepare microporous POPs. The postpolymerization thermal or chemical modification (with CF_3COOH or $ZnBr_2$) led to an increase in the micropore volume and the specific surface area of these POPs. This was ascribed to the removal of *tert*-butyl groups and the formation of additional voids in POPs [36].

In this paper, we report the formation of micropores in polyacetylene-type hyper-cross-linked networks containing 4-methylaniline and 4-methylbenzaldehyde molecules as a covalently attached template. Postpolymerization hydrolytic removal of template molecules led to the transformation of the parent non-porous networks into POPs with a microporous texture and a specific surface area up to 623 m^2/g. At the same time, functional groups (NH_2, CHO) were introduced into the networks. The removal of the template was monitored by solid state NMR spectroscopy which confirmed the high selectivity and efficiency of this process.

2. Experimental section/Methods

2.1. Materials: (Acetylacetonato)(norbornadiene)rhodium(I), [Rh(nbd)acac], (>98%), tetrakis(4-ethynylphenyl)methane, TEPhM (>98%) (both TCI Europe) were used as received. Dichloromethane (99.95%, Lach-Ner) was distilled with P_2O_5. Methanol (99.99% Lach-Ner) was used as obtained. *N*-(4-Ethynylbenzylidene)-4-methylaniline (M1) and *N*-(4-methylbenzylidene)-4-ethynylaniline (M2) were prepared according to Refs. [37,38] Preparation of *N*-(3,5-diethynylbenzylidene)-4-methylaniline (M3) is described in Supporting Information. The following precursors for the synthesis of M1, M2, and M3 were used as received: 4-ethynylaniline (>98%, TCI Europe), 4-ethynylbenzaldehyde (95%, abcr), 3,5-diethynylbenzaldehyde (98% Spectra Group Limited, Inc.), 4-methylaniline (99.7% Sigma-Aldrich) and 4-methylbenzaldehyde (97% Sigma-Aldrich).

2.2. Polymerization: (i) M3 was homopolymerized, (ii) M1 and M2 were copolymerized with TEPhM in CH_2Cl_2 at 75 °C in the sealed thick-wall ampoules. Complex [Rh(nbd)acac] was used as the polymerization catalyst. The mole ratios of the comonomers in the copolymerization feeds were: M1:TEPhM = 4:1, M2:TEPhM = 4:1. The reaction time was 7 days, the overall initial concentration of monomer(s) = 0.3 mol/dm, the concentration of [Rh(nbd)acac] = 15 mmol/dm. In a typical polymerization, 1 g of monomer(s) was used. The polymerizations were started by adding the catalyst solution to the solution of monomer(s). After 7 days, the precipitated polymer network was separated, washed repeatedly with CH_2Cl_2, and dried under vacuum (i) for 2 days at room temperature and then (ii) for 5 h at 110 °C. The yield was determined gravimetrically.

2.3. Hydrolytic detemplating: In a typical experiment, 300 mg of a dry polymer network with azomethine groups were dispersed in methanol (60 ml) containing HCl and stirred in this solution for 5 days at room temperature. The mole ratio of HCl to azomethine groups was 10/1. The hydrolysed network was then washed with water. Hydrolysis of the networks with M1 and M3 units yielded networks containing both benzaldehyde and benzaldehyde dimethyl acetal groups. To convert the benzaldehyde dimethyl acetal groups to benzaldehyde groups the freshly hydrolysed networks were treated with 100 ml of HCl water solution (1 wt %) for 2 days (under stirring) at room temperature. Finally, the networks were washed thoroughly with water and dried under vacuum (i) for 2 days at room temperature and then (ii) for 5 h at 110 °C. The hydrolysis of the network with M2 units provided a network in which the aniline groups were partly protonated. Therefore, the freshly hydrolysed network was treated (under stirring) with 100 ml of aqueous K_2CO_3 solution (10 wt %) for 2 days at room temperature. Finally, the network was washed thoroughly with water and dried under vacuum (i) for 2 days at room temperature and then (ii) for 5 h at 110 °C.

2.4. Techniques: All ^{13}C Cross-Polarization Magic Angle Spinning (CP/MAS) NMR spectra were measured at 11.7 T using a Bruker Avance III 500 WB/US NMR spectrometer (for details see Supporting Information) [39]. The adsorption/desorption isotherms of nitrogen (at 77 K), as well as CO_2 (at 273 and 293 K) on the polymer networks were measured using a Triflex V4.02 apparatus (Micromeritics). Before the sorption was measured, all samples were degassed on a Micromeritics SmartVacPrep instrument as described elsewhere [9]. The Brunauer-Emmett-Teller specific surface area, S_{BET}, was determined utilizing nitrogen adsorption data in the relative pressure range from 0.05 to 0.2. The micropore volume, V_{mi}, was determined on the base of nitrogen amount trapped at $p/p_0 = 0.1$ ($p_0 = 101325$ Pa). The total pore volume, V_{tot}, was determined on the base of nitrogen amount trapped at $p/p_0 = 0.97$.

To evaluate the pore size distribution semi-empirical method of Horvath Kawazoe was used. Model for the slit pore geometry (original Horvath Kawazoe) with carbon-graphite adsorbent was used for calculation of the size of the pores.

3. Results and discussion

Here we report a new path to polymers with permanent microporosity through postpolymerization modification of originally nonporous hyper-cross-linked networks.

Two Schiff-base-type monomers, *N*-(4-ethynylbenzylidene)-4-methylaniline (M1) and *N*-(4-methylbenzylidene)-4-ethynylaniline (M2) were prepared according to Refs. [37,38] Both M1 and M2 contained one polymerizable ethynyl group per molecule and one azomethine group connecting two benzene rings in the molecule (Scheme 1). Monoethynylated aromatic Schiff bases of this type are known to polymerize readily in a chain growth polymerization manner into linear polyacetylenes with Schiff base pendant groups [40–42]. Various Rh(I) complexes were described as efficient catalysts of these polymerizations due to their high compatibility with azomethine groups of the monomers. To prepare polyacetylene networks with monomeric units derived from M1 and M2 we copolymerized (independently) with tetrakis (4-ethynylphenyl)methane (TEPhM) comonomer serving as a cross-linker (Scheme 1). The mole ratios M1:TEPhM and M2:TEPhM in the feed were 4:1, [Rh(nbd)acac] complex was used as a polymerization catalyst [43] (for more details see Experimental part). Both copolymerizations provided quantitative yields of respective polyacetylene networks, P(M1/TEPhM) and P(M2/TEPhM) (Scheme 1).

The networks were brown solids that did not swell in CH_2Cl_2, toluene, tetrahydrofuran, and methanol. The ^{13}C CP/MAS NMR spectra of P(M1/TEPhM) and P(M2/TEPhM) are shown in Fig. 1. A broad, partly

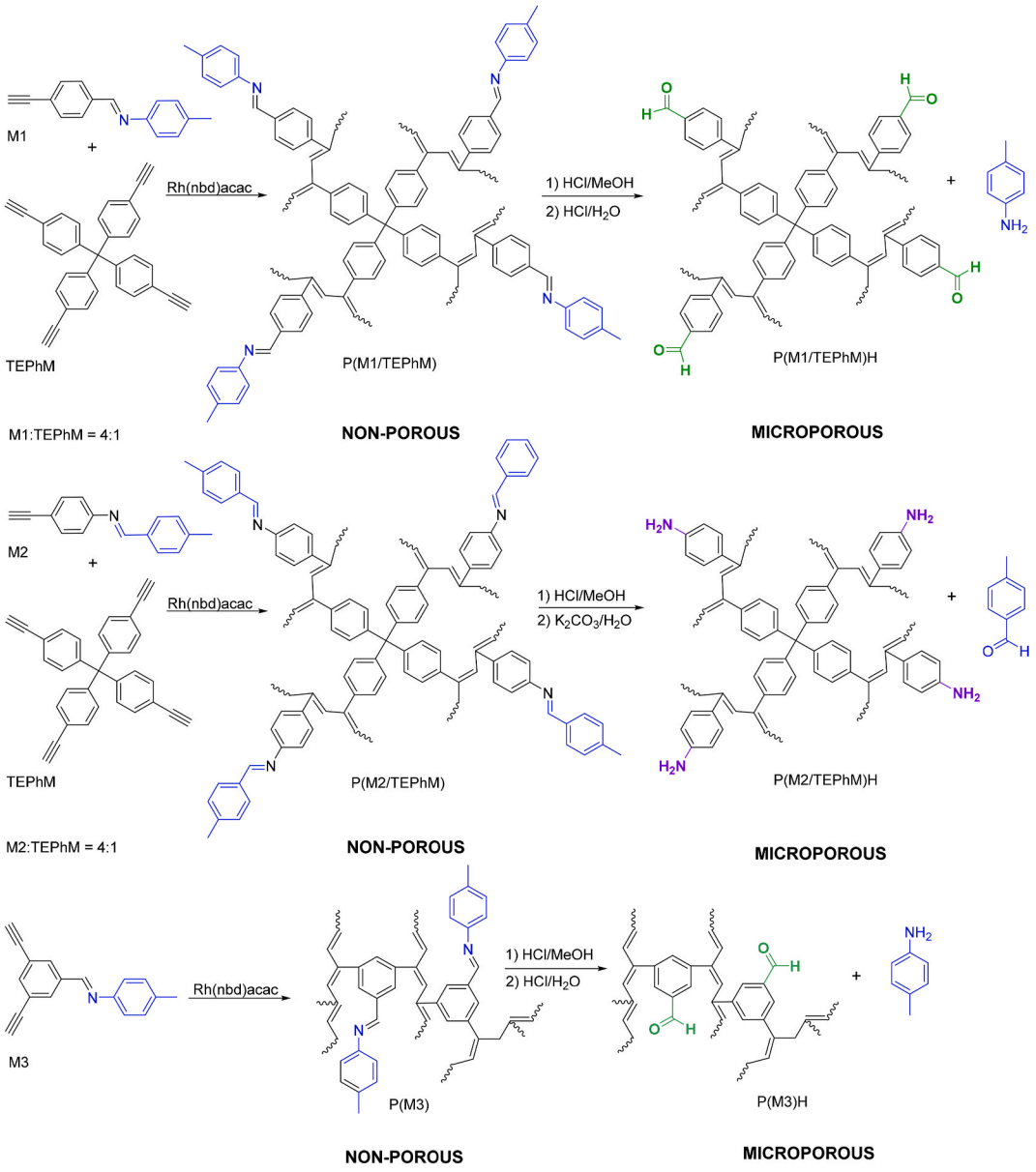

Scheme 1. Preparation of microporous networks via template approach.

resolved signal in the region from $\delta = 120$–150 ppm dominating the ^{13}C CP/MAS NMR spectra of both networks corresponded to the resonance of aromatic carbon atoms and carbon atoms of the unsaturated polyene main chains. The sharp signal at 20 ppm corresponded to the methyl groups of the monomeric units formed from M1 and M2. The weak signal at 65 ppm was due to the central sp^3 carbon of the cross-linking units formed from TEPhM. The ^{13}C CP/MAS NMR spectra of both networks contained the distinct signals at about $\delta = 160$ ppm corresponding to the carbon atoms of azomethine groups that confirmed the preservation of these groups in P(M1/TEPhM) and P(M2/TEPhM). In contrast, the spectra of both networks did not contain pronounced signals characteristic of sp carbon atoms of ethynyl groups (region from $\delta = 70$–90 ppm). This confirmed that not only the ethynyl groups of the monoethynylated M1 and M2 but also most of the four ethynyl groups of the TEPhM cross-linker were transformed to vinylene segments of the main chains during polymerization. The high conversion of the ethynyl groups of TEPhM confirmed a high extent of cross-linking (hyper-cross-linking) of P(M1/TEPhM) and P(M2/TEPhM) networks (see Scheme 1).

P(M1/TEPhM) and P(M2/TEPhM) were characterized using standard nitrogen adsorption/desorption at 77 K (see Experimental) to evaluate the porosity of the networks. However, both networks adsorbed only a negligible amount of N_2 i.e. both networks were virtually non-porous (see Table 1). This was despite the high extent of cross-linking and the rigidity of polyacetylene main chains forming the networks. It should be noted that TEPhM is an efficient cross-linker frequently used for the synthesis of various microporous polymers utilizing both step-growth [44,45] and chain-growth [15] polymerizations.

The chain-growth homopolymerization of TEPhM performed under the conditions used in this study provided highly microporous homopolymer network P(TEPhM) with the Brunauer-Emmett-Teller specific surface area, S_{BET}, of 885 m^2/g (see Supporting Information for details). Therefore we concluded that the non-porous character of P(M1/TEPhM) and P(M2/TEPhM) could reflect the bulkiness of *N*-benzylidene aniline substituents that could occupy the potential micropores in the networks. As can be seen from Scheme 1, the substituents of P(M1/TEPhM) and P(M2/TEPhM) were designed so that the possibility of the post-polymerization reduction of the size of these substituents could be investigated. Thus, P(M1/TEPhM) and P(M2/TEPhM) were submitted to

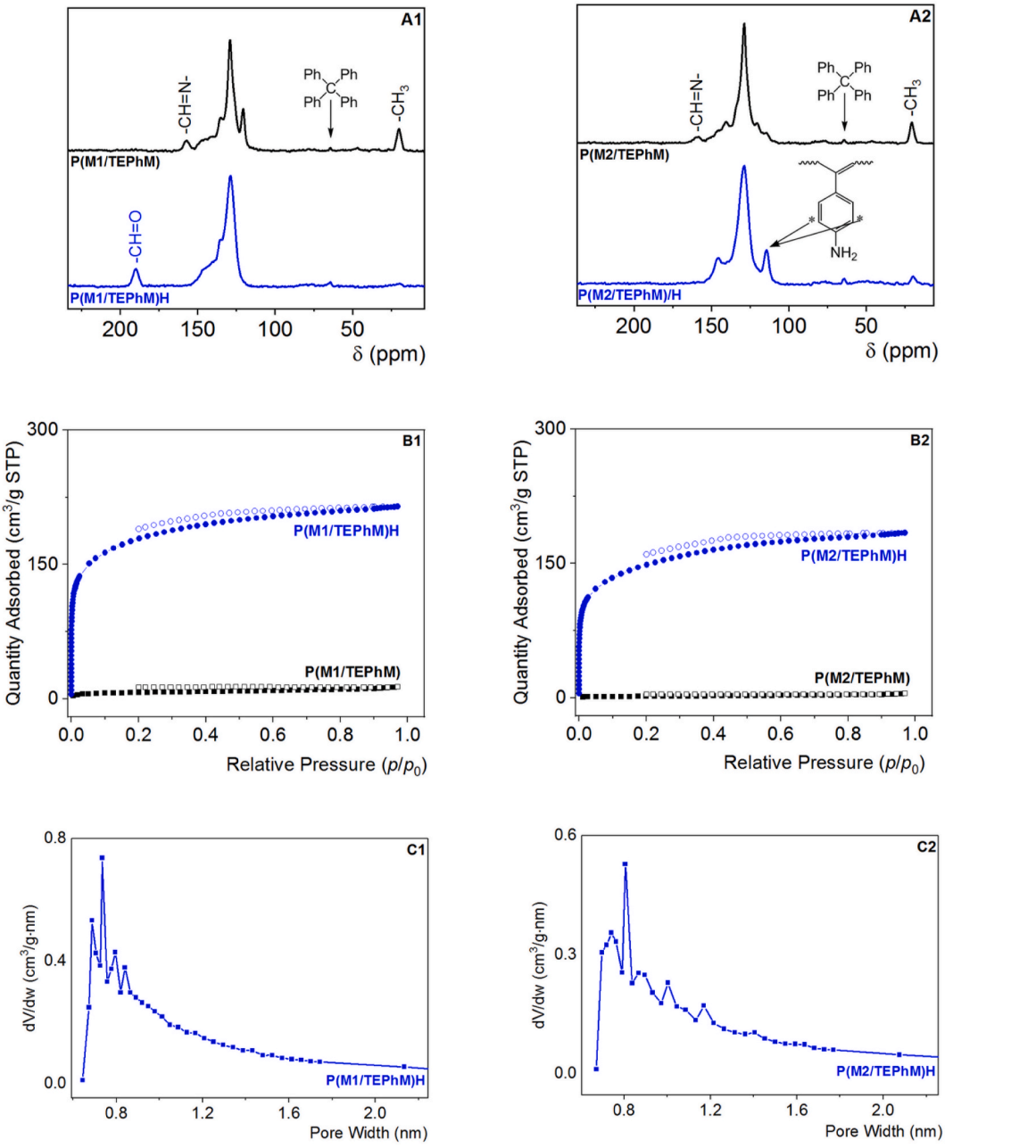

Fig. 1. ^{13}C CP/MAS NMR spectra (A1, A2), N_2 adsorption (full points), and desorption (empty points) isotherms (77 K) (B1, B2) and micropore size distribution (C1, C2).

Table 1
Specific surface area (S_{BET}), micropore volume (V_{mi}), total pore volume (V_{tot}), and adsorption capacities of the networks.

Parent networks		Hydrolysed networks						
Network code	$a_{max,N2}$[a] [mmol N_2/g]	Network code	$a_{max,N2}$[a] [mmol N_2/g]	S_{BET} [m^2/g]	V_{mi} [cm^3/g]	V_{tot} [cm^3/g]	$a_{max,CO2}$[b] [mmol CO_2/g]	$a_{max,I2}$[c] [mmol I_2/g]
P(M1/TEPhM)	0.59	P(M1/TEPhM)H	9.58	623	0.25	0.33	1.73	5.51
P(M2/TEPhM)	0.21	P(M2/TEPhM)H	8.22	522	0.21	0.28	1.58	6.53
P(M3)	0.08	P(M3)H	7.32	464	0.19	0.25	1.67	–

[a] $a_{max,N2}$ amount of nitrogen adsorbed at $p/p_0 = 0.97$ and 77 K.
[b] $a_{max,CO2}$ amount of carbon dioxide adsorbed at $p/p_0 = 0.97$ and 273 K.
[c] $a_{max,I2}$ amount of iodine adsorbed at 25 °C and equilibrium pressure of iodine vapour of 41 Pa.

the hydrolysis in HCl/methanol (see Experimental Part) to decompose CH=N bonds, release 4-methylaniline [from P(M1/TEPhM)] and 4-methylbenzaldehyde [from P(M2/TEPhM)] and reduce the size of the substituents of M1 and M2 monomeric units (Scheme 1). Optimization of the hydrolysis of P(M1/TEPhM) and P(M2/TEPhM) showed that a relatively long reaction time (5 days and intensive mixing) was required to ensure high efficiency of this process.

The hydrolysis of P(M1/TEPhM) with HCl/methanol provided a network in which, in addition to benzaldehyde groups, benzaldehyde dimethyl acetal groups were present (confirmed by ^{13}C CP/MAS NMR spectroscopy). Therefore, subsequent treatment of this network with HCl/H_2O was necessary to convert benzaldehyde dimethyl acetal groups to benzaldehyde groups. The treatment of P(M1/TEPhM) with HCl/methanol and then with HCl/H_2O provided a network labelled as P(M1/TEPhM)H. Similarly, the hydrolysis of P(M2/TEPhM) with HCl/methanol had to be followed by treating the hydrolysed network with an aqueous solution of K_2CO_3 to convert the anilinium chloride groups of the networks to aniline groups. Treatment of P(M2/TEPhM) with HCl/methanol and then with K_2CO_3/H_2O gave the P(M2/TEPhM)H network.

Fig. 1 compares ^{13}C CP/MAS NMR spectra of hydrolysed networks [P(M1/TEPhM)H and P(M2TEPhM)H] and their parent counterparts. The efficient decomposition of azomethine groups of parent networks was manifested by the absence of signals at δ = 160 ppm in ^{13}C CP/MAS NMR spectra of P(M1/TEPhM)H and P(M2TEPhM)H. The intensity of the signals of methyl groups (δ = 20 ppm) in the spectra of the hydrolysed networks was strongly diminished compared to the intensity of these signals in the spectra of the parent networks. This suggested that the decomposition of the azomethine groups covalently attaching 4-methylaniline and 4-methylbenzaldehyde to the networks was accompanied by efficient diffusion of free 4-methylaniline and 4-methylbenzaldehyde molecules from the networks into the liquid phase. ^{13}C CP/MAS NMR spectroscopy further confirmed the presence of new functional groups in the hydrolysed networks: signal at δ = 190 ppm in the spectrum of P(M1/TEPhM)H corresponded to the resonance of carbon atoms of aldehyde groups, the signal at δ = 125 ppm in the spectrum of P(M2/TEPhM)H confirmed the presence of aniline substituents in the network (see Fig. 1 for the assignment). The presence of new functional groups in the hydrolysed networks was confirmed also by IR spectroscopy: the aldehyde groups in P(M1/TEPhM)H were manifested by a strong IR band at 1703 cm^{-1}, the presence of aniline segments in P(M2/TEPhM) was manifested by IR bands at 1604 and 1280 cm^{-1} (see Fig. S5 in Supporting Information for the IR spectra of the hydrolysed networks).

The N_2 adsorption/desorption characterization (77 K) unambiguously showed that the above-described postpolymerization hydrolytic treatment of non-porous P(M1/TEPhM) and P(M2/TEPhM) led to the establishment of a porous texture in both final networks, P(M1/TEPhM)H and P(M2/TEPhM)H. The N_2 adsorption/desorption isotherms on P(M1/TEPhM)H and P(M2/TEPhM)H are shown in Fig. 1. According to IUPAC classification, the shape of adsorption isotherms corresponded to the Type I isotherm characteristic for microporous materials. The micropore volume (V_{mi}) ascertained from the adsorption isotherms was 0.25 cm^3/g in the case of P(M1/TEPhM)H and 0.21 cm^3/g in the case of P(M2/TEPhM)H. In both cases, V_{mi} values represented about 75% of total pore volume, V_{tot} (see Table 1). Both microporous networks had micropore size distributions over a broader range of micropore diameters with maxima at about 0.75 nm. The (apparent) S_{BET} values were 623 m^2/g [P(M1/TEPhM)H] and 522 m^2/g [P(M2/TEPhM)H].

To prepare P(M1/TEPhM)H and P(M2/TEPhM)H, a pair of comonomers differing in their functions had to be used as starting material. The M-type comonomer (M1 or M2) contained covalently attached template molecules, the TEPhM comonomer served as a cross-linker. Subsequently, we managed to combine templating and cross-linking functions of the above comonomers in a new monomer, *N*-(3,5-diethynylbenzylidene)-4-methylaniline (M3) (see Supporting Information for M3 synthesis). The M3 molecule contained a releasable 4-methylaniline segment and two ethynyl groups (on the benzylidene ring), the polymerization of which was to ensure cross-linking of the product (see Scheme 1). The [Rh(nbd)acac] catalysed chain-growth homopolymerization of M3 provided a non-porous polyacetylene network P(M3) in quantitative yield. ^{13}C CP/MAS NMR spectroscopy confirmed the preservation of azomethine groups in P(M3) and revealed that some ethynyl groups remained unreacted in P(M3) (see signals due to sp carbon atoms in the region from δ = 75–85 ppm in ^{13}C CP/MAS NMR spectrum in Fig. 2). Thus, P(M3) contained, in addition to the cross-linking units in which both ethynyl groups were reacted and inbuilt in polyene chains, also linear units in which one ethynyl group remained unreacted. However, P(M3) was totally insoluble in CH_2Cl_2, toluene, tetrahydrofuran, and methanol and did not swell in these solvents. This indicated a sufficient degree of cross-linking of P(M3).

The hydrolysis of P(M3) in HCl/methanol and subsequently in HCl/H_2O provided a network P(M3)H. ^{13}C CP/MAS NMR spectrum of P(M3)H confirmed the high efficiency of cleavage of azomethine groups of P(M3) and efficient removal of free 4-methylaniline template molecules from the network (see Fig. 2).

^{13}C CP/MAS NMR spectroscopy further confirmed the presence of aldehyde groups in P(M3)H (signal at δ = 190 ppm) and showed that a small number of aldehyde groups was remaining in the form of dimethyl acetal in P(M3)H (signals at δ = 54 ppm and 103 ppm due to *C*H$_3$ and *C*H(OMe)$_2$ carbon atoms of benzaldehyde dimethyl acetal segments, respectively, see Fig. 2). We did not manage to fully decompose these residual acetal groups even by additional long-term hydrolysis (10 days) of P(M3)H with HCl/H_2O.

Nitrogen adsorption at 77 K confirmed the microporous texture of P(M3)H (see Fig. 2 for N_2 adsorption/desorption isotherms and micropore size distribution). The S_{BET} and V_{mi} values of P(M3)H, 464 m^2/g, and 0.19 cm^3/g, respectively, were only slightly lower than those achieved for the detemplated copolymer networks P(M1/TEPhM)H and P(M2/TEPhM)H. Evidently, the hydrolytic detemplating of homopolymer network P(M3) was also accompanied by the efficient formation of micropores.

Thermogravimetric Analysis (TGA) confirmed the high thermal stability of detemplated microporous networks P(M1/TEPhM)H, P(M2/TEPhM)H, and P(M3)H (see Fig. S6 in Supporting Information for the TGA curves). A mass loss of 5 wt% was observed at the following values of temperature, $t_{95\%}$: 293 [P(M1/TEPhM)H], 303 [P(M2/TEPhM)H], and 290 °C [P(M3)H]. The values of $t_{95\%}$ of the parent networks P(M1/TEPhM), P(M2/TEPhM), and P(M3) were about 60 °C higher (see Supporting Information), probably due to the compactness of these non-porous networks.

Microporous networks P(M1/TEPhM)H, P(M2/TEPhM)H, and P(M3)H were active in CO_2 adsorption (see Fig. S7 in Supporting Information for CO_2 adsorption isotherms). The CO_2 capture capacities, a_{maxCO2}, achieved at 273 K and CO_2 pressure of 100 kPa ranged from 1.58 to 1.73 mmol/g (see Table 1). The values of isosteric heats of CO_2 adsorption at the lowest amount adsorbed, Q_{st}, obtained from the temperature dependences of CO_2 adsorption isotherms, ranged from 27 to 29 kJ/mol (see Supporting Information, Fig. S8). The values of a_{maxCO2} corresponded to the medium values of CO_2 capture capacities often reported for POPs, the values of Q_{st} were in the range typical for the physisorption nature of CO_2 capture [6,9,46]. It should be noted that the parent polymer networks P(M1/TEPhM), P(M2/TEPhM), and P(M3) also showed some (low) activity in CO_2 capture. The values of a_{maxCO2} achieved at 273 K and CO_2 pressure of 100 kPa were as follows 0.50 mmol/g for P(M1/TEPhM), 0.49 mmol/g for P(M2/TEPhM), and 0.41 mmol/g for P(M3), (see Fig. S9 in Supporting Information). Most likely, the penetration of CO_2 into non-porous networks was due to a certain flexibility of the network segments at 273 K allowing the formation of non-permanent pores in the networks, as already proposed in the literature [47,48].

P(M1/TEPhM)H and P(M2/TEPhM)H were also tested as adsorbents for iodine vapour capture. The adsorption was performed in air at

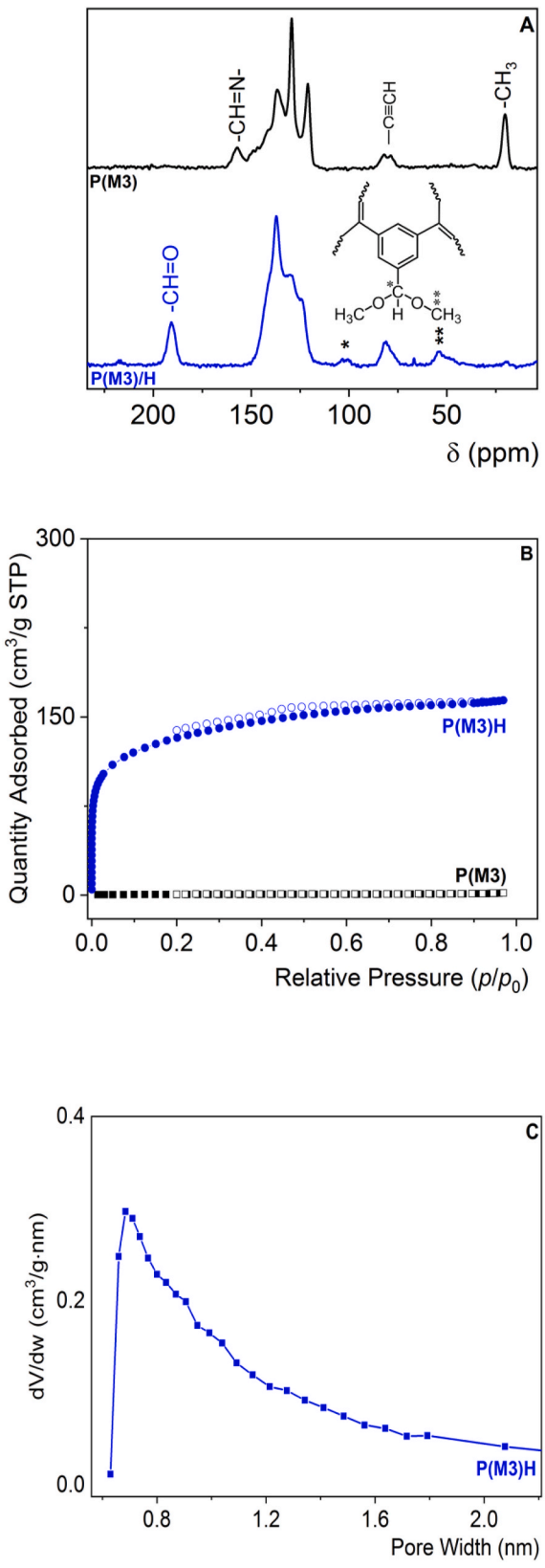

Fig. 2. ^{13}C CP/MAS NMR spectra (A), N_2 adsorption (full points) and desorption (empty points) isotherms (77 K) (B), and micropore size distribution (C).

ambient pressure at 298 K (corresponding iodine vapour pressure of 41 Pa, ref. [49]). The iodine capture capacities, a_{maxI2}, achieved after 3 days of adsorption were as follows: 5.51 mmol/g, i.e. 140 wt% (P(M1/TEPhM)H) and 6.53 mmol/g, i.e. 165 wt% (P(M2/TEPhM)H) (Table 1). Further prolongation of the adsorption time did not lead to a measurable increase in a_{maxI2}. The values of a_{maxI2} achieved on P(M1/TEPhM)H and P(M2/TEPhM)H were among the higher values reported for POPs applied to I_2 sorption under similar conditions [50,51]. Both P(M1/TEPhM)H and P(M2/TEPhM)H were efficient also in the capture of I_2 dissolved in CH_2Cl_2. 10 mg of P(M2/TEPhM)H removed 95% of I_2 from 2 ml of I_2 solution (concentration = 0.2 mg/ml) within 5 h. Using P(M1/TEPhM)H as an adsorbent, the same effective capture was achieved after 240 h. Evidently, P(M2/TEPhM)H decorated with NH_2 groups was more efficient in I_2 capture than P(M1/TEPhM)H decorated with aldehyde groups. The high efficiency of NH_2 containing P(M2/TEPhM)H in I_2 capture is in agreement with the literature describing porous materials with amino groups as promising sorbents for I_2 capture in various applications [51].

4. Conclusions

P(M1/TEPhM)H, P(M2/TEPhM)H, and P(M3)H are microporous polymers in which permanent micropores (diameter ~1 nm) were achieved exclusively by removing covalently attached low-molecular-weight template segments from non-porous precursors. A combination of polyacetylene chemistry and Schiff-base chemistry was used for this purpose. It should be noted that Schiff-base chemistry involving the decomposition or, conversely, the formation of azomethine links is a frequently used tool for the postpolymerization modification of various polymers. In most cases, however, soluble polymer chains or swollen polymer gels with well-solvated segments were modified in this way [52]. In contrast, P(M1/TEPhM), P(M2/TEPhM), and P(M3) were compact non-porous, and non-swellable materials. Nevertheless, we have achieved high efficiency in cleaving azomethine links in these compact networks as well as in removing released aniline and benzaldehyde segments from the networks. The scaffold of networks did not collapse after this detemplating. This was most probably due to the rigidity of the conjugated main chains of the networks, in which double and single bonds alternated between carbon atoms. In addition to the formation of micropores, new functional groups (NH_2 and CHO) were also introduced into the networks through detemplating process. The prepared microporous networks physisorbed the model adsorptives (CO_2, I_2). The sorption capacities were similar to the capacities reported for microporous polymers, microporosity of which was generated during polymerization (i.e. without templating).

Data availability statement

The raw/processed data required to reproduce these findings cannot be shared at this time as the data also forms part of an ongoing study.

Declaration of competing interest

The authors declare that they have no known competing financial interests or personal relationships that could have appeared to influence the work reported in this paper.

Supporting Information is available from the Wiley Online Library or from the author.

Acknowledgements

Financial support from the Czech Science Foundation (Project 21-02183S) and “Grant Schemes at CU“ (reg. no. CZ.02.2.69/0.0/0.0/19_073/0016935) (START/SCI/081) is gratefully acknowledged (L. Havelková).

Appendix A. Supplementary data

Supplementary data to this article can be found online at https://doi.org/10.1016/j.micromeso.2021.111636.

References

[1] J.S.M. Lee, A.I. Cooper, Advances in conjugated microporous polymers, Chem. Rev. 120 (2020) 2171–2214, https://doi.org/10.1021/acs.chemrev.9b00399.

[2] K. Amin, N. Ashraf, L.J. Mao, C.F.J. Faul, Z.X. Wei, Conjugated microporous polymers for energy storage: recent progress and challenges, Nanomater. Energy 85 (2021) 105958, https://doi.org/10.1016/j.nanoen.2021.105958.

[3] J. Huang, S.R. Turner, Hypercrosslinked polymers: a review, Polym. Rev. 58 (2018) 1–41, https://doi.org/10.1080/15583724.2017.1344703.

[4] U.H.F. Bunz, K. Seehafer, F.L. Geyer, M. Bender, I. Braun, E. Smarsly, J. Freudenberg, porous polymers based on aryleneethynylene building blocks, Macromol. Rapid Commun. 35 (2014) 1466–1496, https://doi.org/10.1002/marc.201400220.

[5] S.H. Luo, Z.T. Zeng, H. Wang, W.P. Xiong, B. Song, C.Y. Zhou, A.B. Duan, X.F. Tan, Q.Y. He, G.M. Zeng, Z.F. Liu, R. Xiao, Recent progress in conjugated microporous polymers for clean energy: synthesis, modification, computer simulations, and applications, Prog. Polym. Sci. 115 (2021) 101374, https://doi.org/10.1016/j.progpolymsci.2021.101374.

[6] R. Dawson, A.I. Cooper, D.J. Adams, Chemical functionalization strategies for carbon dioxide capture in microporous organic polymers, Polym. Int. 62 (2013) 345–352, https://doi.org/10.1002/pi.4407.

[7] Y. Byun, S.H. Je, S.N. Talapaneni, A. Coskun, Advances in porous organic polymers for efficient water capture, Chem. Eur J. 25 (2019) 10262–10283, https://doi.org/10.1002/chem.201900940.

[8] B. Lopez-Iglesias, F. Suárez-García, C. Aguilar-Lugo, A. González Ortega, C. Bartolomé, J.M. Martínez-Ilarduya, J.G. de la Campa, Á.E. Lozano, C. Álvarez, Microporous polymer networks for carbon capture applications, ACS Appl. Mater. Interfaces 10 (2018) 26195–26205, https://doi.org/10.1021/acsami.8b05854.

[9] A. Hašková, B. Bashta, Š. Titlová, J. Brus, A. Vagenknechtová, E. Vyskočilová, J. Sedláček, Microporous hyper-cross-linked polymers with high and tuneable content of pyridine units: synthesis and application for reversible sorption of water and carbon dioxide, Macromol. Rapid Commun. 42 (2021) 2100209, https://doi.org/10.1002/marc.202100209.

[10] A.E. Sadak, A comparative gas sorption study of dicarbazole-derived microporous hyper-crosslinked polymers, Microporous Mesoporous Mater. 311 (2021) 110727, https://doi.org/10.1016/j.micromeso.2020.110727.

[11] S.Q. Zhuo, X.H. Wang, L.Y. Li, S. Yang, Y.B. Ji, Chiral carboxyl-functionalized covalent organic framework for enantioselective adsorption of amino acids, ACS Appl. Mater. Interfaces 13 (2021) 31059–31065, https://doi.org/10.1021/acsami.1c09238.

[12] Y.C. Liu, Y.Z. Cui, C.H. Zhang, J.F. Du, S. Wang, Y. Bai, Z.Q. Liang, X.W. Song, Post-cationic modification of a pyrimidine-based conjugated microporous polymer for enhancing the removal performance of anionic dyes in water, Chem. Eur J. 24 (2018) 7480–7488, https://doi.org/10.1002/chem.201800548.

[13] L. Havelková, A. Hašková, B. Bashta, J. Brus, M. Lhotka, E. Vrbková, M. Kindl, E. Vyskočilová, J. Sedláček, Synthesis of hyper-cross-linked microporous poly (phenylacetylene)s having aldehyde and other groups and their chemisorption and physisorption ability, Eur. Polym. J. 114 (2019) 279–286, https://doi.org/10.1016/j.eurpolymj.2019.02.039.

[14] Q. Sun, Z.F. Dai, X.J. Meng, F.S. Xiao, Porous polymer catalysts with hierarchical structures, Chem. Soc. Rev. 44 (2015) 6018–6034, https://doi.org/10.1039/c5cs00198f.

[15] L. Sekerová, M. Lhotka, E. Vyskočilová, T. Faukner, E. Slováková, J. Brus, L. Červený, J. Sedláček, Hyper-cross-linked polyacetylene type microporous networks decorated with terminal ethynyl groups as heterogeneous acid catalysts for acetalization and esterification reactions, Chem. Eur J. 24 (2018) 14742–14749, https://doi.org/10.1002/chem.201802432.

[16] S. Bhunia, B. Banerjee, A. Bhaumik, A new hypercrosslinked supermicroporous polymer, with scope for sulfonation, and its catalytic potential for the efficient synthesis of biodiesel at room temperature, Chem. Commun. 51 (2015) 5020–5023, https://doi.org/10.1039/c4cc09872b.

[17] C.G. Lopez-Calixto, M. Barawi, M. Gomez-Mendoza, F.E. Oropeza, F. Fresno, M. Liras, V.A.D. O'Shea, Hybrids based on BOPHY-conjugated porous polymers as photocatalysts for hydrogen production: insight into the charge transfer pathway, ACS Catal. 10 (2020) 9804–9812, https://doi.org/10.1021/acscatal.0c01346.

[18] S. Rat, A. Chavez-Sanchez, M. Jerigova, D. Cruz, M. Antonietti, Acetic anhydride polymerization as a pathway to functional porous organic polymers and their application in acid-base catalysis, ACS Appl. Polym. Mater. 3 (2021) 2588–2597, https://doi.org/10.1021/acsapm.1c00202.

[19] A.E. Sadak, E. Karakus, Y.M. Chumakov, N.A. Dogan, C.T. Yavuz, Triazatruxene-based ordered porous polymer: high capacity CO2, CH4, and H-2 capture, heterogeneous Suzuki-Miyaura catalytic coupling, and thermoelectric properties, ACS Appl. Energy Mater. 3 (2020) 4983–4994, https://doi.org/10.1021/acsaem.0c00539.

[20] A. Manna, M. Das, S. Mukherjee, S. Das, All-in-One: sensing, adsorptive removal, and photocatalytic degradation of nitro-explosive contaminants by microporous polycarbazole polymer, Macromol. Rapid Commun. 42 (2021) 2000469, https://doi.org/10.1002/marc.202000469.

[21] D.Y. Wang, W.J. Wang, R. Wang, S.C. Xi, B. Dong, A fluorescent covalent triazine framework consisting of donor-acceptor structure for selective and sensitive sensing of Fe3+, Eur. Polym. J. 147 (2021) 110297, https://doi.org/10.1016/j.eurpolymj.2021.110297.

[22] D. Bondarev, R. Sivkova, P. Šuly, M. Polášková, O. Krejčí, R. Křikavová, Z. Trávníček, A. Zukal, M. Kubů, J. Sedláček, Microporous conjugated polymers via homopolymerization of 2,5-diethynylthiophene, Eur. Polym. J. 92 (2017) 213–219, https://doi.org/10.1016/j.eurpolymj.2017.04.042.

[23] C.W. Kang, Y.J. Ko, S.M. Lee, H.J. Kim, J. Choi, S.U. Son, Carbon black nanoparticle trapping: a strategy to realize the true energy storage potential of redox-active conjugated microporous polymers, J. Mater. Chem. A. 9 (2021) 17978–17984, https://doi.org/10.1039/d1ta04782e.

[24] X.P. Wang, B. Chen, W.B. Dong, X.H. Zhang, Z.B. Li, Y.G. Xiang, H. Chen, Hydrophilicity-controlled conjugated microporous polymers for enhanced visible-light-driven photocatalytic H-2 evolution, Macromol, Rapid Commun 40 (2019) 1800494, https://doi.org/10.1002/marc.201800494.

[25] Y.Y. Cui, X.Q. He, C.X. Yang, X.P. Yan, Application of microporous organic networks in separation science, TrAC Trends Anal. Chem. (Reference Ed.) 139 (2021) 116268, https://doi.org/10.1016/j.trac.2021.116268.

[26] H. Chi, X. Qi, X.H. Wang, Y. Wang, X.H. Han, J. Wang, H.W. Wang, Preparative separation and purification of loliolide and epiloliolide from Ascophyllum nodosum using amine-based microporous organic polymer for solid phase extraction coupled with macroporous resin and prep-HPLC, Anal. Methods. 13 (2021) 1939–1944, https://doi.org/10.1039/d1ay00186h.

[27] J.X. Jiang, F. Su, A. Trewin, C.D. Wood, H. Niu, J.T.A. Jones, Y.Z. Khimyak, A. I. Cooper, Synthetic control of the pore dimension and surface area in conjugated microporous polymer and copolymer networks, J. Am. Chem. Soc. 130 (2008) 7710–7720, https://doi.org/10.1021/ja8010176.

[28] G.Y. Li, B. Zhang, J. Yan, Z.G. Wang, The directing effect of linking units on building microporous architecture in tetraphenyladmantane-based poly(Schiff base) networks, Chem. Commun. 50 (2014) 1897–1899, https://doi.org/10.1039/c3cc48593e.

[29] L. Ding, H. Gao, F.F. Xie, W.Q. Li, H. Bai, L. Li, Porosity-enhanced polymers from hyper-cross-linked polymer precursors, Macromolecules 50 (2017) 956–962, https://doi.org/10.1021/acs.macromol.6b02715.

[30] M. Seo, S. Kim, J. Oh, S.J. Kim, M.A. Hillmyer, Hierarchically porous polymers from hyper-cross-linked block polymer precursors, J. Am. Chem. Soc. 137 (2015) 600–603, https://doi.org/10.1021/ja511581w.

[31] J. Lee, M. Seo, Downsizing of block polymer-templated nanopores to one nanometer via hyper-cross-linking of high chi-low N precursors, ACS Nano 15 (2021) 9154–9166, https://doi.org/10.1021/acsnano.1c02690.

[32] S. Kim, M. Seo, Control of porosity in hierarchically porous polymers derived from hyper-crosslinked block polymer precursors, J. Polym. Sci. Part A Polym. Chem. 56 (2018) 900–913, https://doi.org/10.1002/pola.28966.

[33] E. Slováková, M. Ješelnik, E. Žagar, J. Zedník, J. Sedláček, S. Kovačič, Chain-growth insertion polymerization of 1,3-diethynylbenzene high internal phase emulsions into reactive π-conjugated foams, Macromolecules 47 (2014) 4864–4869, https://doi.org/10.1021/ma501142d.

[34] S. Jurjevec, G. Zerjav, A. Pintar, E. Zagar, S. Kovacic, Tunable poly (aryleneethynylene) networks prepared by emulsion templating for visible-light-driven photocatalysis, Catal. Today 361 (2021) 146–151, https://doi.org/10.1016/j.cattod.2020.01.049.

[35] J. Lee, M. Seo, Hyper-cross-linked polymer with enhanced porosity by in Situ removal of trimethylsilyl group via electrophilic aromatic substitution, ACS Macro Lett. 7 (2018) 1448–1454, https://doi.org/10.1021/acsmacrolett.8b00752.

[36] J. Huang, X. Zhou, A. Lamprou, F. Maya, F. Svec, S.R. Turner, Nanoporous polymers from cross-linked polymer precursors via tert-butyl group deprotection and their carbon dioxide capture properties, Chem. Mater. 27 (2015) 7388–7394, https://doi.org/10.1021/acs.chemmater.5b03114.

[37] H. Balcar, J. Cejka, J. Kubista, L. Petrusova, P. Kubat, V. Blechta, Preparation and properties of isomeric N-(4-substituted benzylidene)-4-ethynylanilines and 4-substituted N-(4-ethynylbenzylidene)anilines, Collect. Czech Chem. Commun. 65 (2000) 203–215, https://doi.org/10.1135/cccc20000203.

[38] H. Balcar, J. Sedláček, J. Vohlídal, J. Zedník, V. Blechta, New polyacetylenes with aromatic Schiff's base pendant groups by polymerization of benzylidene-ring-substituted N-benzylidene-4-ethynylanilines with Rh-based catalysts, Macromol. Chem. Phys. 200 (1999) 2591–2596, 10.1002/(SICI)1521-3935(19991201)200:12<2591::AID-MACP2591>3.0.CO;2-N.

[39] J. Brus, Heating of samples induced by fast magic-angle spinning, Solid State Nucl. Magn. Reson. 16 (2000) 151–160, https://doi.org/10.1016/S0926-2040(00)00061-8.

[40] Y. Zhang, K. Gao, Z. Zhao, D. Yue, Y. Hu, T. Masuda, Helical poly(phenylacetylene)s containing schiff-base and amino groups: synthesis, secondary structures, and responsiveness to benzoic acid, J. Polym. Sci. Part A Polym. Chem. 51 (2013) 5248–5256, https://doi.org/10.1002/pola.26955.

[41] H. Balcar, J. Sedláček, J. Zednık, V. Blechta, P. Kubát, J. Vohlıdal, Polymerization of isomeric N-(4-substituted benzylidene)-4-ethynylanilines and 4-substituted N-(4-ethynylbenzylidene)anilines by transition metal catalysts: preparation and characterization of new substituted polyacetylenes with aromatic Schiff base type, Polymer (Guildf) 42 (2001) 6709–6721, https://doi.org/10.1016/S0032-3861(01)00148-3.

[42] J. Ren, B. Ni, H. Liu, Y. Hu, X. Zhang, T. Masuda, Postpolymerization modification based on dynamic imine chemistry for the synthesis of functional polyacetylenes, Polym. Chem. 10 (2019) 1238–1244, https://doi.org/10.1039/C8PY01793J.

[43] O. Trhlíková, J. Zedník, H. Balcar, J. Brus, J. Sedláček, [Rh(cycloolefin)(acac)] complexes as catalysts of polymerization of aryl- and alkylacetylenes: influence of

cycloolefin ligand and reaction conditions, J. Mol. Catal. A Chem. 378 (2013) 57–66, https://doi.org/10.1016/j.molcata.2013.05.022.
[44] J.R. Holst, E. Stockel, D.J. Adams, A.I. Cooper, High surface area networks from tetrahedral monomers: metal-catalyzed coupling, thermal polymerization, and "Click" chemistry, Macromolecules 43 (2010) 8531–8538, https://doi.org/10.1021/ma101677t.
[45] Z. Xie, C. Wang, K.E. deKrafft, W. Lin, Highly stable and porous cross-linked polymers for efficient photocatalysis, J. Am. Chem. Soc. 133 (2011) 2056–2059, https://doi.org/10.1021/ja109166b.
[46] B. Petrovic, M. Gorbounov, S. Masoudi Soltani, Influence of surface modification on selective CO2 adsorption: a technical review on mechanisms and methods, Microporous Mesoporous Mater. 312 (2021) 110751, https://doi.org/10.1016/j.micromeso.2020.110751.
[47] J. Jeromenok, J. Weber, Restricted access: on the nature of adsorption/desorption hysteresis in amorphous, microporous polymeric materials, Langmuir 29 (2013) 12982–12989, https://doi.org/10.1021/la402630s.
[48] S. Petrasova, A. Zukal, J. Brus, H. Balcar, J. Pastva, J. Zednik, J. Sedlacek, New hyper-crosslinked partly conjugated networks with tunable composition by spontaneous polymerization of ethynylpyridines with Bis(bromomethyl) arenes: synthesis, spectral properties, and activity in CO2 capture, Macromol. Chem. Phys. 214 (2013) 2856–2866, https://doi.org/10.1002/macp.201300540.
[49] G.P. Baxter, M.R. Grose, The vapor pressure of iodine between 50° and 95, J. Am. Chem. Soc. 37 (1915) 1061–1072, https://doi.org/10.1021/ja02170a007.
[50] Y.H. Sun, S.A. Song, D.H. Xiao, L.F. Gan, Y.R. Wang, Easily constructed imine-bonded COFs for iodine capture at ambient temperature, ACS Omega 5 (2020) 24262–24271, https://doi.org/10.1021/acsomega.0c02382.
[51] C.Y. Pei, T. Ben, S.X. Xu, S.L. Qiu, Ultrahigh iodine adsorption in porous organic frameworks, J. Mater. Chem. A. 2 (2014) 7179–7187, https://doi.org/10.1039/c4ta00049h.
[52] Y. Xin, J.Y. Yuan, Schiff's base as a stimuli-responsive linker in polymer chemistry, Polym. Chem. 3 (2012) 3045–3055, https://doi.org/10.1039/c2py20290e.

Supporting Information

Microporous Polymers Prepared from Non-Porous Hyper-Cross-Linked Networks by Removing Covalently Attached Template Molecules

Bogdana Bashta[1)], Lucie Havelková[1)], Jiří Sokol[1)], Jiří Brus[2)], Jan Sedláček*[1)]*

[1)]Department of Physical and Macromolecular Chemistry, Faculty of Science, Charles University, Hlavova 2030, 12843 Prague 2, Czech Republic

[2)]Institute of Macromolecular Chemistry, Czech Academy of Sciences, Heyrovský Sq. 2, Prague 6, 162 06 Czech Republic

Synthesis of N-(3,5-diethynylbenzylidene)-4-methylaniline (M3)

575.5 mg (3.73 mmol) of 3,5-diethynylbenzaldehyde (98 %, purchased from ChemApproach) were dissolved in 10 mL of methanol and 400 mg (3.73 mmol) of 4-methylaniline (99.7 %, purchased from Aldrich Chemistry) were dissolved in 2 mL of methanol. These two solutions were mixed and stirred for 48 h at room temperature. After 48 h, the precipitated product was separated by filtration, washed with cold methanol, and dried under vacuum at room temperature. Yield 85 %, m/z (HRMS ESI) measured 244.1123, M+H; calculated 244.1121.

^{1}H NMR (400 MHz, CD_2Cl_2) δ 8.42 (s, H^7), 8.00 (d, J = 1.5 Hz, $2H^5$), 7.69 (t, J = 1.6×(2) Hz, $1H^3$), 7.23-7.13 (m, $2H^9$, $2H^{10}$), 3.22 (s, $2H^1$), 2.37 (s, $3H^{12}$).

^{13}C NMR (100 MHz, CD_2Cl_2) δ 157.4 C^7, 149.1 C^8, 137.9-137.2 C^3,C^6,C^{11}, 132.7 C^5, 130.4 C^{10}, 123.7 C^4, 121.4 C^9, 82.4 C^2, 79.0 C^1, 21.3 C^{12}.

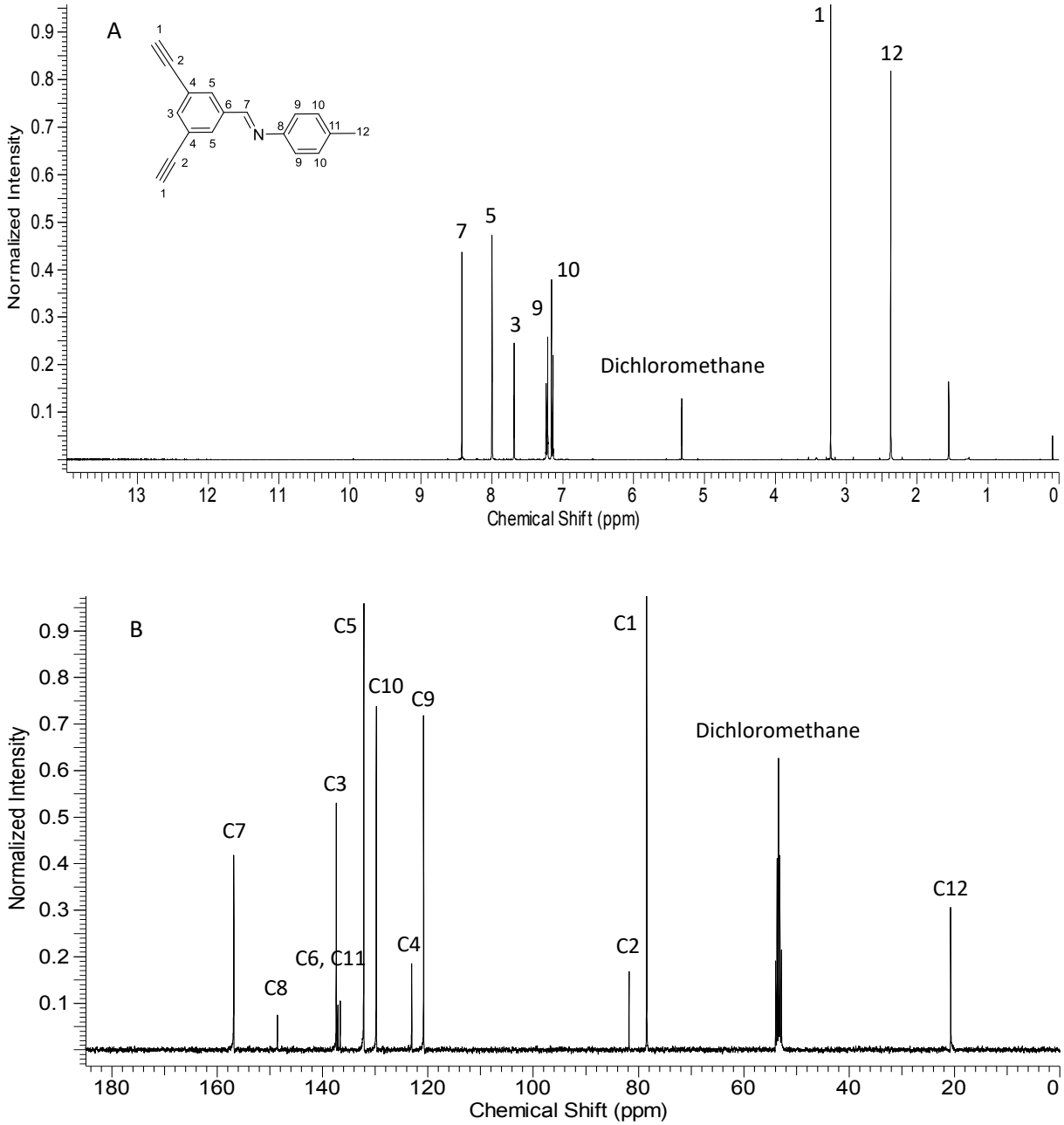

Figure S1. ^{1}H (A) and ^{13}C (B) NMR spectra of monomer M3.

Homopolymerization of tetrakis(4-ethynylphenyl)methane, (TEPhM)

TEPhM was polymerized in CH_2Cl_2 under argon atmosphere at 75 °C using [Rh(nbd)acac] as the polymerization catalyst. The reaction time was 7 days. The initial concentration of monomer was 0.3 mol·dm^{-3}, the concentration of [Rh(nbd)acac] was 15 mmol·dm^{-3}. 400 mg of TEPhM were dissolved in 2 mL CH_2Cl_2. A solution of 14 mg of the catalyst in 1.5 mL of CH_2Cl_2 was added to the solution of the monomer to start the polymerization. After 7 days, the precipitated polymer was separated, washed repeatedly with CH_2Cl_2, and dried under

vacuum for 2 days at room temperature. The quantitative conversion of monomer to poly[tetrakis(4-ethynylphenyl)methane], P(TEPhM) was achieved.

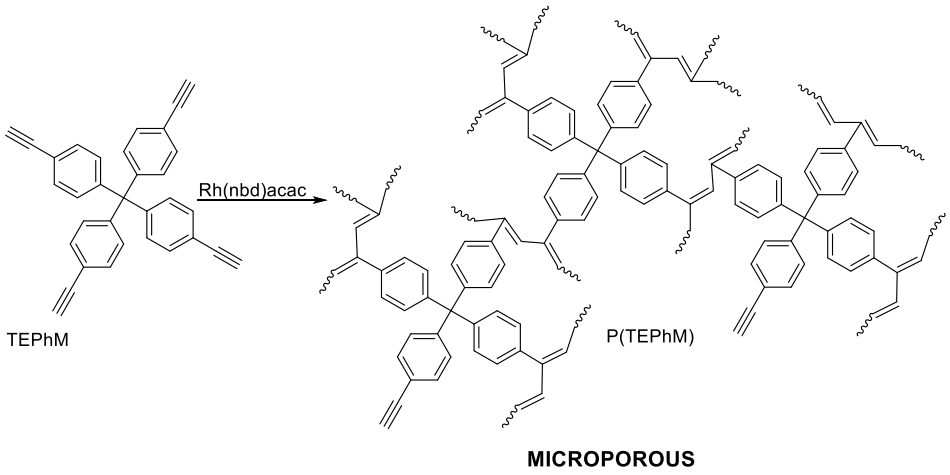

Scheme S1. Homopolymerization of TEPhM.

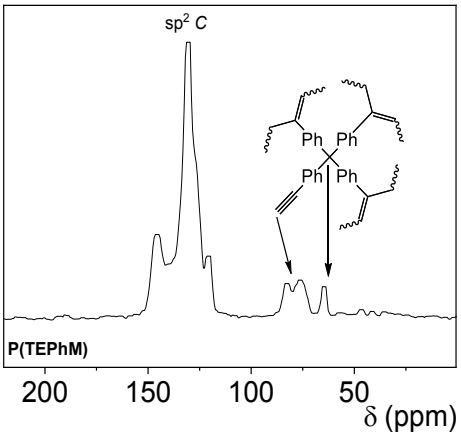

Figure S2. ^{13}C CP/MAS NMR spectrum of P(TEPhM).

All ^{13}C Cross-Polarization Magic Angle Spinning (CP/MAS) NMR spectra were measured at 11.7 T using a Bruker Avance III 500 WB/US NMR spectrometer in a double resonance 4 mm probehead at a spinning frequency of 18 kHz. The length of 90° (^{1}H) pulse was 2.5 μs, the strength of spin-locking field $B_1(^{1}H, ^{13}C)$ expressed in frequency units $\omega_1/2\pi = \gamma B_1$ was 64 kHz, the recycle delay was 6 s and cross-polarization contact time was 3 ms. During the acquisition of NMR signals heteronuclear TPPM (two-pulse phase-modulated) decoupling at $\omega_1/2\pi$ = 89.3 kHz was applied. Active cooling was used to compensate frictional heating of rotating samples.

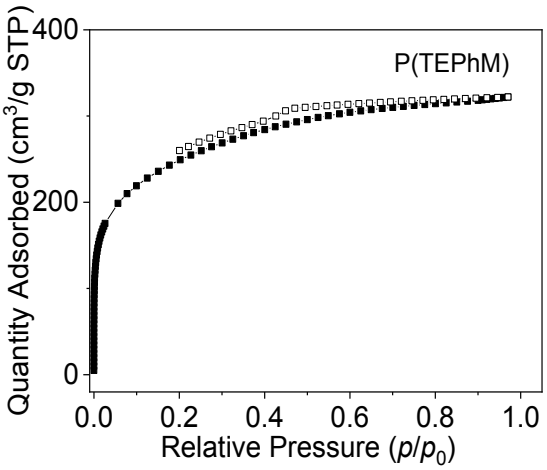

Figure S3. N_2 adsorption (full points) and desorption (empty points) isotherms (77 K) on homopolymer network P(TEPhM).

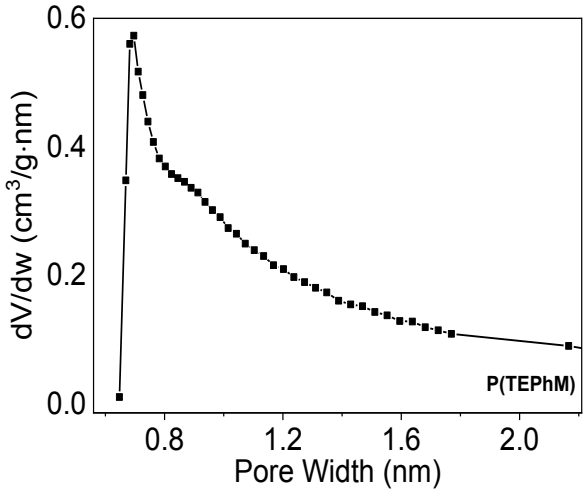

Figure S4. Micropore size distribution in homopolymer network P(TEPhM).

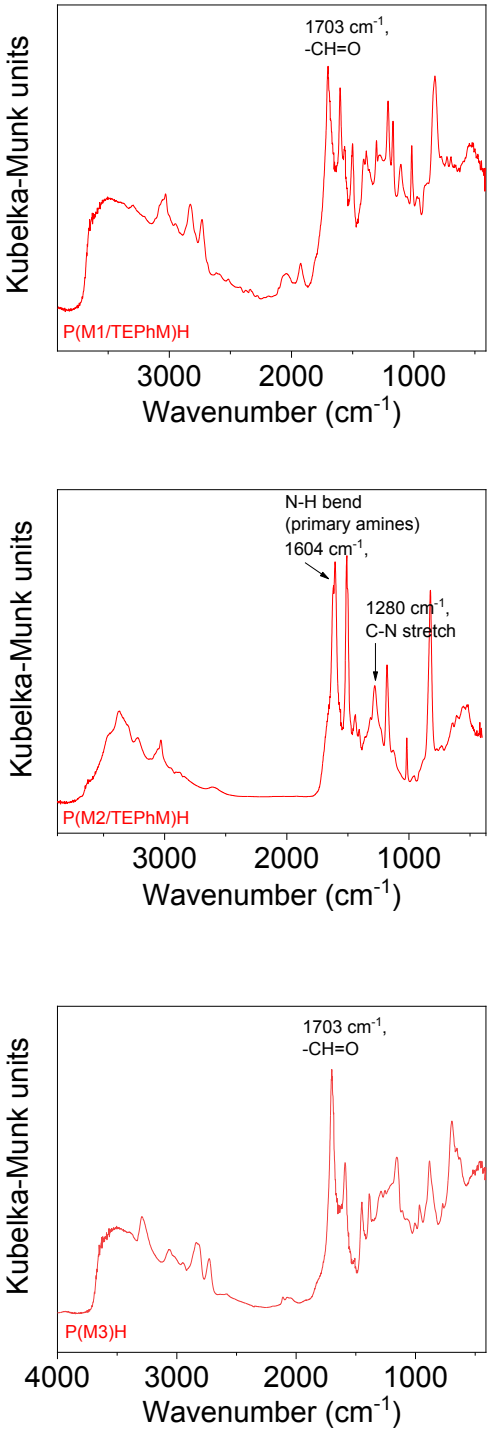

Figure S5. FTIR spectra on hydrolysed networks P(M1/TEPhM)H, P(M2/TEPhM)H, and P(M3)H.

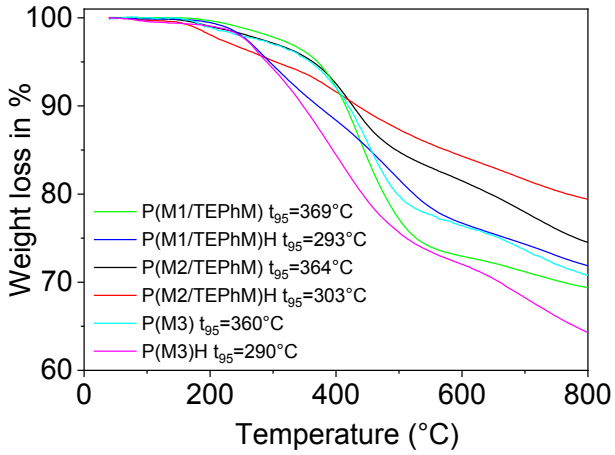

Figure S6. TGA curves of the networks.

CO_2 adsorption on the networks

The adsorption isotherms of CO_2 on the polymer networks were measured using a Triflex V4.02 apparatus (Micromeritics). Prior to the sorption measurements, all samples were degassed on a Micromeritics SmartVacPrep instrument as follows: starting from room temperature the polymer was degassed at 353 K (heating ramp of 0.5 ºC·min^{-1}). Hold pressure 10 mmHg. After a 1 h delay at 353 K, the temperature was further increased up to 383 K with the same heating ramp, and samples were degassed for 5 h.

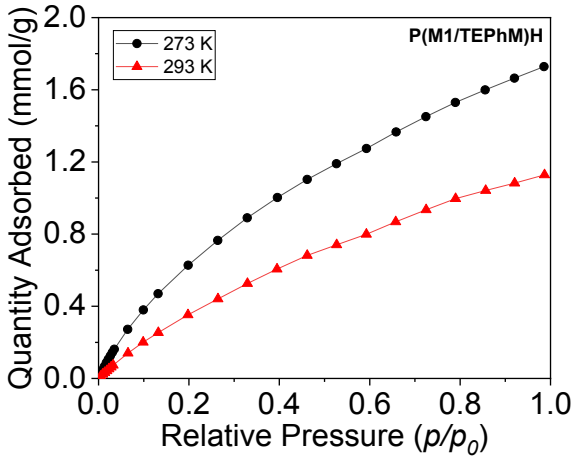

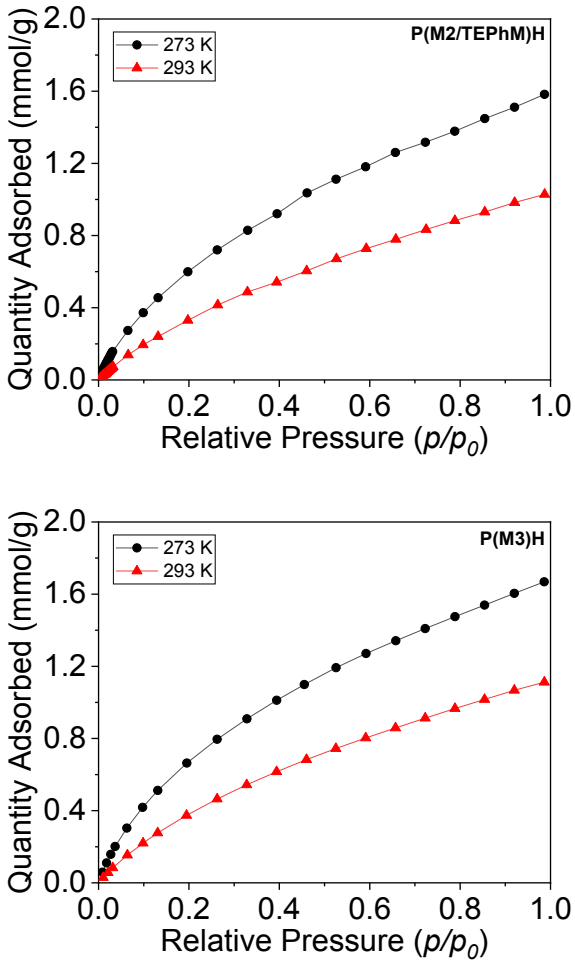

Figure S7. Temperature dependence of CO_2 adsorption isotherms on P(M1/TEPhM)H, P(M2/TEPhM)H, and P(M3)H.

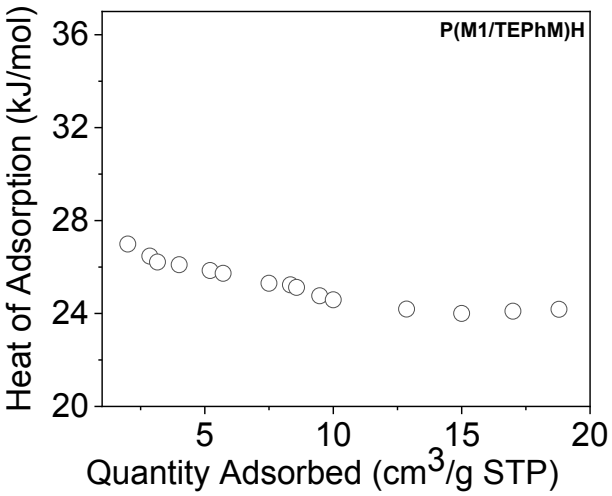

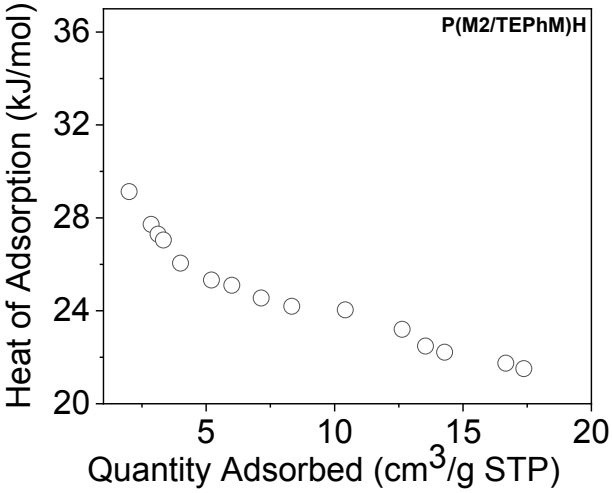

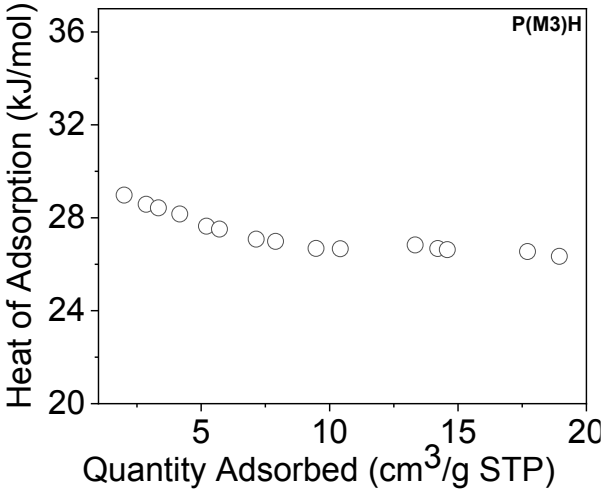

Figure S8. Isosteric heat of CO_2 physisorption on polymer networks.

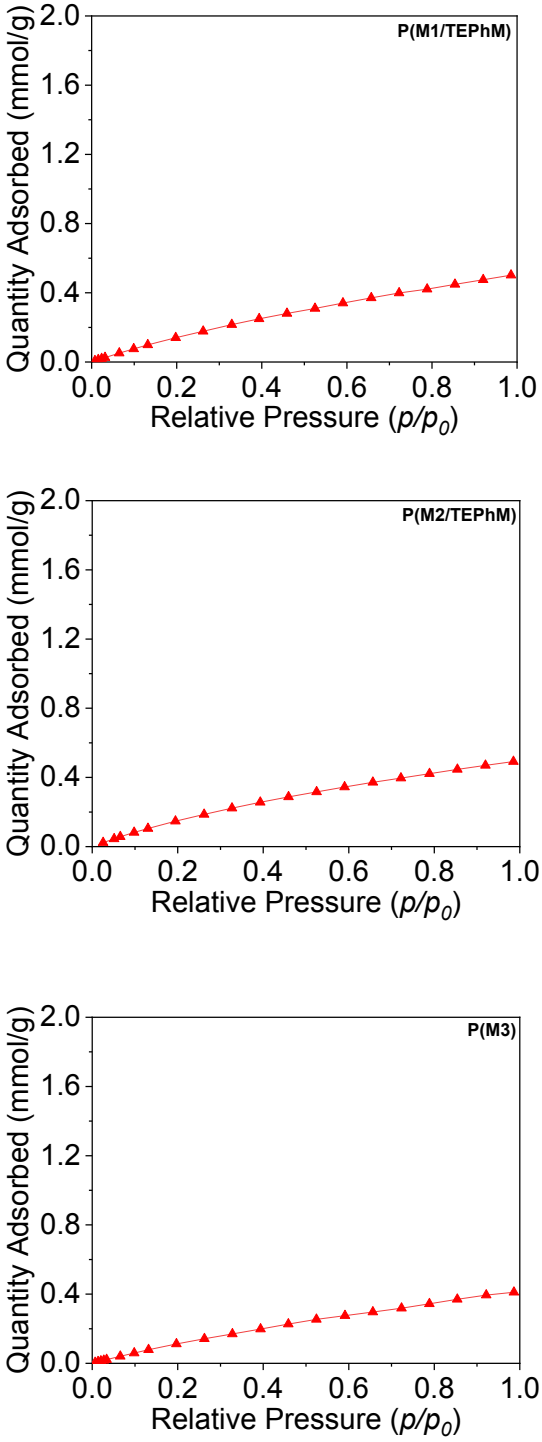

Figure S9. CO_2 adsorption isotherms on P(M1/TEPhM), P(M2/TEPhM), and P(M3) at 273 K.

Iodine adsorption on the networks

Adsorption of iodine vapour

The adsorption of I_2 vapour was performed in air at ambient pressure at 298 K (corresponding iodine vapour pressure of 41 Pa). A vessel containing 100 mg of a network was placed in a closed glass jar in which solid iodine was in the bottom. At given times the vessel with the network was withdrawn and quickly weighed to determine the amount of adsorbed iodine.

Adsorption of iodine dissolved in CH_2Cl_2

10 mg of the network were dispersed in 2 mL of iodine solution (CH_2Cl_2, initial concentration 0.2 $mg \cdot mL^{-1}$). The suspension was subsequently shaken using a lab shaker at room temperature. At given times the concentration of iodine in the liquid phase was determined spectrophotometrically at λ = 504 nm using UV/VIS 2401 PC Shimadzu spectrometer.

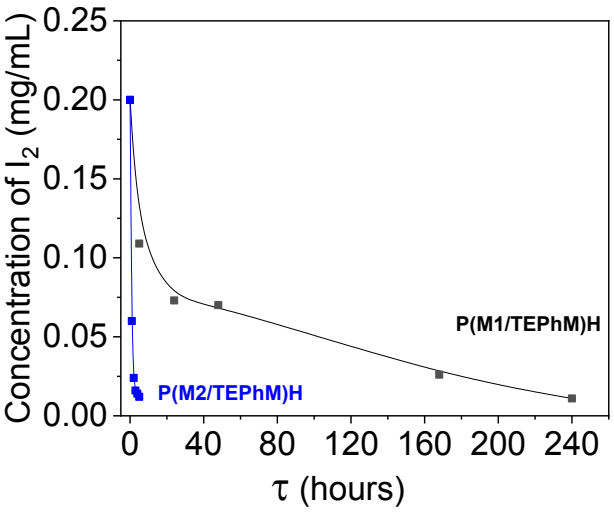

Figure S10. Time decrease of I_2 concentration in CH_2Cl_2 solution due to I_2 adsorption on P(M1/TEPhM)H and P(M2/TEPhM)H (room temperature, 10 mg of network, 2 mL of I_2 solution).